



The New Mexico Journal of Science

Natalie A. Rogers, Editor

THE NEW MEXICO ACADEMY OF SCIENCE

VOLUME 51
DECEMBER 2017

Table of Contents

Editor's Note	3
New Mexico Junior Academy of Science Paper Competition Winners	
<i>The Effects of Vegetable Oil Saturation on Quinine Extraction</i>	5
<i>Magnetic Iron Oxide-Gold Nanoparticles for the Photo-Thermal Dissolution of Protein Aggregates: Implications in Alzheimer Treatment</i>	22
High School Paper Submissions	
<i>The Column-less Stair at Loretto Chapel in Santa Fe: Strength Analysis</i>	33
2017 Award for Outstanding Science Teaching	39
New Mexico Academy of Science Research Symposium	40
About the Research Symposium	40
Keynote Speaker: David Gutzler, PhD	40
Symposium Welcome from 2017 NMAS President	40
About the Symposium Sponsors	41
Concurrent Session Presentation Abstracts	42
Undergraduate Poster Session Abstracts	54
Graduate Student Poster Session Abstracts	63
About the New Mexico Academy of Science	74
Contact Information	74
Officers and Executive Board 2017	74

Editor's Note

The *New Mexico Journal of Science* is a publication of the New Mexico Academy of Science. Each issue of the *Journal*, which has been published since 1906, contains research papers and articles deemed of interest to the scientists, educators, and citizens of New Mexico. Some volumes address scientific topics of social or economic interest to the state, while others emphasize scientific research in areas where New Mexico is particularly active.

The Academy oversees a New Mexico Junior Academy of Science program that sponsors an annual statewide scientific paper competition for students in New Mexico's middle and high schools. This volume of the *Journal* contains the winners from that competition, as well as one additional paper.

The New Mexico Academy of Science Research Symposium was held in Albuquerque, New Mexico on November 4, 2017. Oral and poster presentations at the Symposium described scientific research being conducted by undergraduate students, graduate students, and faculty at New Mexico's colleges and universities, and the abstracts of those presentations are once again included in this year's *Journal*. The New Mexico Academy of Science also presented its annual Outstanding Science Teacher Awards at the meeting. We wish to acknowledge the organizations which co-sponsored the 2017 Research Symposium: the New Mexico Experimental Program to Stimulate Competitive Research (NM EPSCoR), the New Mexico Alliance for Minority Participation (NM AMP) and the University of New Mexico's Center for Water and the Environment.

The *New Mexico Journal of Science* is published in an electronic-only format; it can be freely downloaded from the Academy's website at <http://www.nmas.org>. This enables the Academy to reach a much wider readership without incurring the considerable costs associated with the printing and distribution of paper copies.

Natalie A. Rogers, Editor
New Mexico Journal of Science

Public Relations Specialist
New Mexico EPSCoR
University of New Mexico
nrogers@epscor.unm.edu

New Mexico Junior Academy of Science Paper Competition Winners

Lea Godret-Miertschin

The Effects of Vegetable Oil Saturation on Quinine Extraction

Sanjiv Harikumar

Magnetic Iron Oxide-Gold Nanoparticles for the Photo-Thermal Dissolution of Protein Aggregates: Implications in Alzheimer Treatment

High School Paper Submissions

Anita Sumali

The Column-less Stair at Loretto Chapel in Santa Fe: Strength Analysis

The Effects of Vegetable Oil Saturation on Quinine Extraction

Lea Godret-Miertschin, Sandia High School

While quinine remains a useful drug in treating malaria, industrial extraction methods utilize harmful organic solvents. A sparsely researched yet more environmentally friendly method utilizes vegetable oil for the initial extraction. This study investigated the viability of this method and the impact of unsaturation on quinine yield. Three oils with varying degrees of unsaturation were used to extract quinine from cinchona bark: safflower (monounsaturated), sunflower (diunsaturated), and flaxseed (triunsaturated). It was found that flaxseed oil extracted the most quinine; the determined average percent yield values were 0.0128%, 0.0175%, and 0.0201%, for safflower, sunflower, and flaxseed oil, respectively. As these differences in yields are relatively significant, it is proposed that oils with higher levels of unsaturation extract more quinine than more saturated oils.

INTRODUCTION

Cinchona bark has a long medicinal history of treating malaria, dating back to the Spanish conquistadors (Petrovaska, 2012; Roth 2013). The active ingredient is quinine, one of the four cinchona alkaloids (quinine, quinoline, cinchonine, and cinchonidine) that can be extracted from trees in the Rubiaceae family (Carroll, 2012; Xu, 2012). Although quinine was synthetically manufactured in 1944, the process is costly and the primary method for obtaining quinine today remains cinchona bark extraction (Xu, 2012).

Many industrial extraction methods use lime and toxic organic solvents (benzene, alcohol, ether, or chloroform) and pH solubility properties to extract and isolate the alkaloid (Sukhdev, 2008). However, the unique work of Kallimopoulos (2012) suggests that alkaloid extraction with vegetable oils is possible.

The use of non-toxic solvents in extractions is intriguing as there is little research, especially regarding quinine, and if viable it would allow for a greener extraction process. The present investigation tested the viability of using vegetable oils to initially extract quinine from the bark. Further, the impact of oil unsaturation was investigated as no previous research could be found discussing its effect on extraction yield. Safflower oil, flaxseed oil, and sunflower oil were chosen because each has a different composition of unsaturated fatty acids (Zambiasi, 2007; Vesna 2012).

METHODS

Background and Methodology Theory

Extraction of alkaloids using solubility

Extraction of cinchona alkaloids occurs in two solubility steps: (Figure 1)

1. Removing compounds from the plant material
2. Changing solvent pH to isolate the desired compound from undesired structures (Xu, 2012; Morrow, 2016)

Based on the alkaloids' solubility fluctuations at various pH (Caine, 1911; Sasidharan, 2011; Carroll, 2012;

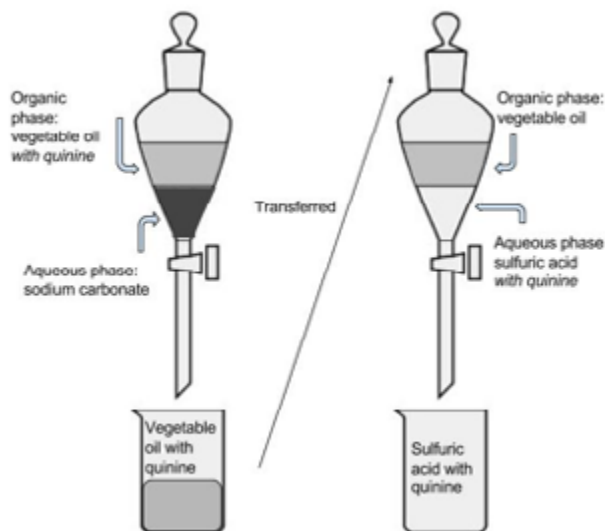


Figure 1. Solubility of Quinine throughout Extraction Process. (Made by student researcher) The extraction process as the quinine is transferred via pH changes from organic phase (vegetable oil) to aqueous phase (sulfuric acid).

Kallimopoulos, 2012; Xu, 2012), the alkaloids are extracted from powdered bark using vegetable oil concurrent with sodium carbonate, solvating the alkaloids in the immiscible vegetable oil organic phase and thereby separating the alkaloids from other compounds in the bark (Kallimopoulos, 2012; Morrow, 2016). The oil is then separated from sodium carbonate and acidified with sulfuric acid, dissolving alkaloids into an acidic aqueous phase (Morrow, 2016) where the quinine can be identified through fluorescence properties (Harley, 1885; University of Kentucky, 2005; Garcias, 2009).

Fluorescent properties of alkaloids

To reduce variables which would otherwise be introduced in crystallization, the amount of quinine extracted was determined using fluorescence. Quinine and quinidine (quinoline alkaloids) contain a methoxy group which exhibits fluorescence properties in the presence of oxygenated acids (Morrow, 2016), while cinchonine and cinchonidine do not (Kurian, 2007; Roman, 2016). A linear calibration curve plotting the concentration of standard quinine solutions in relation to emitted fluorescence intensity was used to calculate the unknown concentration of quinine solutions based on the measured intensity. Although quinine does not have a linear relationship between concentration and emission intensity at high concentrations due to quenching, previous research shows an accurate linear relationship for small amounts, e.g. below 5mg/L (University of Kentucky, 2005).

Fatty Acid Content in Vegetable oils

Fatty acid content in vegetable oil was isolated as the independent variable. Safflower, flaxseed, and sunflower oils were chosen due to their distinctive compositions of oleic, linoleic, and alpha-linolenic fatty acids. Each fatty acid is 18 carbon bases with varying degrees of unsaturation (Table 1). Unsaturation is when a hydrocarbon

contains one or more double bond between carbons, reducing the overall number of hydrogens present and forcing the molecule to assume a “bent” shape. This folds the oil’s triglycerides (Morrow, 2016), potentially affecting quinine’s ability to solvate and therefore the extraction yield. Because each oil is composed primarily of one fatty acid, it is assumed that extraction yield can be directly related to degree of unsaturation.

Variables Tested and Controlled

The independent variable is the degree of unsaturation in vegetable oil fatty acids. The dependent variable is the percent yield of quinine extracted from cinchona bark as compared to literature percent yield values. All other variables were kept as consistent as possible, including:

- Bark source (Penn Herb Co. LTD). While various species can be used (Kurian 2007; Sasidharan, 2011), the bark used was *Cinchona succirubra*
- Fluorospectrometer settings: excitation at 350nm, emission range of 400-600, and slit widths of 5nm (See Appendix II)
- Volume of sample tested in Fluorospectrometer (3mL)
- Cuvette used/orientation

Procedure

The brief outline of reagents and separation time from Kallimopoulos (2012) was used as general scaffolding for the current procedure as no other research concerning alkaloid vegetable oil extraction could be found (see Appendix I). The final procedures, including specific reagents, filtration processes, oils, and times were detailed by the student researcher.

Extraction of Alkaloids

Day 1: Alkaloid extraction from bark.

Three samples are made in labeled Erlenmeyer flasks consisting of:

	Oleic acid (monounsaturated; 1 double bond) (g fat/tbsp. oil^a)	Linoleic acid (diunsaturated; 2 double bonds) (g fat/tbsp. oil^a)	Alpha-Linolenic acid (triunsaturated; three double bonds) (g fat/tbsp. oil^a)
Safflower Oil	10.2	2.0	0.0
Sunflower Oil	2.7	8.9	0.0
Flaxseed Oil	2.5	2.2	8.0

Table 1. Fatty Acid Compositions of Selected Vegetable Oils. Note a: units g/tbsp. verbatim from: Anderson, 2007

- 25.005g (+/- 0.005g) powdered cinchona bark
- 40mL of oil (either safflower, flaxseed, or sunflower)
- 50mL 0.03M sodium carbonate.

The flasks are stirred into a homogenous mixture using a magnetic stir plate (30-45min), and left for eight hours.

Day 2: Liquids filtered from bark and phase separation.

A Buchner vacuum system filters liquid phases (See Appendix I). In stages, the bark sludge is placed into the funnels, 10-15 mL of bark sludge at a time, until no liquid drips through funnel. The filtered bark is removed before more wet bark is placed in funnel. The filter paper is replaced every 3rd filtration. After all sludge is filtered, filtrate (oil and sodium carbonate) is transferred into a 120-mL separatory funnel and sits overnight. To prevent possible pressure build-up, a paper is placed between greased stopper and funnel opening.

Day 3: Quinine moved to aqueous, sulfuric acid phase.

Oil and sodium bicarbonate phases are drained into separate beakers and oil phase is transferred to a clean separatory funnel. 40mL of 3M sulfuric acid is added

and carefully shaken, with pressure released frequently, to create an emulsion which then sits for one hour. The lower acidic phase is drained, measured, and stored until fluorescence testing.

For each oil, at least 5 trials were done (Materials, equipment, chemicals, and diagrams in Appendix I).

Testing Fluorescence using Fluorospectrometer

To measure fluorescence of samples, 3mL of the sample is taken from the middle (to avoid remaining residue oil on top and bark contaminates from bottom) with a pipette and transferred to a cuvette. The cuvette is placed into the fluorospectrometer, and fluorescence intensity is recorded using an excitation wavelength of 350nm, slit widths of 5nm, and emission window of 400-600nm. The peak emission wavelength is recorded as well as the corresponding intensity (see Appendix II).

RESULTS

Below are the crucial graphs and average data gathered. Raw data including concentration, amount quinine, % composition, and % yield in Appendix IV.

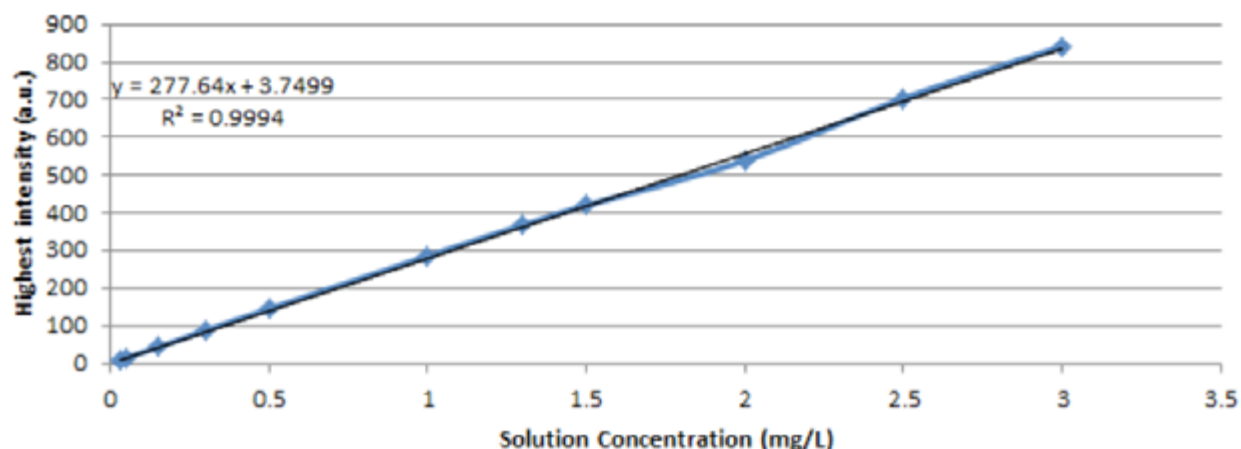


Figure 2: Calibration Curve Graph. The linear relationship between quinine concentration of standardized samples and absorption intensity at 450nm. The linear trend is reliable and accurate, with an r^2 value of 0.999. Using this graph, the concentrations for each trial can be found, by measuring the intensity and using the best-fit line equation to back-calculate quinine concentration (created by student researcher, see Appendix II).

Oil	Percent composition averages ^b	Percent yield
Safflower	0.000255% +/- 0.000008%	0.0128%
Flaxseed	0.000403% +/- 0.00009%	0.0201%
Sunflower	0.000350% +/- 0.0.0001%	0.0175%

Table 2: Average Percent Compositions and Yields. Average percent compositions of quinine based on calculated concentrations and percent yields based on industrial yields (calculations following) **Note b:** Averages do not include the tests that were saturated (Over 1000 intensity) or duplicate fluorescence tests of some trials, as including those data would skew average (See Appendix IV).

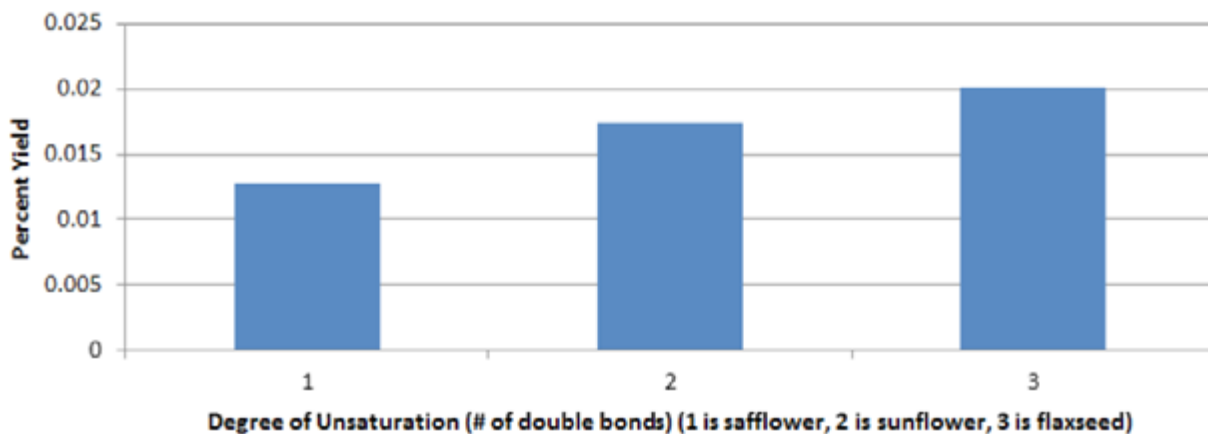


Figure 3: Comparison of Unsaturation to Percent Yield. Table 2 data in graphic form, showing percent yield quinine increasing with higher degrees of unsaturation.

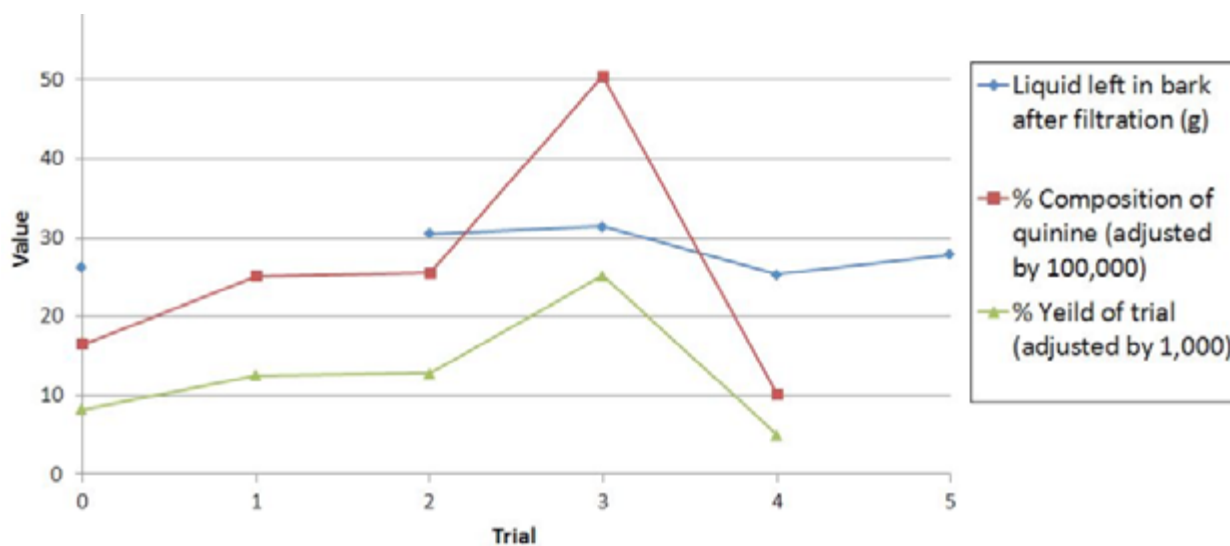


Figure 4: Comparing Filtration Efficiency, % Composition, and % Yield in Safflower Trials.^{c,d}

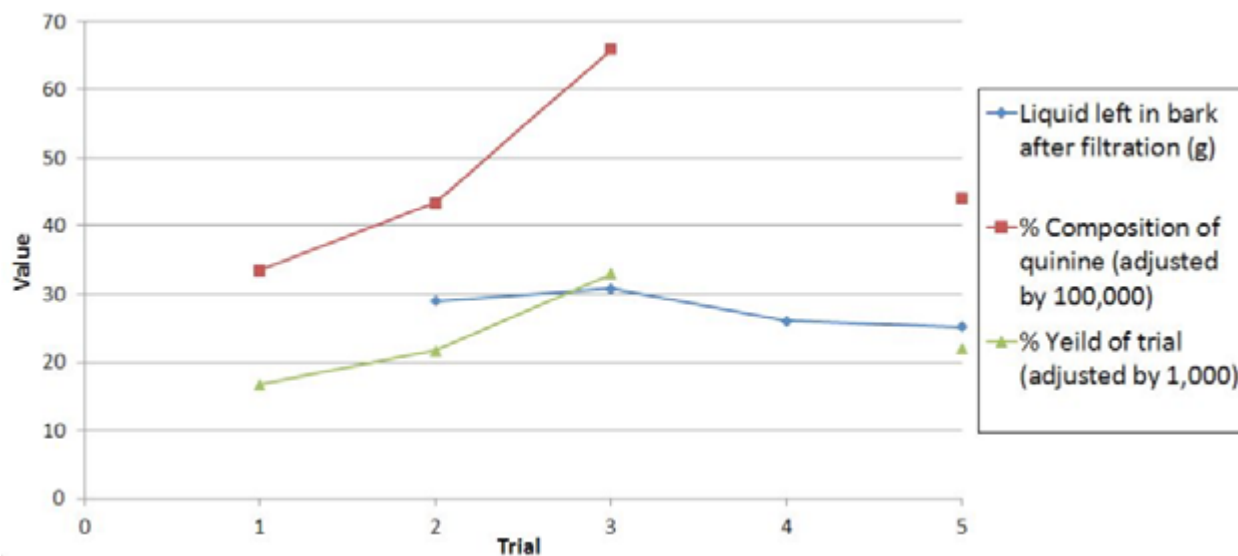


Figure 5: Comparing Filtration Efficiency, % Composition, and % Yield in Flaxseed Trials.^{c,d}

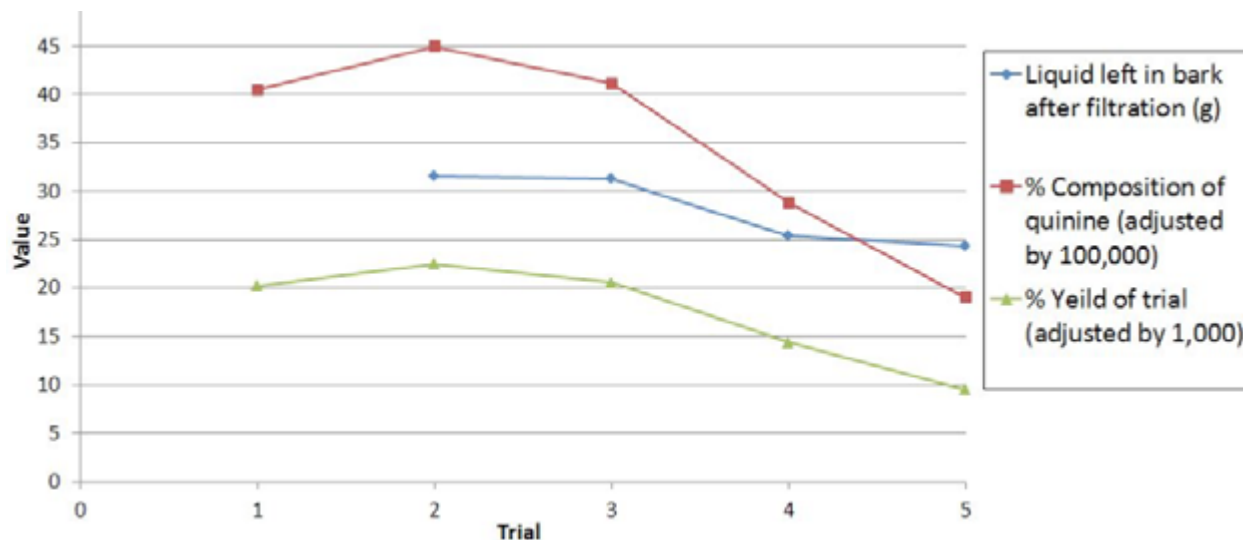


Figure 6: Comparing Filtration Efficiency, % Composition, and % Yield in Sunflower Trials.^{c,d}

Figures 4-6, Note c: Graphs display proportional relationships, not actual, because the data trends needed to be compared by trial on the same scale. Therefore, the % yield and % composition were multiplied by a factor of ten (as shown in legend) to make all trends comparable on the same y-axis scale. The amount of liquid left in bark is graphed (rather than just the amount of oil) because proportions of oil to sodium bicarbonate in filtrate are unknown (as measuring oil recovered to calculate oil left in bark would cause quinine to be lost in transfer and increase random error).

Figures 4-6, Note d: Some data points are missing due to trials that were saturated in fluorescence intensity, and therefore concentration was not calculated (Table 7, Appendix IV).

Figures 4-6 compare filtration efficiency (measured by the difference in bark weight before and after extraction and filtration) to the general trends of percent compositions and percent yield for all three oils over the 5 trials conducted. As percent yield values were extremely low, this analysis examined the possible direct effect that filtration inefficiency had upon the yields.

Calculations

The percent yield of quinine is calculated as follows:

1. Quinine concentration is found using fluorescence intensity values and the calibration curve best fit line (Table 7 and Figure 3).

$$y = 277.64x + 3.7449 \quad (\text{Best fit line: } y \text{ is intensity and } x \text{ is quinine concentration})$$

$$x = \frac{y - 3.4779}{277.64} \quad (\text{Rearranging equation to solve for concentration})$$

Example (intensity 500 a.u.):

$$\text{quinine concentration} = \frac{500 - 3.4779}{277.64}$$

$$\text{quinine concentration} = 1.79 \text{ mg/L} \pm 0.05 \text{ mg/L}$$

2. Amount of quinine in sample found by:

$$\text{amount quinine} = \frac{(\text{quinine concentration}) \text{ mg}}{L} \times (H_2SO_4) L$$

Example (continuing previous example, volume of 0.03L H₂SO₄):

$$\text{amount quinine} = \frac{1.79 \text{ mg}}{L} \times 0.03 \text{ L } H_2SO_4$$

$$\text{amount quinine} = 0.054 \text{ mg} \pm 0.0002$$

3. Percent composition found by:

$$\% \text{ composition} = \frac{(\text{amount quinine}) \text{ mg}}{(\text{original amount of bark}) \text{ mg}} \times 100$$

Example (continuing previous example, 25.0g bark originally):

$$\% \text{ composition} = \frac{0.054 \text{ mg}}{25000 \text{ mg}} \times 100$$

$$\% \text{ composition} = 0.000216\% \pm 0.000008$$

Percent yield from averages of each oil was then found by:

$$\% \text{ yield} = \frac{\text{Experimental yield (average \% compositions)}}{\text{Theoretical yield (based on research)}}$$

Example (continuing previous example):
Theoretical yield used was 2% ± 1% (Bartholow, 1893) (Xu, 2012)

$$\% \text{ yield} = \frac{0.000216}{2} \times 100$$

$$\% \text{ yield} = 0.0108\%$$

Assumptions

First, it was assumed that the bark used was of comparable quality to that used in industrial extraction to allow for comparisons of experimental quinine yield to that of industrial values. Second, it was assumed that no other reactions, such as formation of quinine sulfate, would interfere with the extraction or fluorescence processes. In relation to this, fluorescence intensity was assumed to be accurate and be attributed entirely to quinine due to the low percent composition of quinidine within cinchona bark when compared to quinine (Bartholow, 1893). Finally, the solubility properties to separate the cinchona alkaloids from bark material were assumed to be viable due to quinine's pKa of 8.56 (PubChem, 2012; Morrow 2016).

DISCUSSION

The percent yields for safflower, sunflower, and flaxseed oil are 0.0128%, 0.0175%, and 0.0201% respectively. Based on the samples' average percent yields of quinine, flaxseed oil performed best, followed by sunflower oil, with safflower much lower. This suggests that highly unsaturated fatty acids, such as the linoleic and alpha-linolenic present in sunflower and flaxseed oil respectively, extract quinine more efficiently. Hypothetically, this is explained by looking at the structures caused by unsaturation. More double bonds cause 'kinks' in the fatty acid chain, potentially increasing the oil's ability to isolate quinine molecules. As the triglycerides have weaker intermolecular attractions due to the crookedness, the oils can dissolve quinine better as it is more difficult for the triglycerides to stick to other triglycerides. The increase in double bonds also causes the polarity of these triglycerides to increase, possibly allowing for the intermolecular bonds between oil and quinine to be stronger. Furthermore, each new double bond is a chance for a different stereoisomer to occur,

creating a more diverse environment and theoretically enabling quinine to dissolve in the vegetable oil better. However, due to the complex structure of quinine and unknown reactions between quinine and solvent, it is difficult to know precisely why the increase in unsaturation increases the ease of solubility. Another possibility is that unsaturated oils break down cinchona bark cell walls more effectively, although this speculation is complex and requires investigation into cinchona bark structure.

Analysis of Methods

The meaning of the data gathered, assumptions made, and the design flaws that the data demonstrates will now be explained. Although not directly relating to the effects of unsaturation, this is pertinent to the investigation as it impacts further research and helps form some main conclusions that can be drawn from this investigation.

The filtration may have seriously impeded accurate and precise results. Figures 4, 5, and 6, which compare filtration efficiency to percent composition and percent yield, show a correlation between liquid left in bark and final results for each trial. The data trends correlate proportionally, showing that the more liquid left in bark, the higher the percent yield. Moreover, the filtration seems to have affected these results in a drastic, non-linear way. For example, a difference of 1g liquid left in bark (mixture of oil and sodium bicarbonate) could increase percent yield as much as 0.01% (safflower and flaxseed trials 2, 3). The reasons for this are unclear.

The reliability of fluorescence must also be considered as the data formed a basis for calculations and conclusions. However, the use of quinine's fluorescent properties to determine concentration is considered reliable for several reasons:

1. Standard samples' excitation was found to be ~ 350nm and emission ~ 450, consistent with previous research (University of Kentucky, 2005), and the wavelength peaks of the extracted samples were close to the standards, falling between 440.00 and 451.00.
2. The intensity values of measured samples fall about a third of the way up the calibration curve, and therefore display clear peaks.
3. The disparity between the excitation wavelengths of quinine based and cinchonine based alkaloids (Grant, 1950) and the fact that only dications of

cinchonine alkaloids have been known to fluoresce (Pharmacognosy, 2012) led to the assumption that emission intensity was overwhelmingly due to the quinine based alkaloids.

4. For trial 1, the fluorescence was retested on a different day to confirm that exposure to sunlight over time would not affect fluorescence intensity. It was found that the intensity did not markedly change. This shows that while the trials were measured different times after extraction was completed, all are still comparable.

The calibration curve (Figure 2) is also reliable. It shows what would be expected based on previous research; the concentration of quinine is directly proportional to fluorescence emission intensity at low concentrations (Artxy, 2012). Although a concentration at 5mg/L was found to be saturated (over 1000), below 3mg/L concentration and intensity were found to be linear. In fact, the r-squared value is 0.9994, showing that the data is close to the linear best fit line and therefore viable to calculate quinine concentration based on fluorescence intensity.

Reliability of Investigation

There are several possible sources of error. First, if the bark used was not industrial quality, then comparing results to industrial yields is inaccurate.

There was also significant room for error in filtration. While the Buchner funnel vacuum filtration method was found to be most efficient, Table 6 demonstrates how an average of 28g of liquid remained in the bark, showing that the amount of quinine extracted is uncertain, as the amount left in bark is unknown. Further, not all Buchner funnels were equal in filtration efficiency, as shown through lack of consistency in liquid left in bark in Figures 4, 5, 6.

Random error is present due to loss of material in glassware transfers, especially pronounced due to the small sample size. Further, as many values were used to calculate further measurements and analysis, the final percent composition and percent yield values have a higher chance of being affected by random mathematical error and uncertainty.

There is also possible error in the fluorescence tests. As many of the fluorescent readings had two peaks at slightly different wavelengths, usually lower than the 450 shown in the standard solutions, there are probably

impurities. The second peak could indicate the presence of quinidine. However, as quinine in each sample was too small to crystalize and perform purity tests on (such as melting point or TLC), the purity of the sample remains unknown. As the sample was impure, there could have been unknown quenching factors.

Finally, with only 5 trials for each oil (some of which excluded from averages due to saturated intensity) random errors have a larger impact on final averaged results.

Reliability of Sources

As web based sources are not always reliable, the procedure and concepts applied in this type of extraction were verified with supervisor Valerie Varoz and Dr. Morrow, as well as other web pages and books. The Google Patent (Kallimopoulos, 2012) was relied upon for proportions of reagents and general procedure because it was the sole source found with numerical amounts mentioned for the extraction process. For other information, multiple webpages, books, and accepted literature were utilized to confirm correct information. However, verification was not always possible, and the accuracy of some particulars (such as percent composition quinine in cinchona bark), remain unclear.

Conclusions

Presently, the data leads to the conclusion that fatty acids with more unsaturation sites are the best extractors. Although percent yields are low compared to the average 2% composition of industrial methods (Xu, 2012), this vegetable oil extraction method does appear to be viable, assuming further process optimization. Although methods seem inefficient, this investigation does demonstrate that extraction with vegetable oil is possible and that the oil's unsaturation has an impact upon the extraction yield of quinine.

It is thought that vegetable oil extraction is much cleaner and "greener" chemistry than industrial extraction methods, and has potential for making other alkaloid extractions less toxic. However, there are limitations to using vegetable oil; although the flaxseed oil was shown to produce the highest yield, it was also a difficult solvent. If allowed to dry inside glassware, it formed a hard residual that was difficult to remove. Also, this investigation was small scale, and the ability to upscale remains unknown.

Further Research and Unanswered Questions

Not all questions could be addressed. Data gathered could give a preliminary answer to the research question posed, but more testing is required to confirm these results and reduce the impact of random error. Especially as the current methods had many limitations, other procedures should be done to confirm that the yield was due to the oil composition and not the method. However, the methods here could be used to determine the ideal conditions, including times for each step, conducting multiple washes with sulfuric acid, temperature, reagent amounts/concentrations, and effects of several vacuum filtrations to remove more oil. Investigation of these variables aid in developing a procedure which maximizes the efficiency of vegetable oil extraction. There are also several expansions upon the original question that could be investigated, such as testing other cinchona bark species or different unsaturated oils, such as soybean oil, to see if all highly unsaturated oils are as effective.

ACKNOWLEDGMENTS

I would first like to thank my teacher, Valerie Varoz for allowing me to complete my testing during the summer. In addition, I want to thank Dr. Ho for showing and allowing me to use the fluorospectrometer at the University of New Mexico. I would also like to thank Dr. Cary J. Morrow for his time in helping me answer questions about organic chemistry.

REFERENCES

A. Quinine (2012). In *Pharmacognosy*. Retrieved from <http://www.epharmacognosy.com/2012/07/quinine-obtained-from-bark-of-cinchona.html>.

Albert-Garcia, J.R., Antón-Fos, G.M., Duarte, M.J., Lahuerta Zamora, L., Martínez Calatayud, J. (2009). Theoretical prediction of the native fluorescence of pharmaceuticals. In *Talanta*. Retrieved May 7, 2016.

Anderson (2007). Fatty Acid composition of fats and oils. *PDF*. Retrieved from http://www.uccs.edu/Documents/danderso/fats_oils.pdf.

Bartholow, R. (1893). *A Practical Treatise on Materia Medica and Therapeutics* (p. 545). N.p.: Materia Medica. Retrieved from Google Books.

Carroll, A., Kavanagh, D., McGovern F., Reilly, J., and J. Walsh, (2012). Nature's Chiral Catalyst and Anti-Malarial Agent: Isolation and Structure Elucidation of Cinchonine and Quinine from *Cinchona calisaya*. *Journal of Chemical Education*, 89, 1578-1581.

Cain, J. C. (1911). *Journal of the Chemical Society Transactions* (Vol. 99, pp. 1254-1261). London: Gurney and Jackson. Retrieved from Internet Archive.

Experiment 6: Molecular Florescence Spectroscopy: Quinine Assay (2005). *PDF*. Retrieved from http://www.chem.uky.edu/courses/che226/Labs/060-Quinine_Fluor.pdf.

Grant, H. S., & Jones, . (1950). Spectrophotometric determination of cinchona alkaloids. In *PDF*. Retrieved from <http://pubs.acs.org/doi/abs/10.1021/ac60041a017?-journalCode=ancham>.

Hertzler, A. A. (1986, January). Perception of nutrient density and information links of college students. *Journal of The American Dietetic Association*, 86(1), 792.

Harley, W. N. (1885). *The Absorption Spectra of the Alkaloids* (Vol. 176, pp. 487-521). London: Royal Society. Retrieved from JSTOR.

Kurian, A. M., & Sankar, A. (2007). *Medicinal Plants* (p. 82). N.p.: New India Publishing. Retrieved from Google Books.

Kallimopoulos, T. (2012). Methods for isolating alkaloids from plants EP 2475374 A2. In *Google Patents*. Retrieved May 7, 2016, from <https://www.google.com/patents/EP2475374A2?cl=en&dq=quinine+alkaloid+extraction&hl=en&sa=X&ved=0ahUKEwiqls-PnJnMAhXqloMKHW0DDj4Q6AEINzAD#npl-citations>.

Petrovska, B. B. (2012). Historical review of medicinal plants' usage. In *National Center for Biotechnology Information*. Retrieved October 11, 2016, from <https://www.ncbi.nlm.nih.gov/pmc/articles/PMC3358962/>.

Lab Report on Excitation and Emission Spectra of Quinine Sulfate Solution (2012). In *Artxy*. Retrieved from <http://www.art-xy.com/2009/10/lab-report-on-excitation-and-emission.html>.

Quinine (2012). In *PubChem*. Retrieved from <https://pubchem.ncbi.nlm.nih.gov/compound/8549#section=pKa>.

Quinoline Alkaloids (2012). In *Epharmacognosy*. Retrieved from <http://www.epharmacognosy.com/2012/07/quinoline-alkaloids.html>.

Roman, C., & Smith, Z. (2016, May 31). Fluorescence. In *LibreTexts*. Retrieved from http://chem.libretexts.org/Core/Physical_and_Theoretical_Chemistry/Spectroscopy/Electronic_Spectroscopy/Fluorescence.

Roth, K., & Streller, S. (2013). From Pharmacy to the Pub - A Bark Conquers the World Part 1. In *Chemistry Views*. Retrieved from http://www.chemistryviews.org/details/ezone/4701281/From_Pharmacy_to_the_Pub_A_Bark_Conquers_the_World_Part_1.html.

Sasidharan, S., Chen, Y., Saravanan, D., Sundram, K. M., & Yoga Latha, L. (2011). Extraction, Isolation and characterization of bioactive compound from plant's extracts. In *African Journal of Traditional, Complementary and Alternative Medicines*. Retrieved from <http://www.ajol.info/index.php/ajtcam/article/view/60483/48716>.

Sharp, J. T. (1989). *Practical Organic Chemistry: A Student Handbook of Techniques* (pp. 129-134). New York: Chapman and Hall.

Sukhdev Swami Handa, Suman Preet Singh Khanuja, Gennaro Longo, Dev Dutt Rakesh, . (2008). *Extraction technologies for medicinal and aromatic plants*. Retrieved

from http://agritech.tnau.ac.in/horticulture/extraction_techniques%20_medicinal_plants.pdf.

Xu, R., Ye, Y., & Zhao, W. (2012). *Introduction to Natural Products Chemistry* (pp. 40-68). Boca Raton, FL: CRC Press.

Zubrick, J. W. (2001). *The Organic Chem Lab Survival Manual: A student's guide to techniques* (pp. 129-134). New York: John Wiley.

Zambiasi, R., Przybylski, R., & Mendonca, C. (2007). Fatty Acid composition of vegetable oils and fats. In *PDF*. Retrieved from <http://www.nononsensecosmethic.org/wp-content/uploads/2015/01/fatty-acid-oil-composition.pdf>.

AUTHOR INFORMATION

Lea Godret-Miertschin
Sandia High School
7801 Candelaria Road NE
Albuquerque, NM 87110
leagodret@gmail.com

APPENDIX I

Procedure as Outlined in Patent

The text below is the exact wording and amount of information given in the patent in regards to extracting quinine.

“Example 4- Extraction of Quinine Alkaloids from Cinchona. Bark Fifty seven grams Na_2CO_3 were dissolved in 192 ml water in a 500 ml extractor. One hundred grams of ground (< 0.5mm) Cinchona bark and 150g rapeseed oil were added. The mixture was thoroughly mixed and left to stand at ambient temperature (approx. 25°C) for 19 hours. The mixture was stirred occasionally... The solid compounds in the mixture were removed by filtration and discarded. The oil phase was separated from the filtered emulsion and extracted with 300 ml 3% H_2SO_4 at pH 2. The aqueous phase was recovered after its separation and washed with 50 ml cyclohexane. Then, the aqueous phase was extracted with 125 ml of a 1:4 (v/v) mixture of 25% aqueous NH_4OH and cyclohexane at pH 11. The resulting emulsion was broken by addition of 5ml methanol. The organic phase was separated, dried over MgSO_4 , and the solvent was evaporated to obtain 0.145g of a mixture of cinchona alkaloids. The content of quinine in this mixture of cinchona alkaloids was 47%.” (Kallimopoulos, 2012)

Materials and Equipment

As there were three different procedures carried out (extraction, reading samples' fluorescence, and making fluorescence calibration curve) the materials lists have been separated out respectively.

For extraction (all amounts for one extraction sample):

- Digital mass balance
- Weighing boat
- 1 Erlenmeyer flask
- Electronic stir plate and rod
- 1 Vacuum filter flask (Erlenmeyer flask with spout)
- 1 Plastic piece of tubing (for sink attachment in vacuum filtration)
- 1 Buchner funnel with rubber stopper for flask
- 2-3 quantitative filter papers
- Scoopula
- 100mL graduated cylinders
- 2 (120mL) separatory funnels and stoppers; so each separation avoids previous residue
- Waste beakers
- Storage container

- Sharpie for labeling
- Parafilm
- Papertowels

For testing fluorescence of samples:

- 1 cuvette
- 1 (1,000ul - 5,000ul) pipette, set at 3,000ul
- Fluorospectrometer

For fluorescence calibration curve (amount of materials needed to make stock sulfuric acid quinine solutions (30 mg/L and 3 mg/L) and 1 dilution):

- 2 (1L) volumetric flasks
- 1 (50mL) volumetric flask
- Electronic mass balance
- Weigh boat
- Scoopula
- 1 (1,000ul - 5,000ul) micro pipette
- Beakers (for pouring stock solutions into for easier access)
- 1 (10mL) volumetric flask (one needed for each dilution made)
- Vortex (an instrument which mixes small solutions)
- Cuvette (4 mL)
- Fluorospectrometer (Cary Eclipse program)

Chemicals/Reagents

Reagents used for each procedure have been separated out accordingly:

List of reagents for extraction (all amounts for one extraction trial/process):

- 25g cinchona bark (bought from [Penn Herb Co. LTD](#))
- 40 mL oil (safflower, flaxseed, or sunflower)
- 50 mL 0.03M sodium carbonate
- 40 mL 3.00M sulfuric acid

List of reagents for testing fluorescence of samples:

- Extracted sample
- 0.05M sulfuric acid for needed dilutions

List of reagents for fluorescence calibration curve (for stock quinine solutions, stock sulfuric acid solution, and 1 dilution of quinine):

- 18M sulfuric acid
- Powdered, lab grade quinine
- Deionized water

Diagrams and Pictures

Figure 7: Set-up Diagram and Picture for Buchner Vacuum Filtration (diagrams and pictures by student researcher)

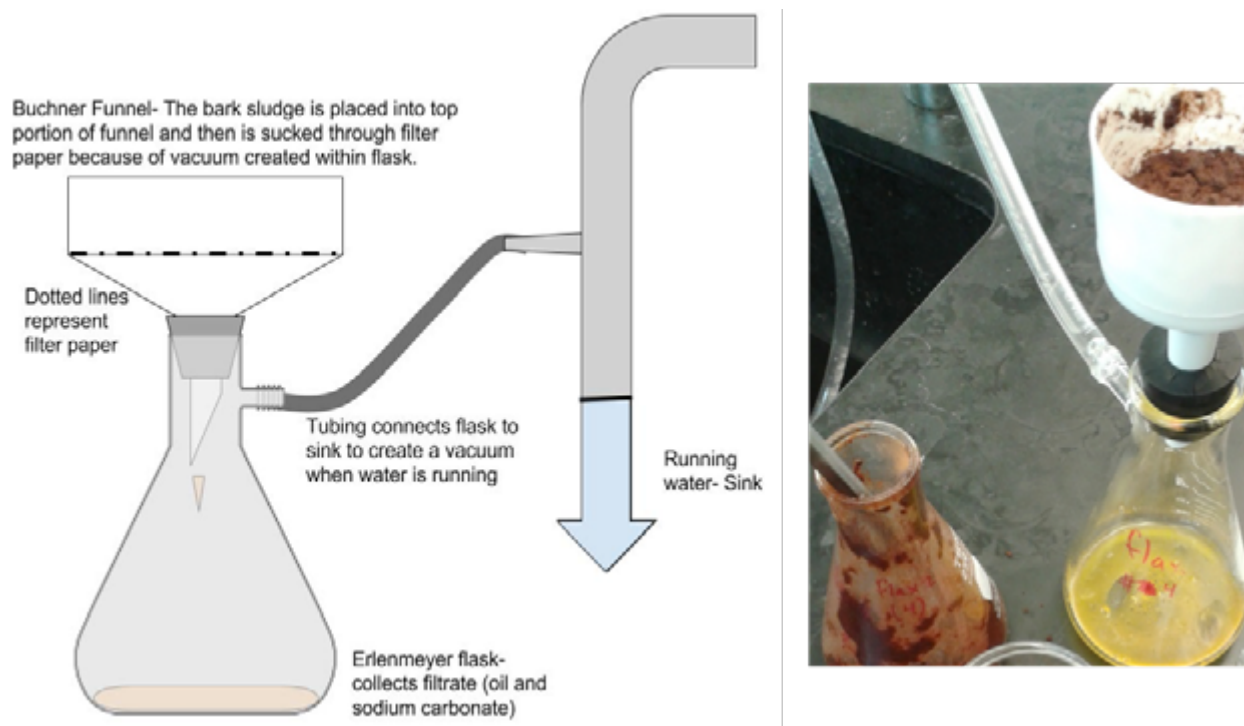


Figure 8: Set-up Diagram and Picture for Separatory Funnel (picture taken by student researcher)

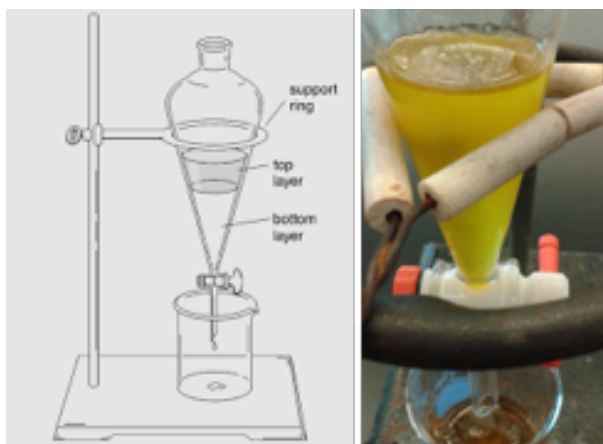


Figure 9: Pictures of Phase Separation between oils and sodium carbonate (pictures taken by student researcher)



APPENDIX II

Creation of Calibration Curve

To make the curve, 1L stock solution of 38.7mg/L was prepared with 0.0387g of reagent grade standard quinine, 50.00mL of 1M H₂SO₄, and deionized water. Gradual 10mL dilutions of the stock, ranging from 5mg/L to 0.003mg/L, were made (sample calculations below) and mixed thoroughly using a vortex (mixing apparatus). To measure fluorescence, 3mL of the sample was inserted into a clean cuvette using a micropipette and placed into the fluorospectrometer. The resulting emission intensity and wavelength was recorded and graphed as concentration (mg/L) vs. wavelength intensity (a.u.) (Figure 3).

Sample Calculations for Making Standard Quinine Solutions

The stock solution used to start all dilutions was 38.7 mg/L. To make dilutions, the equation $M_1V_1=M_2V_2$ was rearranged to solve for the first volume (how much stock was needed) to get general formula:

$$x = \frac{n \times 10 \text{ mL}}{s}$$

(where n is the new desired concentration, s is the concentration of the stock used, and x is the amount (in mL) of the stock needed to make a 10 mL dilution)

Although the original stock was used to make dilutions of 5mg/L and 3mg/L, to make more dilute solutions, a 3mg/L dilution of 50mL was made and used for all further dilutions. The following is an example calculation, where the 5mg/L dilution was made using the original 38.7mg/L stock.

$$x = \frac{5.00 \times 10 \text{ mL}}{38.7 \text{ mg/L}} = 1.29 \text{ mL}$$

Table 3. Volumes used to make Standard Quinine Dilutions for Calibration Curve

Dilution concentration (mg/L) +/- 0.005	Concentration of stock used (mg/L) +/- 0.005	Amount of stock (mL) added to make 10 mL dilution +/- 0.0005mL
5.00	38.70	1.290
3.00	38.70	3.876 ^e
2.50	3.00	8.333
2.00	3.00	6.666
1.50	3.00	5.000
1.30	3.00	4.335
1.00	3.00	3.335
0.50	3.00	1.665
0.30	3.00	1.000
0.15	3.00	0.500
0.05	3.00	0.166
0.03	3.00	0.100

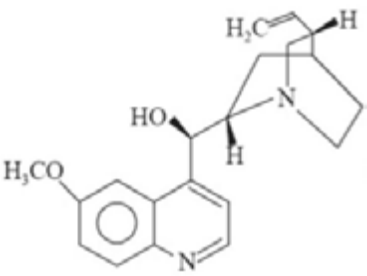
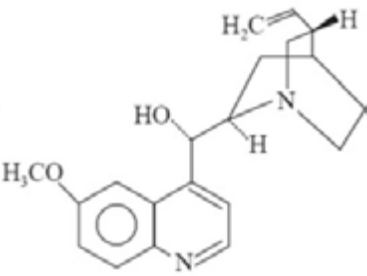
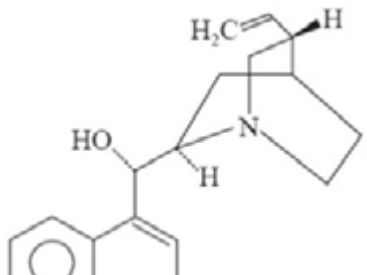
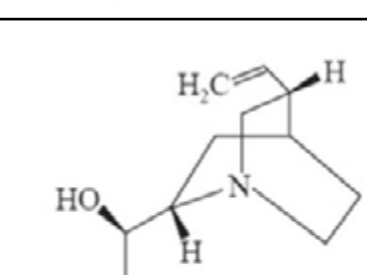
Note e: This amount was used to make a 50mL solution, rather than 10mL, which is why it is higher than others.

Table 4. Fluorescence Calibration Curve Data

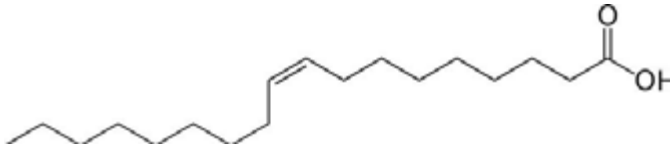
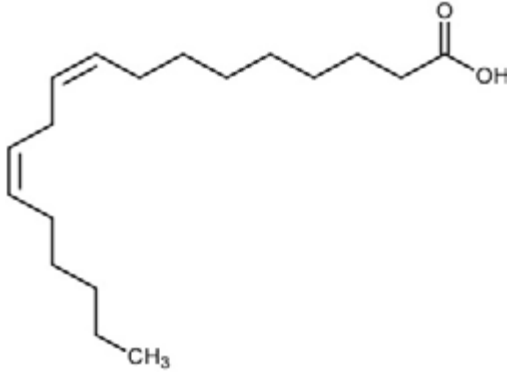
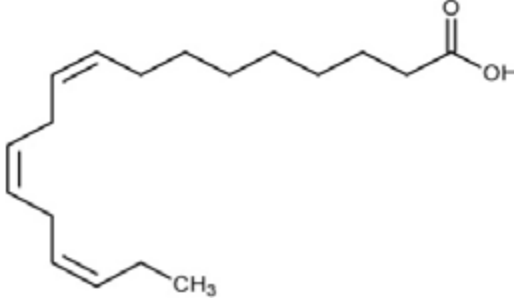
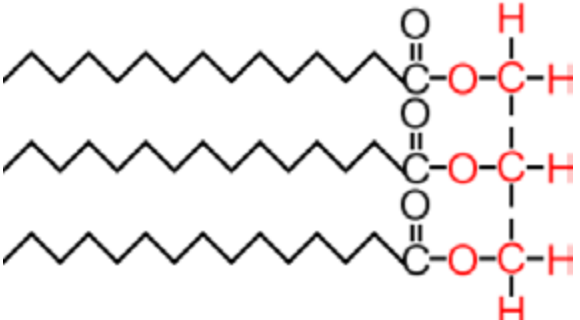
Concentration of quinine (mg/L)	Highest Intensity (a.u.)	Wavelength peak (nm)
5.0	>1,000	425.00 - 481.00
3.0	841.38	448.90
2.5	704.02	451.96
2.0	538.94	451.96
1.5	420.20	456.06
1.3	368.06	456.96
1.0	285.55	456.06
0.50	145.82	453.03
0.30	89.243	458.93
0.15	44.465	450.00
0.05	16.249	446.06
0.03	10.590	450.00

APPENDIX III

Cinchona alkaloids (structures and properties from Pharmacognosy, 2012)

<p>Quinine Formula: $C_{20}H_{24}N_2O_2$ Molar Mass: 324.42 g/mol Important functional groups: methoxy (H_3CO) allows for fluorescence, Nitrogen in upper right allows for protonation and therefore solubility properties. Solubility properties: highly soluble in acidic conditions Fluorescent properties: fluorescent</p>	
<p>Quinidine Formula: $C_{20}H_{24}N_2O_2$ Molar Mass: 324.42 g/mol Important functional groups: methoxy (H_3CO) allows for fluorescence, Nitrogen in upper right allows for protonation and therefore solubility properties. Solubility properties: highly soluble in acidic conditions Fluorescent properties: fluorescent</p>	
<p>Cinchonine Formula: $C_{19}H_{22}N_2O$ Molar Mass: 294.39g/mol Important functional groups: Nitrogen in upper right allows for protonation and therefore solubility. An additional H to each nitrogen produced dications of this molecule. (Dr. Morrow) Solubility properties: soluble in acidic conditions Fluorescent properties: not fluorescent (except dication)</p>	
<p>Cinchonidine Formula: $C_{19}H_{22}N_2O$ Molar Mass: 294.39g/mol Important functional groups: Nitrogen in upper right allows for protonation and therefore solubility. An additional H to each nitrogen produced dications of this molecule. Solubility properties: soluble in acidic conditions Fluorescent properties: not fluorescent (except dication)</p>	

Oils and Fatty Acids

<p>Oleic Acid (Monounsaturated)</p> <p>$C_{18}H_{34}O_2$</p> <p>Mainly in Safflower oil</p>	
<p>Linoleic Acid (Polyunsaturated)</p> <p>$C_{18}H_{32}O_2$</p> <p>Mainly in Sunflower oil</p>	
<p>Alpha-Linolenic Acid (Polyunsaturated)</p> <p>$C_{18}H_{30}O_2$</p> <p>Mainly in Flaxseed oil</p>	
<p>Sample triglyceride</p> <p>Each black chain represents a fatty acid, and red groups are glycerin. The actual fatty acids used (above) are not shown here, as the complexity would confuse the basic structure of a triglyceride.</p>	

APPENDIX IV

Raw Data

Table 5: Relevant Data Collected During Extraction

Oil and Trial	H ₂ SO ₄ (L) +/- 0.0005	Mass of dry bark (g) +/- 0.001	Bark mass after filtration (g) +/- 0.001
Safflower (0)	0.0720 ^{note a}	50.015	76.316
Safflower (1)	0.0711 ^{note a}	25.005	Note b
Safflower (2)	0.0750 ^{note a}	25.006	55.554
Safflower (3)	0.0403	25.002	56.473
Safflower (4)	0.0392	25.004	50.323
Safflower (5)	0.0390	25.009	52.887
Flaxseed (1)	0.0680 ^{note a}	25.008	Note b
Flaxseed (2)	0.0390	25.005	54.000
Flaxseed (3)	0.0418	25.004	55.832
Flaxseed (4)	0.0390	25.006	51.017
Flaxseed (5)	0.0390	25.008	50.196
Sunflower (1)	0.0682 ^{note a}	25.004	Note b
Sunflower (2)	0.0396	25.001	56.604
Sunflower (3)	0.0409	25.003	56.330
Sunflower (4)	0.0389	25.007	50.479
Sunflower (5)	0.0390	25.009	49.395

Note a: The volumes of H₂SO₄ that are around 70mL were due to the fact that for the first few trials, a higher amount of H₂SO₄ was used until it was realized that not much product was needed to test fluorescence. Therefore, the amount added was reduced to 40 mL for trials afterward. Some of the trials show volumes higher than 40 as this was not measured out precisely.

Note b: For the first trial, the weights of the bark after filtration were not recorded because of misjudgment.

Table 6: Change in Bark Weight before and after Filtration

Oil	Liquid left in bark after filtration (g) +/- 0.002 ^{note b}
Safflower (0)	26.301
Safflower (1)	Note a
Safflower (2)	30.548
Safflower (3)	31.471
Safflower (4)	25.319
Safflower (5)	27.878
Flaxseed (1)	Note a
Flaxseed (2)	28.995
Flaxseed (3)	30.828
Flaxseed (4)	26.011
Flaxseed (5)	25.188
Sunflower (1)	Note a
Sunflower (2)	31.603
Sunflower (3)	31.327
Sunflower (4)	25.472
Sunflower (5)	24.386

Note a: The mass of bark after filtration for trial 1 was not measured.

Note b: These values were calculated by subtracting mass of bark from mass after filtration. (Table 5)

Table 7: Fluorescence of Samples

Oil ^{note a}	Highest intensity (a.u.) +/- approx. 0.0000001	Wavelength peak ^{note b} (nm) +/- approx. 0.01
Safflower (0)	322.18	440.00
Safflower (0re)	262.32	443.93
Safflower (1)	248.61	455.00
Safflower (1re)	245.10	451.06
Safflower (2)	240.05	446.96
Safflower (3)	872.13	448.93
Safflower (4)	183.62	448.93
Safflower (5)	Over 1,000 ^{note d}	Note c
Flaxseed (1)	345.77	448.93
Flaxseed (1re)	355.01	451.06
Flaxseed (2)	776.15	448.03
Flaxseed (3)	Over 1,000 ^{note d}	Note c
Flaxseed (4)	Over 1,000 ^{note d}	Note c
Flaxseed (5)	787.08	448.93
Sunflower (1)	416.13	448.03
Sunflower (1re)	433.1735229	445.00
Sunflower (2)	792.05	446.96
Sunflower (3)	702.77	448.03
Sunflower (4)	518.72	445.00
Sunflower (5)	342.79	446.06

Note a: The (#) refers to trial, “re” refers to retesting the trial on a different day.

Note b: These values were not used for any calculations, but rather as a quality reference.

Note c: As the samples were saturated, no wavelength was recorded.

Note d: Some samples had unregularly high concentrations and because the fluorescence was saturated (over 1,000), the highest intensity peak could not be seen.

Table 8: Calculated Data for each Sample

Oil note a	Concentration of quinine in sample (mg/L) +/- 2.58% note b	Quinine in sample (mg) +/- 3.48% note b	% composition quinine in bark +/- 3.484% note b	% yield +/- 50% note e
Safflower (0)	1.15	0.0826	0.000165%	0.0086%
Safflower (0re)	0.931	0.0671	0.000134%	“ “ note f
Safflower (1)	0.882	0.0627	0.000251%	0.013%
Safflower (1re)	0.869	0.0618	0.000247%	“ “ note f
Safflower (2)	0.851	0.0638	0.000255%	0.013%
Safflower (3)	3.13	0.126	0.000504%	0.25%
Safflower (4)	0.648	0.0254	0.000102%	0.0051%
Safflower (5)	Note c	Note c	Note c	Note c
Flaxseed (1)	1.23	0.0838	0.000335%	0.017%
Flaxseed (1re)	1.265	0.0860	0.000344%	“ “ note f
Flaxseed (2)	2.782	0.1085	0.00043%	0.022%
Flaxseed (3)	Note c	Note c	Note c	0.033% note d
Flaxseed (4)	Note c	Note c	Note c	Note c
Flaxseed (5)	2.8214	0.11003	0.00044%	0.022%
Sunflower (1)	1.4853	0.1013	0.00041%	0.020%
Sunflower (1re)	1.5467	0.1055	0.00042%	“ “ note f
Sunflower (2)	2.8393	0.1124	0.00045%	0.022%
Sunflower (3)	2.5177	0.103	0.00041%	0.021%
Sunflower (4)	1.8548	0.0722	0.00029%	0.014%
Sunflower (5)	1.2211	0.0476	0.00019%	0.0095%

Note a: The (#) refers to trial, “re” refers to retesting the trial on a different day. (also, refer to note a in table 7)

Note b: The percentages do not refer to a unit or absolute uncertainty, but the percentage uncertainty.

Note c: There are no values for the saturated solutions (over 1000) when fluorescence was tested, as the concentration was not calculated.

Note d: This was only calculated for flaxseed trial 3 because this trial, although saturated, was diluted to find fluorescence and then concentration could be found. However, as this trial was not used in any other calculations other than the percent yield in the figures 4,5,6, the other data was not included. This trial was done while other were not diluted, as when testing fluorescence for the other trials, there were no materials to make accurate dilutions.

Note e: This percent uncertainty is high because the percent uncertainty for the 2% industrial yield (used in calculating percent yield of extraction) is 50%.

Note f: As the first trials were tested twice on two different days, the compositions were averaged to calculated percent yield, leading to both rows having the same value in this column.

Magnetic Iron Oxide-Gold Nanoparticles for the Photo-Thermal Dissolution of Protein Aggregates: Implications in Alzheimer Treatment

Sanjiv Harikumar¹, Las Cruces High School

Aggregation of Beta Amyloid ($A\beta$) and Tau peptides are known to cause Alzheimer's Disease. This research proposed a method that can potentially disaggregate the Beta Amyloid peptides and slow the process of neurodegeneration. Since $A\beta$ is dangerous, this research used calcium depleted A-Lactalbumin proteins that possess similar aggregation properties to $A\beta$. A bio-compatible solution consisting of iron-oxide nanoparticles ($Fe_2O_{3(s)}$) coated with gold nanoparticles (AuNPs) was synthesized and localized on A-Lactalbumin proteins. This solution was then subjected to a laser that was calibrated to emit light energy in the AuNP's absorption region. The photo thermal properties of AuNPs dispensed quanta of heat energy that broke the hydrogen bonds between the protein aggregates thus resulting in their disaggregation. TEM images were taken at different stages of the experiment to characterize the process of disaggregation. Future research can exploit the magnetic properties of $Fe_2O_{3(s)}$ to transport the bio-compatible solution through the blood brain barrier.

INTRODUCTION

Alzheimer's Disease

Alzheimer's Disease is a neurodegenerative disorder in which certain proteins known as Beta Amyloid ($A\beta$) form aggregates (plaques) within neuron synapses. Such aggregates can constrict neural axons and impede the flow of neurotransmitters over time, incurring memory loss. The $A\beta$ Aggregates can cause physical changes in the brain in later phases of Alzheimer's Disease as shown in Figure 1.

It is unclear what causes Alzheimer's Disease, and there are some methods to treat Alzheimer's, such as chemotherapy. Chemotherapy can be inefficient (Jordan et al., 1999) because the heat produced can destroy healthy tissue surrounding the unhealthy tissue, thereby hurting the patient during treatment. This project proposes an approach that uses photothermal properties of hybrid gold and iron-oxide nanoparticles to disaggregate the $A\beta$ aggregates without causing damage to healthy tissue.

Therapeutic Applications of Iron-oxide and Gold Nanoparticles

Iron-oxide nanoparticles² ($Fe_2O_{3(s)}$) suspended in an aqueous-based medium are biocompatible fluids attracted towards magnetic fields; the 'iron-liquid' moves based on the magnet's direction without its components separating, via surface tension of the particles.³ This

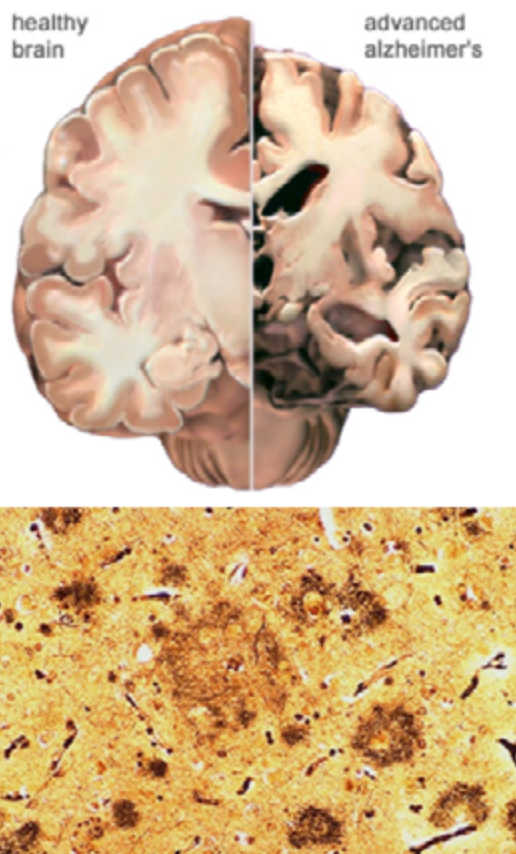


Figure 1: (Top) Brain before and after Alzheimer's Disease. (Bottom) The dark spots represent Beta-Amyloid plaques in the brain [1] [2].

property is useful for research in biomedical fields such as magnetic drug delivery i.e. the ability to transport drugs using iron-oxide nanoparticles to various parts of the human body where a lesion such as a cancer tumor occurs (Takeda et al., 2006). Figure 2 represents some TEM images of commercial iron-oxide nanoparticle clusters (scale: 20 nm.), which provide a typical depiction of them, displaying how small in volume they are, as well as showing the nanoparticles dispersed in solution.

Colloidal gold nanoparticles (i.e., AuNPs) are small sodium citrate-stabilized atoms of gold. AuNPs are mainly regarded for their photothermal 'light-scattering' properties (also called Rayleigh Scattering), which involves visible light irradiating the electrons of AuNPs to generate heat. The photothermal properties of AuNPs are useful as therapeutic agents in, for example, destroying cancer tumors [4]. Figure 3 represents general, commercially available AuNPs in various sizes and concentrations. Depending on the molarity (concentration) of the solutions, the color may vary slightly (i.e. 'red' solutions have smaller concentrates of AuNPs, and the 'purple' solutions have greater concentrates of AuNPs).

A Hybrid Gold and Iron-oxide Nanoparticle Fluid as a Therapeutic against Alzheimer's

From *Therapeutic Applications of Iron-oxide and Gold Nanoparticles*, it is discerned the particles, overall, have the potential to be biocompatible (Lyon et al., 2004) since they are soluble (due to iron-oxide's aqueous base), demonstrating promise as a treatment for Alzheimer's. This project is an attempt to exploit the light-scattering properties of AuNPs to dissipate the A β aggregates in the brain. This requires several steps to be accomplished. The first task involves crossing the Blood Brain Barrier (BBB) to reach the A β aggregates as depicted in Figure 1. One possible method to accomplish this is using the magnetic and biocompatible nature of iron-oxide nanoparticles to transport the AuNPs through the endothelial junctions of the BBB. The question of transporting the AuNPs, however, is important only if the AuNPs can successfully disaggregate the A β Aggregates. This project addresses the following two research questions:

1. Is it possible to create a biocompatible synthesis that consists of an iron-oxide core bonded with AuNPs?
2. Using the light scattering properties of AuNPs, is it possible to generate therapeutic levels of heat energy to successfully disaggregate the protein aggregates?

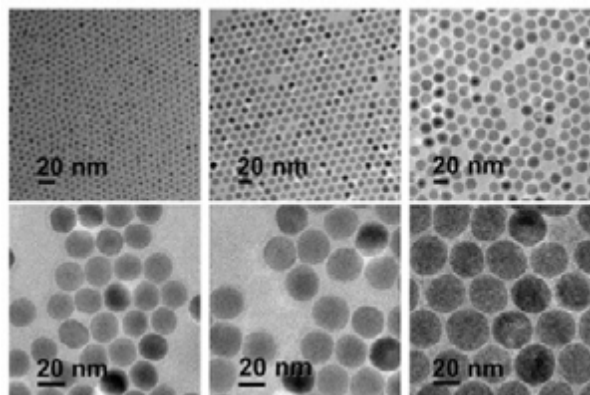


Figure 2: TEM images of 20 nm. iron-oxide nanoparticles [3]. From left to right, each image is zoomed in to characterize the spherical shape of the nanoparticles.

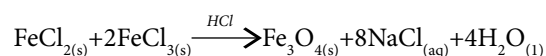


Figure 3: Various solutions of AuNPs [5].

MATERIALS & METHODS

Synthesis of Iron (II, III) Oxide Nanoparticles

The procedure used to synthesize the hybrid iron-oxide AuNPs fluid is based on the method described by Lyon et al. (2004). Each reagent used for the experiment was taken in proportions described in the following paragraphs to prevent any acidity among the solution, as well as maximizing the output of iron (II, III) oxide nanoparticles. A solution of 0.3749 g. concentrated hydrochloric acid (HCl) in 0.0250 L water (H₂O) was created to dissolve 5.4 g of ferric chloride (FeCl₃·6H₂O) with 2.0 g ferrous chloride (FeCl₂·4H₂O). Next, 0.250 L of the solution was added dropwise to a solution of 1.5 M sodium hydroxide (NaOH), with vigorous stirring, until a black precipitate was formed and the acid was neutralized. The following equation describes the process:



Iron (III) Oxide Nanoparticles Dispersed in Aqueous Medium

The precipitate, $\text{Fe}_3\text{O}_{4(s)}$, was then isolated via magnetic decantation and washed twice with 0.1 L of water and twice with 100 mL of 0.1 M of tetramethylammonium hydroxide (TMAOH), a surfactant used to bond the $\text{Fe}_3\text{O}_{4(s)}$ with an aqueous medium (water). Figure 4 provides a schematic of the synthesis of $\text{Fe}_3\text{O}_{4(s)}$ nanoparticles as well as an overview of the surfactant's properties to bind water molecules to the iron particles.

The $\text{Fe}_3\text{O}_{4(s)}$ precipitate was centrifuged at 6000-9000 rpm for 10 min to remove any inert chemicals or impurities that might have been present in the synthesis. Finally, the precipitate was dissolved in 100 mL of 0.1 M TMAOH and over time the $\text{Fe}_3\text{O}_{4(s)}$ nanoparticles oxidized into $\text{Fe}_2\text{O}_{3(s)}$ nanoparticles⁴ (Figure 4). Note, the oxidation has no effect on the properties of the iron-oxide solution, because $\text{Fe}_3\text{O}_{4(s)}$ and $\text{Fe}_2\text{O}_{3(s)}$ have similar properties described in *Therapeutic Applications of Iron-oxide and Gold Nanoparticles*.

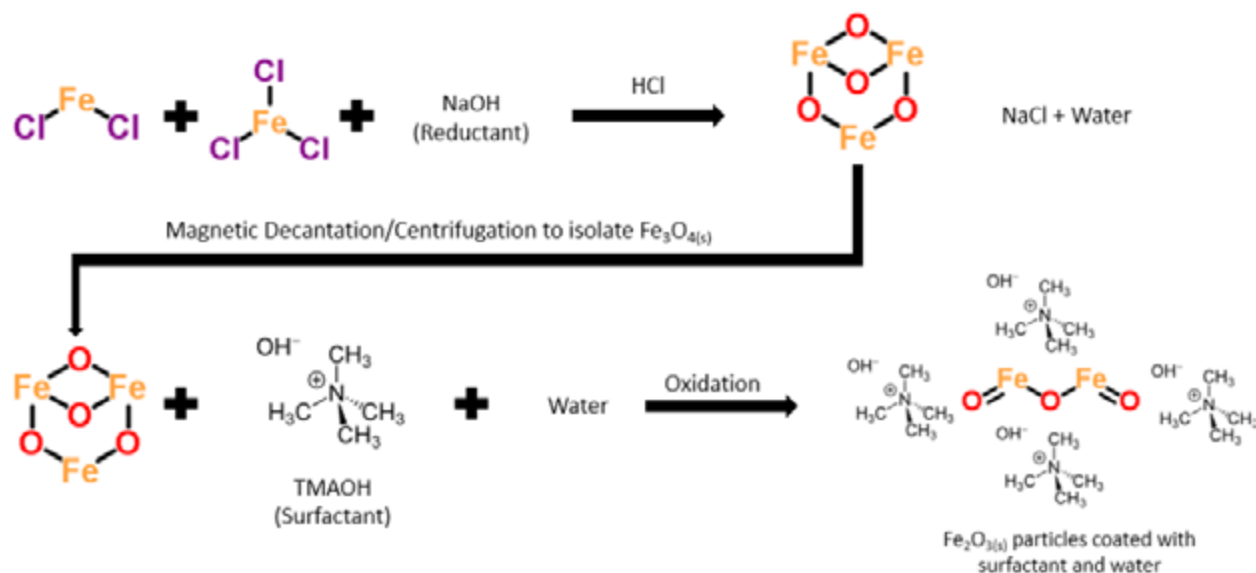


Figure 4: Synthesis of $\text{Fe}_3\text{O}_{4(s)}$ scheme. Notice how $\text{Fe}_3\text{O}_{4(s)}$ oxidizes to $\text{Fe}_2\text{O}_{3(s)}$ over time.

Stabilizing AuNPs on Iron (II, III) Oxide Nanoparticles

Figure 5 depicts the final solution of $\text{Fe}_2\text{O}_{3(s)}$ to be coated with AuNPs. Accordingly, 0.2 M hydroxylamine ($\text{H}_3\text{NO}\cdot\text{HCl}$ or $\text{NH}_2\text{OH}\cdot\text{HCl}$) and 1% chloroauric acid (HAuCl_4) were added incrementally to the $\text{Fe}_2\text{O}_{3(s)}$ solution. It was important to add the reagents in increments to prevent aggregation of the AuNPs.

A molecule of chloroauric acid contains an Au atom, which was extracted to create Au ions, and eventually AuNPs. Hydroxylamine induced metallic bonding between AuNPs and iron-oxide nanoparticles. Next, 7.5 mL of $\text{Fe}_2\text{O}_{3(s)}$ nanoparticle solution was diluted to 1.1 mM using 140 mL water. The solution was stirred with 7.5 mL of 0.1M sodium citrate for 10 min. Sodium citrate is a reducing agent designed to stabilize AuNPs

from an ionic state to a neutral state, as well as prevent AuNPs from aggregating. This is known as the Turkevich Method [6] and is given by the equation below:

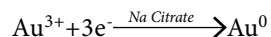


Table 1 gives different measurements for each iteration of hydroxylamine and chloroauric acid added to the $\text{Fe}_2\text{O}_{3(s)}$ solution, as well as the % of moles (mol) of Au nanoparticles and % mol. of iron-oxide nanoparticles. Note: it is not necessary to achieve the exact % mol. count given in the table if there is an observation of an increase in AuNPs (by the browner color of the solution). Finally, the 'iron-oxide AuNPs' fluid responded to various magnets placed near the fluid confirming the iron-oxide nanoparticles were attracted to the magnet and that they 'pulled' the AuNPs.

¹Iterations of Hydroxylamine and HAuCl₄ may vary. This is a general overview.

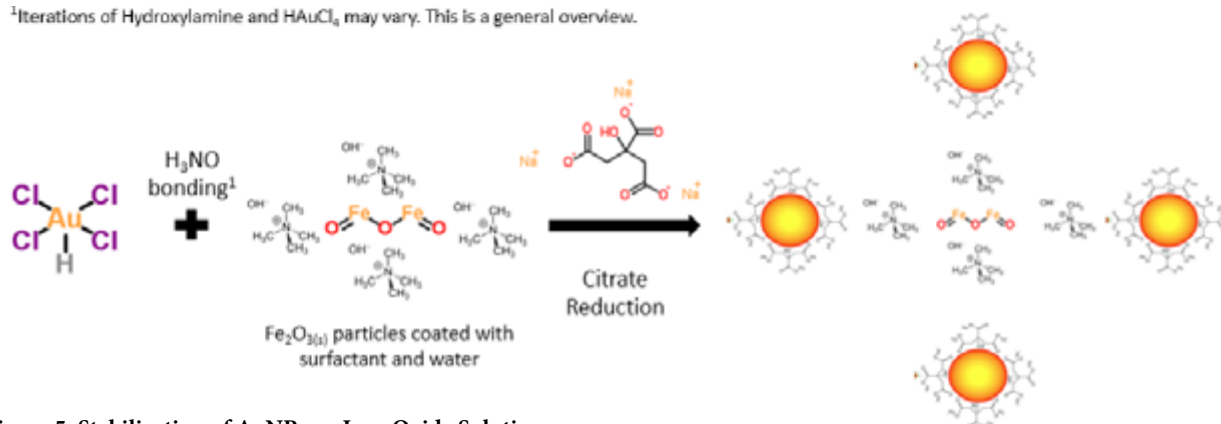


Figure 5: Stabilization of AuNPs on Iron Oxide Solution.

Iteration	0.2 M NH ₂ OH·HCl (mL)	1% HAuCl ₄ (mL)	Total mol. % Au	Total mol. % Fe oxide
1	0.750	0.625	69	31
2	0.281	0.500	80	20
3	0.188	0.500	85	15
4	0.188	0.500	88	12
5	0.281	0.500	90	10

Table 1: Increments of hydroxylamine and HAuCl₄ added to the solution, % mol. of Au nanoparticles, and % mol. of Iron Oxide nanoparticles (Lyon et al., 2004).

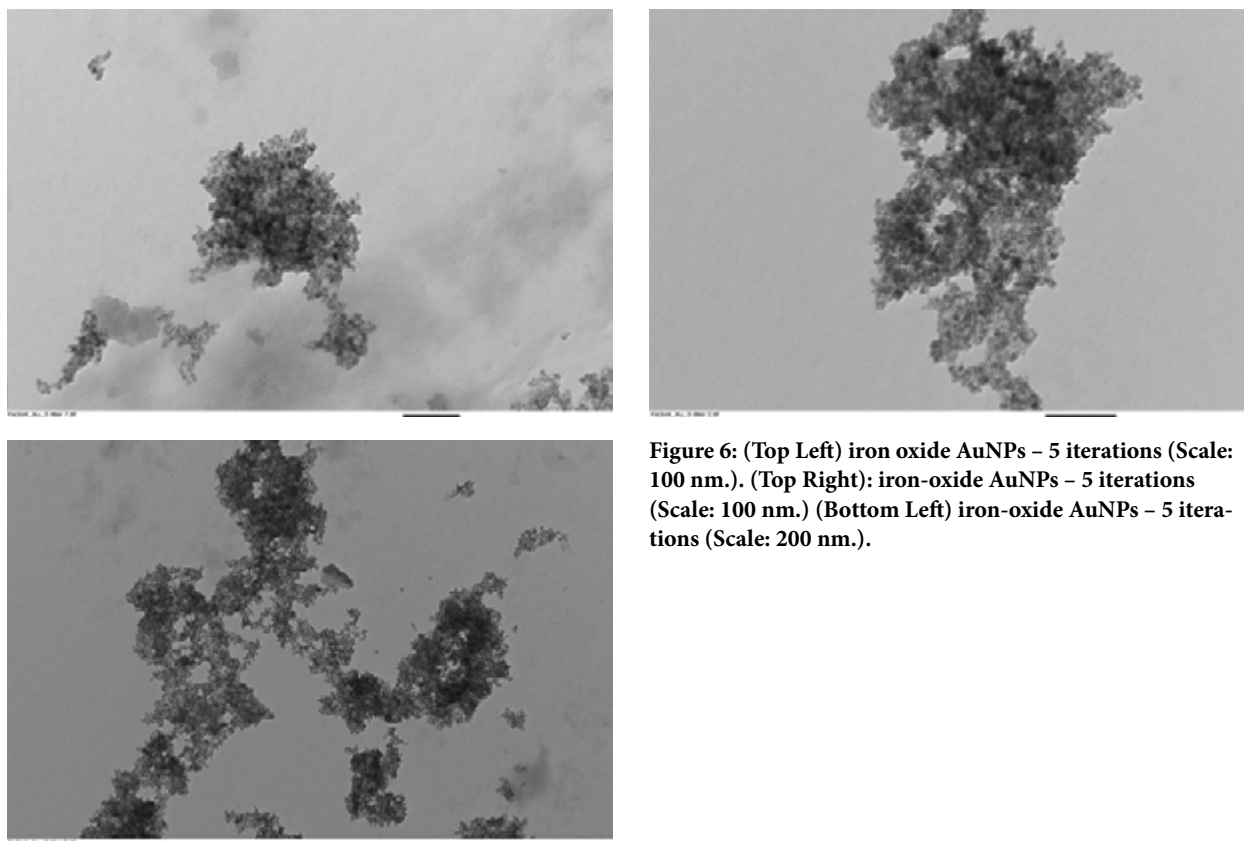
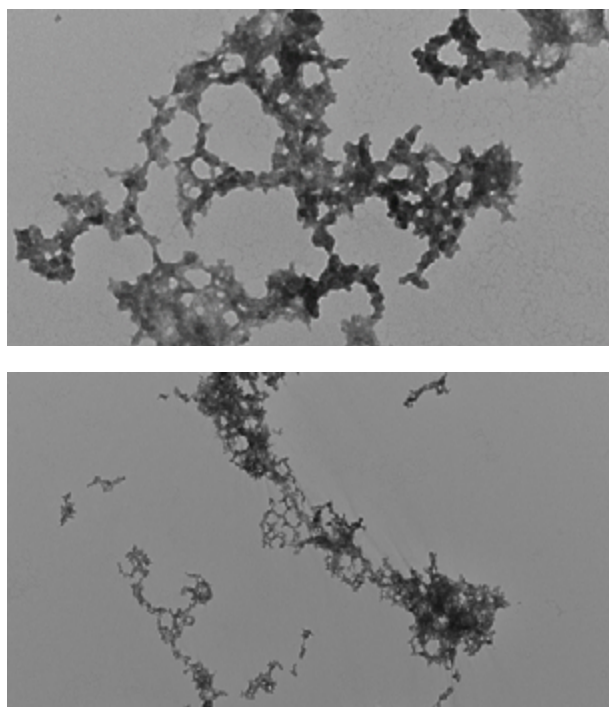


Figure 6: (Top Left) iron oxide AuNPs – 5 iterations (Scale: 100 nm.). (Top Right): iron-oxide AuNPs – 5 iterations (Scale: 100 nm.) (Bottom Left) iron-oxide AuNPs – 5 iterations (Scale: 200 nm.).

For potential penetration through the BBB, the sizes of the individual nanoparticles should typically be less than ~50 nm (Shubayev, 2009). From the synthesis created in this procedure and the TEM images, the sizes of each iron-oxide AuNP nanoparticles are less than 50 nm, and are featured in clusters. This, however, did not affect their magnetic properties nor interaction with AuNPs. Notice the grayish-black circles and the black circles in the nanoparticle clusters. Unfortunately, given the sizes of the nanoparticles, it was hard to zoom into the clusters without blur.

The iron-oxide AuNPs created were clustered into large groups as seen in Figure 6. The fluid's physical properties resembled a black-brownish color with some shades of red, probably due to oxidation of the iron-oxide AuNPs



over time (Lyon et al., 2004).

Creation of A-Lactalbumin Aggregates

To assess the viability of the iron-oxide AuNPs solution, it was necessary to gain access to an A β solution; however, access to A β proteins was strictly prohibited due to their characteristics. A-lactalbumin, a primary protein found in milk, was manipulated to aggregate and resemble conditions similar to Beta-Amyloid (Liu, 2011). Figure 7 presents TEM images of A-lactalbumin aggregates before any change in their structural integrity was made. To create the aggregates, the A-lactalbumin received was calcium depleted and stored at 0 degrees Celsius, and eventually stored in a pH of 7.4, the same pH the human body retains.

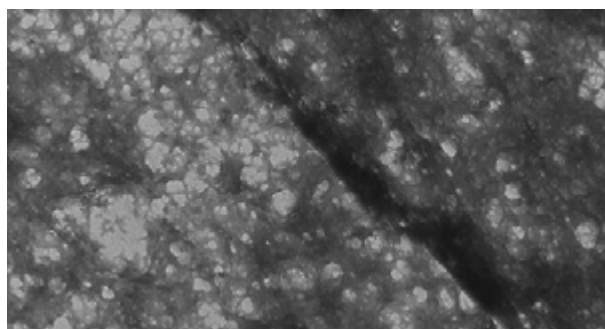


Figure 7: (Top Left and Bottom Left): A-lactalbumin aggregates (Mixture 6) w/o iron-oxide AuNPs (Scale: 100 nm. and 600 nm., respectively.). (Top Right) A-lactalbumin aggregates (Mixture 4) w/ iron-oxide AuNPs (Scale: 200 nm.). The folding seen is caused by the protein's secondary structure's Alpha Helix, composed of hydrogen bonds.

Mixture #1	2 mL of Phosphate Buffer Saline (PBS) + 4 mL DI water.
Mixture #2	2 mL nanoparticles of (5 iterations) + 3 ml phosphate buffer saline.
Mixture #3	2 mL nanoparticles of (3 iterations) + 3 mL DI water + 3 ml phosphate buffer saline.
Mixture #4	2 mL nanoparticles of (5 iterations) + 3 mL phosphate buffer saline + 0.2 g. A-Lactalbumin.
Mixture #5	2 mL nanoparticles of (3 iterations) + 3 ml DI water + 3 mL phosphate buffer saline + 0.2 g. A-Lactalbumin.
Mixture #6	A-Lactalbumin in PBS, no iron-oxide AuNPs (was not lased because proteins do not absorb light at 532 nm, rather they absorb light between 200-280 nm.)

Table 2: Mixtures #1-6. All mixtures except Mixture #6 were lased to measure temperature changes in the iron oxide AuNPs. As a note, 'nanoparticles' refer to iron-oxide AuNPs and the number of iterations for the iron-oxide AuNPs represent the increments of hydroxylamine and HAuCl₄ added to it.

Creation of Mixtures and Laser Tests

This section provides a description of the different mixtures synthesized for this experiment. Table 2 contains the description of six different mixtures that were created to be lased and to determine the effect of iron-oxide AuNPs with A-lactalbumin Aggregates.

Mixture #1 was a control mixture of phosphate buffer saline (pH 7.4) and water to determine if the iron-oxide AuNPs' aqueous base mediated any heat. Mixtures #2 & #3 determined the temperature properties of concentrated and dilute iron-oxide AuNPs, respectively. Mixtures #4 & #5 are the same as Mixtures #2 & #3, except the mixtures contain small samples of the A-lactalbumin

aggregates. Finally, Mixture #6 is the A-lactalbumin without the iron-oxide AuNPs, to determine the structure of the protein.

AuNPs contain various light scattering properties. A 532 nm, 460.8 mW Millennia VIII Laser (Figure 8) was used to lase each mixture (except Mixture #6) to determine temperature changes in the fluid and assess the structure of the A-lactalbumin aggregates before and after the temperature changes in the fluid. Typically, AuNPs absorb light within 500-800 nm. [7], which is why a 532 nm laser was used. To confirm this, Figure 9 represents the absorbance peaks of the AuNPs in the iron-oxide AuNPs.

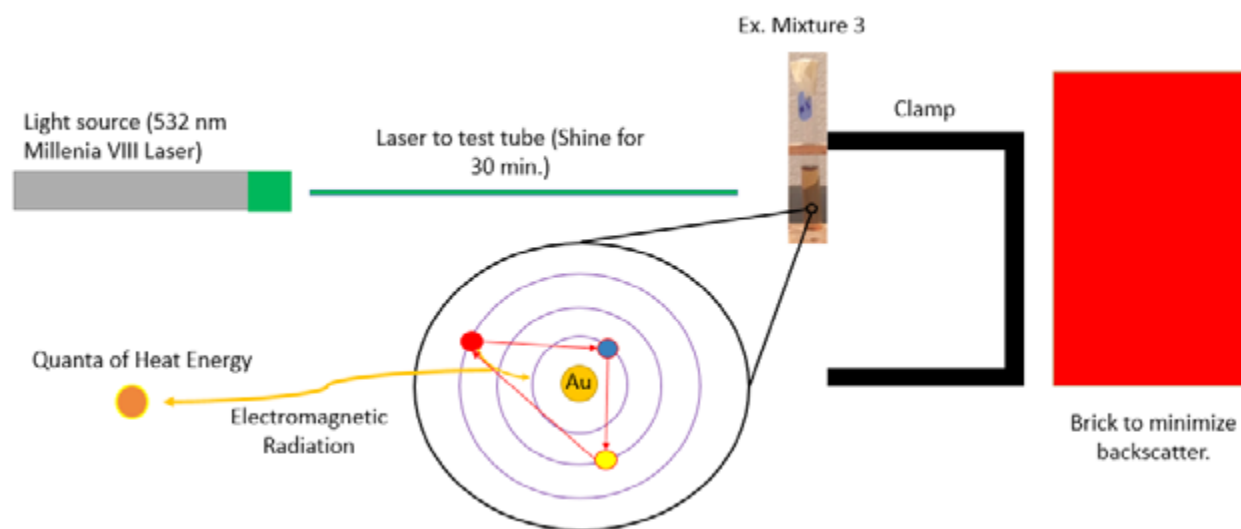


Figure 8: Laser Tests on Mixtures #1-5 Scheme.

RESULTS

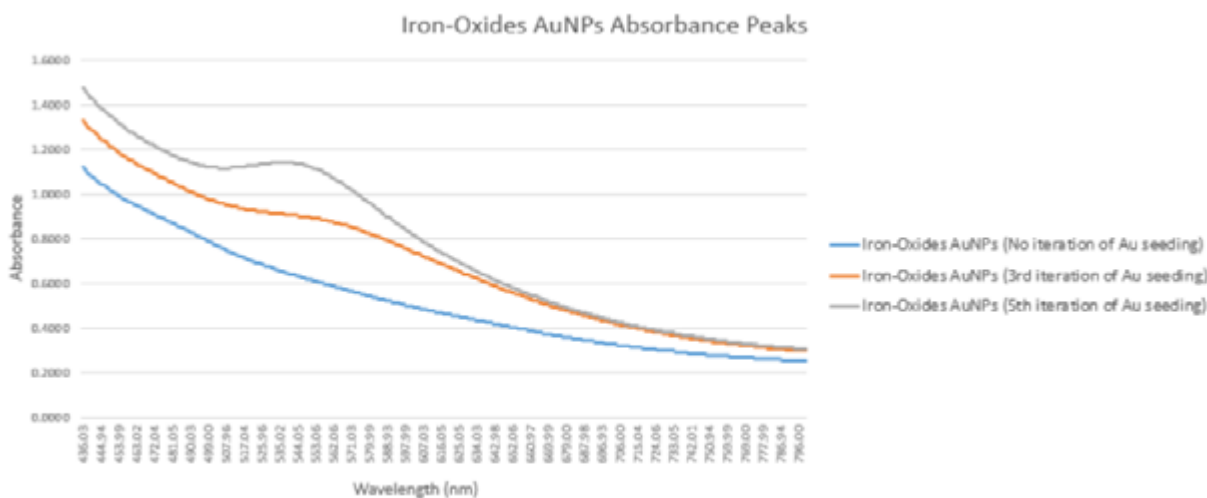
Absorbance of Iron-Oxide AuNPs

All the lased mixtures showed temperature changes⁵. From the recorded data (Figures 6 and 9), it was clear the AuNPs bonded with the iron-oxide nanoparticles; the fluid responded to various magnets, and absorbed/mediated heat in 532 nm, since AuNPs absorb light within that region. The iron-oxide AuNPs fluid with the highest Au concentration (5th iteration of Au seeding) had the highest peak absorbance rate, followed by the iron-oxide AuNPs with 3 iterations of Au seeding and the iron-oxide nanoparticles without any addition of AuNPs. The iron-oxide nanoparticles without the Au seeding (blue line) did not mediate heat in the 532 nm. range.

Figure 10 shows the change in temperature of the mixtures with time. The temperatures of the iron-oxide AuNPs mediated heat as the time they were lased was increased. Temperature changes were recorded every minute, for a total of 30 minutes. After 30 min., the particles stopped increasing in temperature. The temperature of the iron-oxide AuNPs solutions increased to a maximum temperature of 30-40 degrees Celsius. Mixture #1 cooled to room temperature as time increased because PBS and water do not mediate heat. Mixture #2 had the highest temperature between 35-40 degrees Celsius, and Mixture #3 had the third highest temperature, between 30-35 degrees Celsius. Mixtures #4 and #5's initial temperature (between 5-15 degrees Celsius) was below the other Mixtures (between

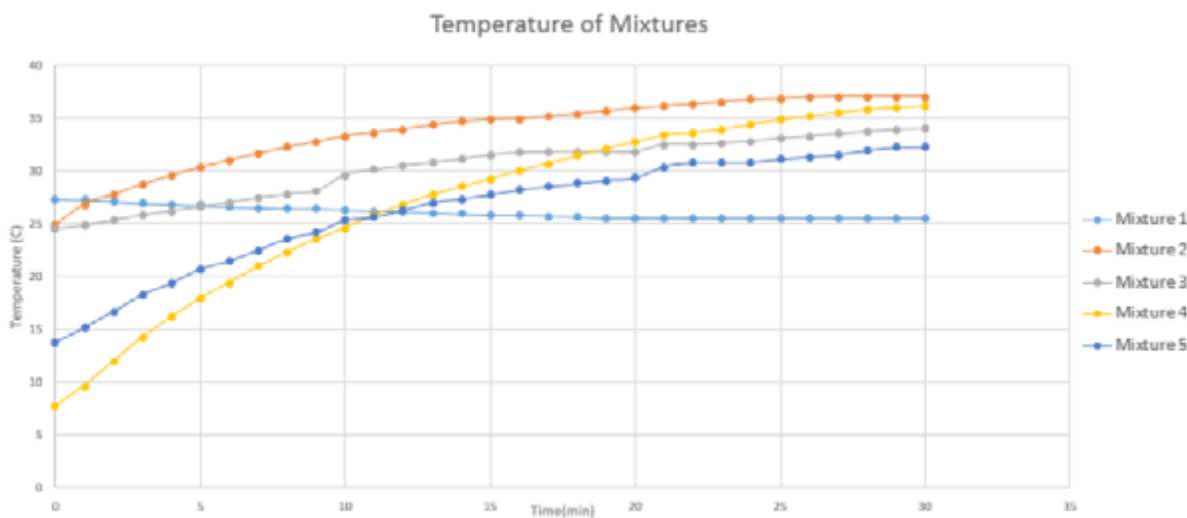
25-30 degrees Celsius) because #4 and #5 contained the iron-oxide AuNPs and the protein samples, which were kept frozen to preserve the protein's shape/aggregates

for testing. Both Mixtures #4 and #5 had the highest increase in temperature, but attained the same maximum temperature as #2 and #3.



Iron Oxide-AuNPs' absorbance peaked at 532 nm.

Figure 9: Absorbance Spectrum of Iron-Oxide AuNPs.



Temperature changes of Mixtures #1-#5.

Figure 10: Temperature changes in iron-oxide AuNPs during the laser tests. Based on the data, Mixture #2 has the highest temperature reading, followed by #4, #3, #5, and #1. The Appendix contains the raw data of the temperature readings.

Protein Structure after Laser Tests

After the laser tests, A-lactalbumin fragmented into smaller particles, and smaller aggregates. From the TEM images in Figure 11, it is possible the heat dispersed from the AuNPs triggered the proteins to unfold and destroy the secondary and tertiary structure where the protein's hydrogen bonds and hydrophobic bonds reside (see the yellow arrows in Figure 11) to create the

smaller fragments of the protein (see the red arrows). The destruction of these bonds leads to the unfolding of the protein, thereby denaturing the protein aggregates of A-lactalbumin [8]. Since these structures were broken, the protein did not have a backbone structure (its Alpha Helix) to preserve its shape, resulting in fragmentation and non-uniformity [8]. While Aβ and A-lactalbumin are different proteins, both have the propensity to

aggregate under the same conditions, granting the potential for AuNPs to disaggregate A β plaques. Results of A-lactalbumin were gathered several days after the laser tests, with the mixtures kept in an environment below 0 degrees Celsius to preserve the structure of the protein.

As an important note, a previous work used AuNPs alone against A β Aggregates (Kogan et al, 2009), but it has not answered the question of transporting AuNPs⁶ to the target site or assessing the biocompatibility of AuNPs. This research answers those questions by

using iron-oxide nanoparticles as a potential magnetic transport for AuNPs to a target site, and ensuring the hybrid fluid is biocompatible by treating the iron-oxide nanoparticles on a water-based medium (see *Therapeutic Applications of Iron-oxide and Gold Nanoparticles*). Finally, for consistency, the hybrid fluid is tested against protein aggregates to measure if (a) the AuNPs can mediate heat energy despite being attached to iron-oxide AuNPs and (b) the hybrid fluid can disaggregate proteins.

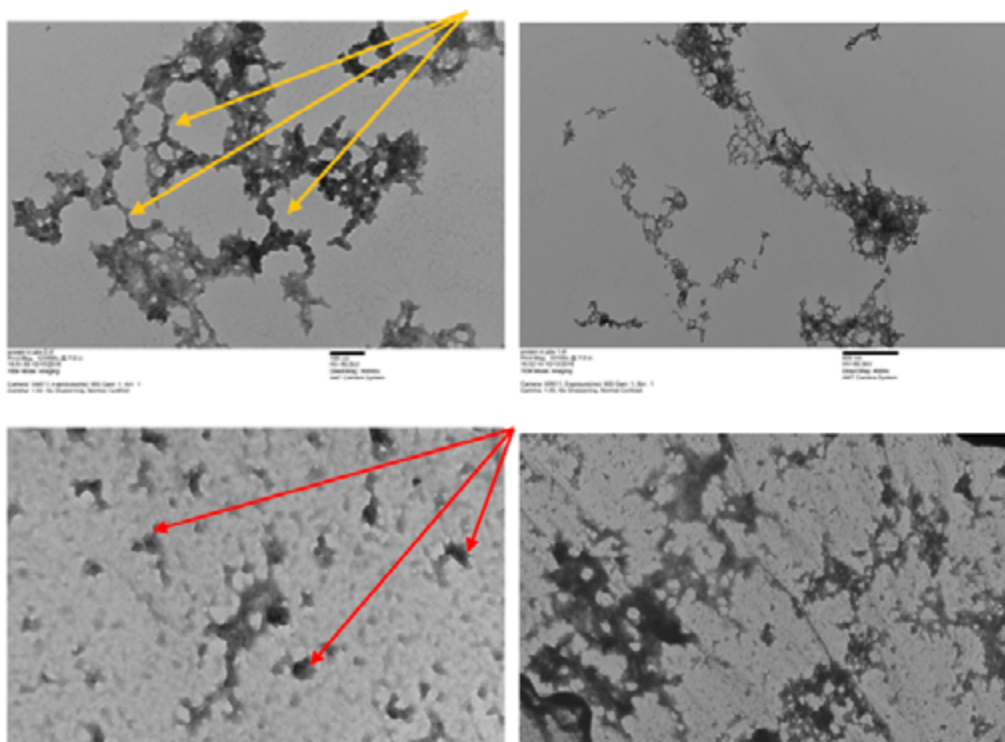


Figure 11: (Top Left and Top Right) A-Lactalbumin before laser test (100 nm and 200 nm respectively). Both images are from Figure 7. The yellow arrows point to protein bonds. **(Bottom Left and Bottom Right) A-Lactalbumin after laser test (100 nm and 500 nm respectively).** The red arrows point to protein fragments.

CONCLUSIONS & DISCUSSION

This research used an in-vitro approach to treating Alzheimer's Disease using hybrid iron-oxide AuNPs fluids from Lyon et al. (2004) as photothermal mediators to heat and denature protein aggregates. The synthesis of iron-oxide AuNPs was successful and stable, confirming the metallic bonding process mentioned in *Stabilizing AuNPs on Iron (II, III) Oxide Nanoparticles*. Iron-oxide AuNPs mediated heat without any problems. The AuNPs partially coated the iron-oxide nanoparticles but metallic bonding induced most of the bonding between gold and

iron. Based on the TEM images, the protein's peptide structure was damaged by the irradiation from the iron-oxide AuNPs causing breakage of hydrogen bonds in the protein [9].

One of the main concerns of nanotherapeutic treatment involves crossing the Blood-Brain Barrier or BBB (Figure 12) to treat A β plaques. According to Gu et al. (2015), the Blood-Brain Barrier consists of a monolayer of capillary endothelial cells with tight junctions between each other to limit intake of foreign substances into the Central Nervous System. Other cells including

Peripheral and Astrocyte cells surrounding the endothelial cells maintain the development of the Blood-Brain Barrier. Methods to pass the BBB include sending the nanoparticles in the form of lipids (the BBB is lipophilic), invasive injection into the brain, and recently, the development of ultrasound robots to open a minute gap in the BBB for transportation of drugs [10].

There are still a few paths to explore in this research. Typical in-vivo Laser-Therapy research uses wavelengths in the order of 800 nm., but recent research has shown Laser-Therapy research within 450-800 nm. wavelength range (Hart, 2016), making iron-oxide AuNPs an encouraging tool for further in-vivo research. There are multiple sources of literature which suggest laser therapy can be used for treatments of different injuries in the brain, but should be used in moderation to prevent neuronal apoptosis (Cakir et al., 2016). Well known literature from Parrington (1972) and Sandor (1973) used visible-light and laser therapy for in-vivo research.

Sending lasers into the brain requires a pathway for the laser to travel. Small ultrasound robots [10] can partially open the BBB to allow for substances such as lasers to penetrate through. Once the laser passes through the BBB, it has the potential to target the iron-oxide AuNPs and excite them with light.

However, given iron-oxide AuNPs are biocompatible within the body, the fluid itself cannot target A β aggregates within the brain, since many neurons are surrounded by other proteins, including gene-expression proteins [12]. Biomarkers can be attached to AuNPs to detect Amyloid Beta aggregates (Kogan, 2009), to filter the aggregates from the healthy proteins. Finally, new research has shown the potential for protein aggregates to be toxic after they unfold (Kabiraj, 2016). Therefore, a possible removal of aggregates immediately after heat induction needs to be assessed. This project does not address the mechanics of this transportation of the biocompatible iron-oxide AuNPs through the BBB and the safe disposal of disaggregated proteins and leaves it for future research.

ACKNOWLEDGMENTS

I would like to thank the UTEP Chemistry department for letting me use their laboratory, so I may synthesize

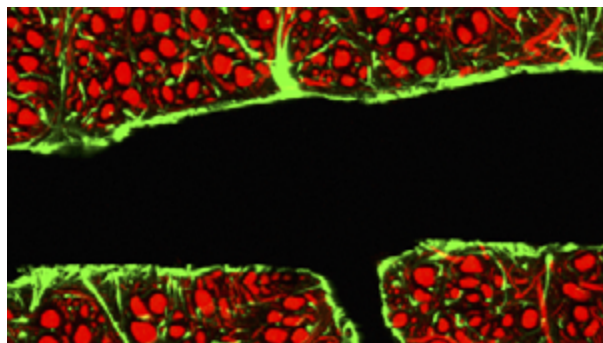


Figure 12: Endothelial cells wedged together to form the BBB preventing foreign substances from entering the brain [11].

the iron-oxide AuNPs, WSMR for allowing me to use their Millennia VIII Laser for the protein experiment, NMSU for letting me use the TEM machine, and UNM and Texas State University for patiently answering my questions on biocompatibility of iron-oxide nanoparticles and use of Lasers, respectively. Lastly, I would like to thank the anonymous reviewers at the 2016-Society for Neuroscience Conference held in San Diego for their useful suggestions, and NMJAS Paper Competition judges for their feedback on my presentation.

REFERENCES

- Cakir, M., Colak, A., Calikoglu, C., Taspinar, N., Sagsoz, M. E., Kadioglu, H. H., ... & Seven, S. (2016). Once the Light Touch to the Brain: Cytotoxic Effects of Low-Dose Gamma-Ray, Laser Light, and Visible Light on Rat Neuronal Cell Culture. *The Eurasian journal of medicine*, 48(2), 76.
- Gu, X., Chen, H., & Gao, X. (2015). Nanotherapeutic strategies for the treatment of Alzheimer's disease. *Future Science*, 6(2), 177-195.
- Hart, N. S., & Fitzgerald, M. (2016). A New Perspective on Delivery of Red-Near-Infrared Light Therapy for Disorders of the Brain. *Discovery Medicine*, 22(120), 147-156.
- Jordan, A., Scholz, R., Wust, P., FShling, H., & Felix, R. (1999). Magnetic fluid hyperthermia (MFH): Cancer treatment with AC magnetic field induced excitation of biocompatible superparamagnetic nanoparticles. *Journal of Magnetism and Magnetic Materials*, 201, 413-419.
- Kabiraj, P., Marin, J. E., Varela-Ramirez, A., & Narayan, M. (2016). An 11-mer Amyloid Beta Peptide Fragment Provokes Chemical Mutations and Parkinsonian Biomarker Aggregation in Dopaminergic Cells: A Novel Road Map for "Transfected" Parkinson's. *ACS Chemical Neuroscience*, 7(11), 1519-1530.

Kogan, M., Bastus, N., Amigo, R., Grillo-Bosch, D., Araya, E., Turiel, A., & Puntès, V. (2006). Nanoparticle-Mediated Local and Remote Manipulation of Protein Aggregation. *Nano Letters*, 6(1), 110-115.

Liu, D., Zhou, P., Liu, X., & Labuza, T. P. (2011). Moisture-Induced Aggregation of Alpha-Lactalbumin: Effects of Temperature, Cations, and pH. *Journal of food science*, 76(6), C817-C823.

Lyon, J. L., Fleming, D. A., Stone, M. B., Schiffer, P., & Williams, M. E. (2004). Synthesis of Fe oxide core/Au shell nanoparticles by iterative hydroxylamine seeding. *Nano Letters*, 4(4), 719-723.

Shubayev, V. I., Pisanic, T. R., & Jin, S. (2009). Magnetic nanoparticles for theragnostics. *Advanced drug delivery reviews*, 61(6), 467-477.

Websites

[1] https://www.alz.org/braintour/images/alzheimer_brain.jpg

[2] <http://library.med.utah.edu/WebPath/CNSHTML/CNS090.html>

[3] <http://www.sigmaaldrich.com/content/dam/sigma-aldrich/articles/technology-spotlights/iron-oxide-nanoparticles/20-nm-diameter-iron-oxide-nanoparticles.jpg>

[4] <http://www.news.cornell.edu/stories/2013/10/goldplated-nano-bits-find-destroy-cancer-cells>

[5] <http://www.sigmaaldrich.com/materials-science/nanomaterials/gold-nanoparticles.html>

[6] https://en.wikipedia.org/wiki/Colloidal_gold#Turkevich_method

[7] <https://www.itp.uni-hannover.de/~zawischa/ITP/scattering.html>

[8] http://academic.brooklyn.cuny.edu/biology/bio4fv/page/alpha_h.htm

[9] <http://chemistry.elmhurst.edu/vchembook/568denaturation.html>

[10] <http://sunnybrook.ca/media/item.asp?i=1351>

[11] <http://www.brainfacts.org/brain-basics/neuroanatomy/articles/2014/blood-brain-barrier>

[12] <http://www.proteinatlas.org/humanproteome/brain>

ENDNOTES

1. Corresponding author: Email: legosan9@yahoo.com
2. As a note, a nanoparticle is a nanoscale particle (molecule), with dimensions typically less than 100 nm. For reference, a nanometer (nm) is 1.0×10^{-9} meters.
3. Iron oxide nanoparticles can be synthesized through various means. One of the more common, simple, and biocompatible methods involves the use of iron (II) and iron (III) chloride dissolved in HCl, coated with a surfactant and water to act as an aqueous base for the particles to flow in. This research uses a similar procedure in the synthesis of iron-oxide nanoparticles.
4. Please note, the scheme mentions 'Fe₂O₃(s) particles'. It is implied the term 'particles' refers to 'nanoparticles'. Moreover, Fe₂O₃(s) and 'iron-oxide' are used interchangeably throughout this paper.
5. Occasionally, the phrase 'iron-oxide AuNPs mediated heat' is mentioned, but as a reminder, it is the AuNPs alone which mediate heat energy, with iron-oxide acting as a carrier/base. For clarification, please see *Therapeutic Applications of Iron-oxide and Gold Nanoparticles*.
6. Previous research from Cornell University's Ludwig Institute for Cancer Research has actually used Iron Oxide as a transport for AuNPs to destroy cancer tumors, but such a hybrid fluid has not been used for Alzheimer's Disease [4].

AUTHOR INFORMATION

Sanjiv Harikumar
Las Cruces High School
1755 El Paseo Rd.
Las Cruces, NM 88001
legosan9@yahoo.com

APPENDIX

This appendix contains raw data pertaining to the temperature changes of the mixtures represented in Figure 10 of this paper.

TEMPERATURES OF MIXTURES									
Mix # 1 (6 mL)		Mix # 2 (5 mL)		Mix # 3 (8 mL)		Mlx # 4 (5 mL + 0.2 g. Protein)		Mlx # 5 (8 mL + 0.2 g. Protein)	
Time (min)	Temp, C	Time (min)	Temp, C	Time (min)	Temp, C	Time (min)	Temp, C	Time (min)	Temp, C
0	27.3	0	24.8	0	24.5	0	7.7	0	13.8
1	27.2	1	26.8	1	24.8	1	9.6	1	15.2
2	27.1	2	27.7	2	25.3	2	11.9	2	16.7
3	26.9	3	28.7	3	25.8	3	14.2	3	18.3
4	26.8	4	29.5	4	26.2	4	16.1	4	19.4
5	26.7	5	30.3	5	26.6	5	17.9	5	20.7
6	26.6	6	31	6	27	6	19.4	6	21.5
7	26.5	7	31.6	7	27.4	7	20.9	7	22.5
8	26.4	8	32.2	8	27.8	8	22.3	8	23.6
9	26.4	9	32.7	9	28.1	9	23.5	9	24.2
10	26.3	10	33.3	10	29.6	10	24.6	10	25.3
11	26.2	11	33.6	11	30.1	11	25.8	11	25.6
12	26.1	12	33.9	12	30.5	12	26.8	12	26.3
13	26	13	34.3	13	30.8	13	27.7	13	27
14	25.9	14	34.6	14	31.1	14	28.5	14	27.3
15	25.8	15	34.8	15	31.5	15	29.2	15	27.7
16	25.8	16	34.9	16	31.7	16	30	16	28.2
17	25.7	17	35.1	17	31.8	17	30.7	17	28.5
18	25.6	18	35.4	18	31.8	18	31.4	18	28.8
19	25.5	19	35.6	19	31.8	19	32.1	19	29.1
20	25.5	20	35.9	20	31.8	20	32.7	20	29.3
21	25.5	21	36.1	21	32.5	21	33.4	21	30.4
22	25.5	22	36.3	22	32.5	22	33.6	22	30.8
23	25.5	23	36.5	23	32.6	23	33.9	23	30.8
24	25.5	24	36.7	24	32.8	24	34.4	24	30.8
25	25.5	25	36.8	25	33.1	25	34.8	25	31.1
26	25.5	26	36.9	26	33.3	26	35.2	26	31.3
27	25.5	27	37	27	33.5	27	35.5	27	31.5
28	25.5	28	37	28	33.7	28	35.8	28	31.9
29	25.5	29	37	29	33.9	29	36	29	32.2
30	25.5	30	37	30	34	30	36.1	30	32.2

The Column-less Stair at Loretto Chapel in Santa Fe: Strength Analysis

Anita Sumali, La Cueva High School

A spiral staircase in Loretto Chapel in Santa Fe, New Mexico, has no center column to provide structural strength and stability. Some estimates say that the stair should have collapsed at first use. This article presents a stress analysis of the stair using a finite element model. The loading is 16 persons on steps 1, 3, 5, ..., 31 of the stair, the weight of the stair, and the weight of the railing. The analysis shows that the center spiral is severely stressed. The maximum Von Mises stress, which occurs near the top of the center spiral, is 1.7MPa. (The ultimate strength of strong Engelmann spruce is 2.0MPa.) The absence of the center column is significant because a center column would reduce the maximum stress in the stair to about 0.3MPa.

INTRODUCTION

The Loretto Chapel in Santa Fe, the capital of New Mexico, has a spiral staircase with no center column to provide structural strength and stability. Some estimates say that the stair should have collapsed at first use (Black, 2014). Yet, the stair has been used daily since its genesis in 1878 (Loretto Chapel web site, 2017). Explanations of the source of the structural integrity ranges from simple 'physics' (e.g., Carter, 2010) to attribution to miracle (e.g., Black, 2014). A popular landmark in the historic Old Town area of Santa Fe, the staircase has been the subject of many articles. A popular story about the genesis of the stair has been re-enacted in television shows and movies including "Unsolved Mysteries" and the 1998 television movie entitled "The Staircase" (Wikipedia, 2017).

This article provides finite element calculations to show:

1. The stresses in the staircase structure under heavy loading.
2. Which parts of the structure may be stressed most heavily.
3. How a center column would reduce the stress.

DATA

Figure 1 shows the structure of the stair. The figure is an artist's rendition; but the only difference between the figure and photographs of the actual stair is that the figure eliminates the railing. The strength analysis in this paper will include the railing as a load, not part of the load-bearing structure. (For the first two years of its

use, the stair had no railing (Loretto Chapel home page, 2017).) Table 1 shows data used in the strength analysis. Specific weight is used to calculate the loading of the stair structure due to its own weight. Young's modulus is a measure of the stiffness of the material, i.e., how much the material stretches when it is pulled. When a rod of a certain material is pulled at its end, the rod gets longer, but it also gets thinner proportionally. Poisson's ratio is the thinning over the elongation. The ultimate strength and the shear strength of the material (assumed here to be Engelmann spruce) are used not in the calculation but instead compared to the maximum stress in the stair structure.



Figure 1: Staircase structure. (Black, 2014)

Parameter, unit	Value	Notes
Height, m	6.706	
Outside radius, m	1.224	Excludes railing structure
Inside radius, m	0.300	Excludes railing structure
Number of steps	32	The 33rd step is the balcony floor
Thickness of boards, mm	5.08	Assumed for all boards
Thickness of inner and outer helices, mm	76.2	
Material	Spruce	
Specific weight, N/m ³	3434*	Specific density = 350 kg/m ³
Young's modulus, Pa	8.4E9*	Assumed isotropic
Poisson's ratio	0.26*	
Ultimate strength, Pa	2.0E6*	Engelmann spruce
Shear strength, Pa	4.07E6*	Weakest direction (parallel to grain)
Loading	Persons	Based on Fig. 3
Weight of railing structure, N/m	200	Rough estimate. Small compared to other loads.
Number of persons on stair	16	Heavy load based on Fig. 3
Weight of each person, N	800	Conservatively heavier than persons in Fig. 3

Table 1: Data used in strength analysis. *=Matweb.com, 2017. 1 kg = 9.81 Newtons (N).

METHOD OF ANALYSIS

A measure of loading severity, stress is force per unit area (similar to pressure). Stress is the result of the calculations presented in this article. If stress at any point is greater than the material's ultimate strength, then the material will break at that point. Stress is a measure of the severity of loading on the material. Unlike pressure, stress has several components that depend on direction. A measure that sums up all components of stress is the Von Mises stress. Von Mises stress can be compared to the ultimate strength of the material. If at any point the stress is higher than the strength, then the material breaks at that point.

The stresses that the stair material has to endure is calculated below with a finite element model built and run in Abaqus CAE (Dassault Systemme, 2016). The finite element method divides the stair into many finite (i.e., small) elements, and calculates the stress in each element as the element is loaded by its neighboring elements. Some elements are loaded by loads such as the weight of the persons on the stair. Those elements transfer the loads onto other elements. A mesh is a system of the many finite elements, created from the geometry of the stair. Figure 2 shows the mesh created and used throughout this analysis. Figure 3 is a photograph illustrating a

heavy loading scenario. Figure 4 is a model of the loads used in the stress analysis: Sixteen persons weighing 800N each stand on steps number 1, 3, 5, 7, ..., 31. The weight of each person is assumed evenly distributed over the tread. The stair is also loaded by its own weight, plus the weight of the railings.

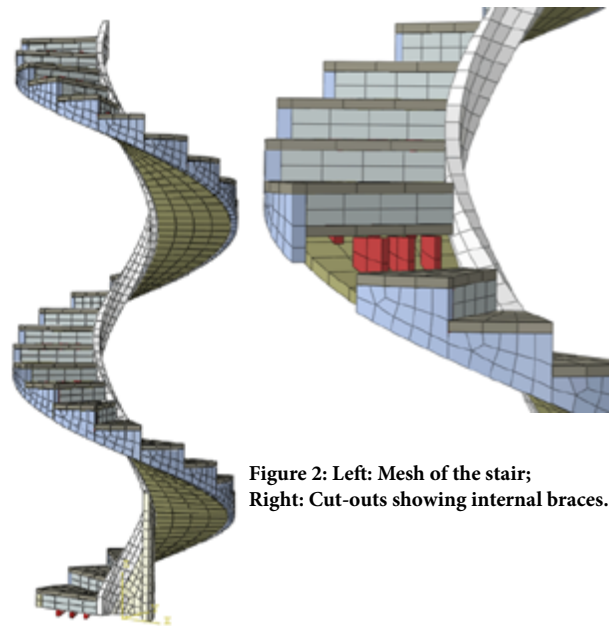


Figure 2: Left: Mesh of the stair; Right: Cut-outs showing internal braces.



Figure 3: Photograph used to estimate loads.

Stress Caused by the Loading

Figure 5 shows that the center helix is heavily stressed. At the location with the highest stress, near the top of the inner helix, the Von Mises stress is about 1.7 MPa. If the material is Engelmann spruce (a strong structural wood), it would break at its ultimate strength of 2.0MPa. Thus, if more weights load the stair (for example, a heavy person on each step), it is quite possible that the weights and the weight of the stair together will break the stair structure. The most likely location of the fracture is the center helix. It is also possible that the stair material is an even stronger Sitka spruce whose ultimate strength is 4.0MPa (Green, 2001). However, the cold location where Sitka spruce grows is many hundreds of miles away from Santa Fe, and it would have been difficult in the 1870's to transport the wood to Santa Fe. On the other hand, Engelmann spruce grows in New Mexico (Picea Engelmannii, Wikipedia, 2017).

The above result confirms the assessment that it is difficult for the stair to bear its own weight plus the load.

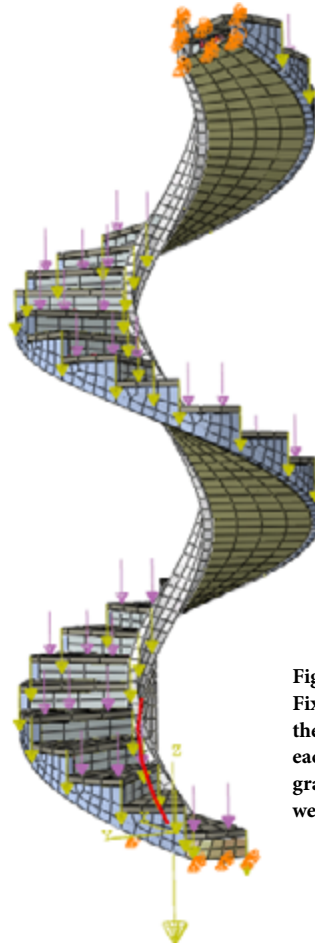


Figure 4: Boundary conditions: Fixed on the top and bottom of the stair. Loading: one person each on steps 1, 3, 5, ..., 31; gravity (weight of stair), and weight of railings.

Thus, the fear that the stair might have collapsed upon loading was justified. A spiral stair without a center column is not only uncommon but also difficult to design. Though downplayed by some experts (e.g. Carter, 2010), the absence of a center column may well be significant. The next section of this article offers a numerical measure of the importance of a center column to the strength of any spiral staircase.

The Importance of a Center Column

Figure 5 shows that the center helix, especially the top part of it, is by far the most heavily stressed part of the stair. Suppose, then, that the center helix were replaced by a more complete hollow column that supports the stair from the ground, as illustrated in Fig. 6. Then, this support would reduce the stresses around the center of the stair. The stress reduction would give a numerical value to the importance of a center column. Below, the above analysis process is applied to the hypothetical design in Fig. 6. The boundary conditions and loads are the same as those shown in Fig. 4

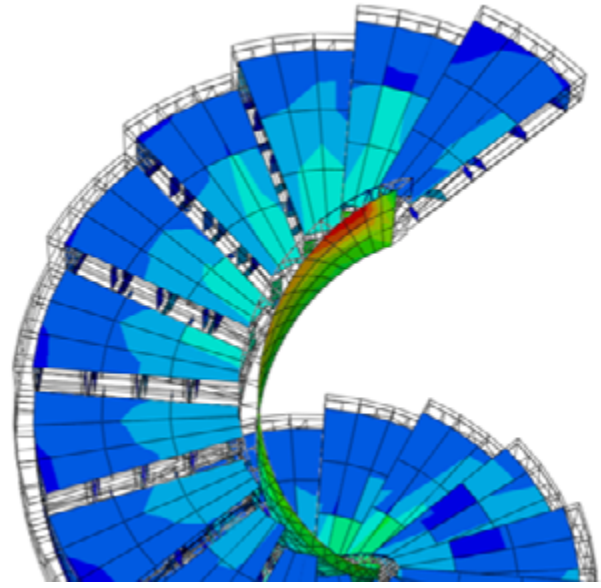
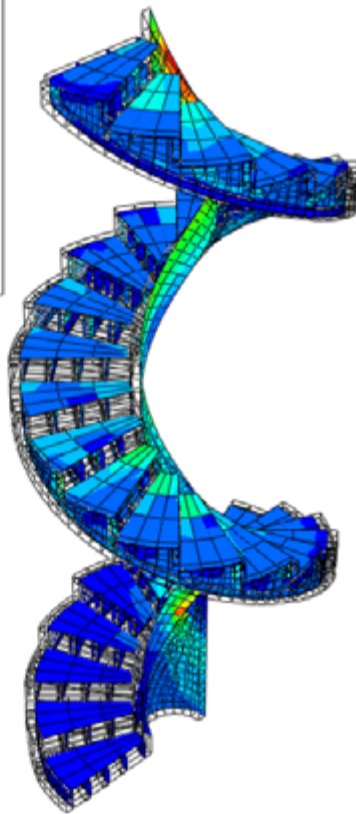
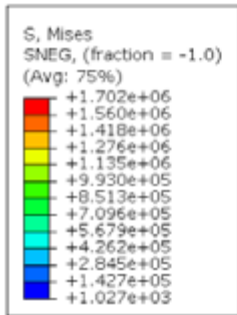


Figure 5: Von Mises stress (left) Side View; (right) View from above

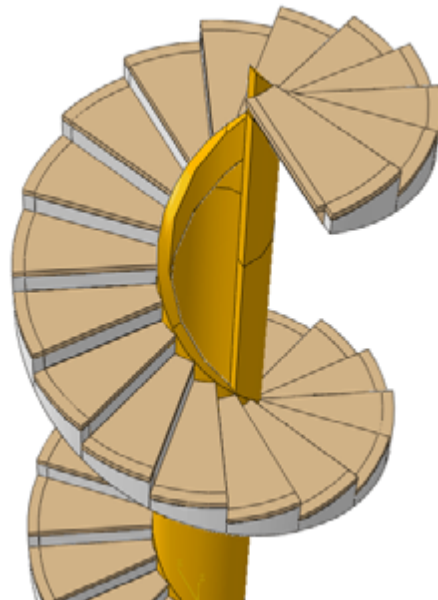
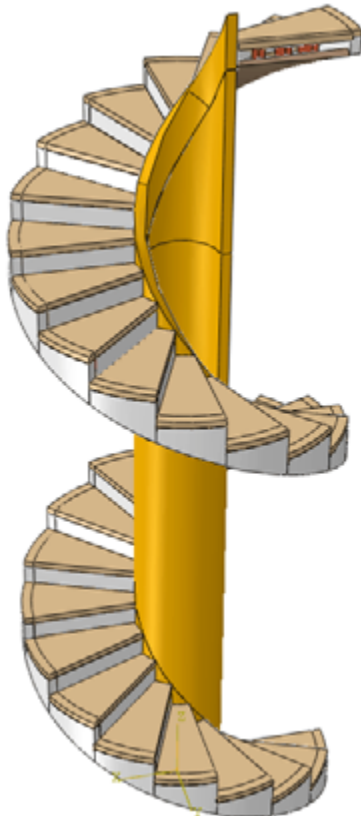


Figure 6: A hypothetical design, the same as the original design but with a center column.

Figure 7 shows that, with a center column, the highest stress in the stair is now around 0.3MPa. The location of the highest stress is on the outside wall at the top of the stair, near the place where the balcony supports the stair. The highest stress around the center of the stair is just around 0.28 MPa. Those stresses are about eight times lower than the stress around the center helix of the stair without center column. Thus, the stair without a center column is about eight times weaker than an equivalent stair with a center column. This analysis shows that a center column is very important to the strength of the spiral stair.

CONCLUSION

When loaded with one person every other step, the column-less stair is heavily stressed. The center helix sustains the heaviest stress, especially at the top where the stair is attached to the balcony. The highest stress is about 1.7MPa. Thus, the center helix material must be a strong wood like Engelmann spruce which can sustain stresses up to about 2.0MPa, or a stronger wood. If more weights load the stair (for example, a heavy person on each step), it is quite possible that those weights and the weight of the stair together will break the stair structure. The absence of a center supporting column is quite significant. When loaded with the same load as the column-less stair, a similar stair design with a center column would be stressed to just about 0.3MPa maximum.

ACKNOWLEDGEMENTS

Abaqus Student Edition (Dassault Systemme, 2016) was used to build the finite element models. I thank my AP Physics teacher Ms. Lena Eddings and my genius friend Brad Zhang for their guidance.

REFERENCES

- Black, John. "The mysterious helix staircase of the Loretto Chapel". *Ancient Origins*. 2014. Retrieved from <http://www.ancient-origins.net/unexplained-phenomena/mysterious-helix-staircase-loretto-chapel-001295>.
- Staircase, *Loretto Chapel web site*. 2017. Retrieved from <https://www.lorettochapel.com/info/staircase>.

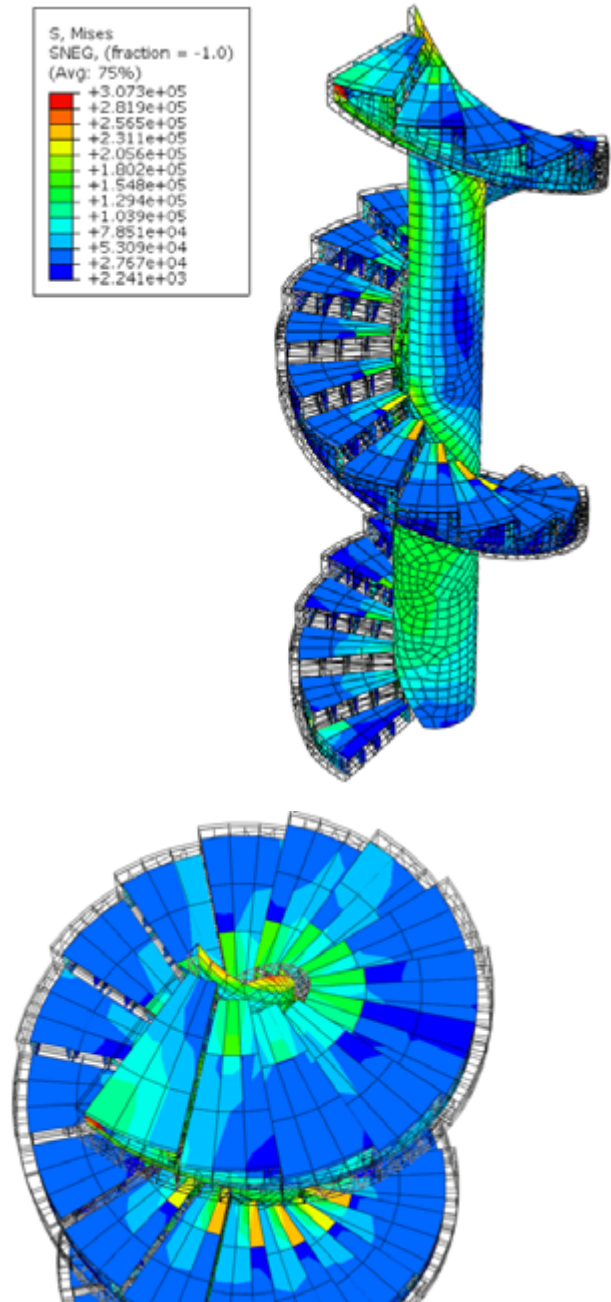


Figure 7: Von Mises stress in a stair with center column. Left: Side View; Right: View from above.

Carter, Tim. "The Loretto Chapel staircase: A lesson in physics, not miracles." *The Washington Post*. January 16, 2010. Retrieved from <http://www.washingtonpost.com/wp-dyn/content/article/2010/01/15/AR2010011501810.html>.

Dassault Systemme. *Abaqus CAE*. 2016. Retrieved from <https://www.3ds.com/products-services/simulia/products/abaqus/abaquscae/>.

Dassault Systemme. *Abaqus Student Edition*. 2016. <https://academy.3ds.com/en/software/abaqus-student-edition>.

Green, D.W. "Wood: Strength and Stiffness." *Encyclopedia of Materials: Science and Technology*. Forest Products Laboratory. 2001. Retrieved from <https://www.fpl.fs.fed.us/documnts/pdf2001/green01d.pdf>.

Loretto Chapel. *Wikipedia*. 2017. Retrieved from https://en.wikipedia.org/wiki/Loretto_Chapel.

Matweb. "North American Engelman Spruce Wood". 2017. Retrieved from <http://www.matweb.com/search/DataSheet.aspx?MatGUID=972210a797e2437982460bd800c31dc3>.

Picea Engelmannii, *Wikipedia*. 2017. Retrieved from https://en.wikipedia.org/wiki/Picea_engelmannii.

AUTHOR INFORMATION

Anita X. Sumali
La Cueva High School
7801 Wilshire Ave NE
Albuquerque, NM 87122
dolphinator7@gmail.com

New Mexico Academy of Science 2017 Award for Outstanding Science Teaching

Jessica Sanders

Berrendo Middle School, Roswell



Jessica Sanders (third from left) is the 2017 Outstanding Science Teacher of the Year. Presenting her award at the NMAS Research Symposium are Donivan Porterfield, left, and Ning Xu, second from left, of the Central New Mexico Local Section of the American Chemical Society, and David Peters, right, President of the New Mexico Academy of Science (photo courtesy of the *Albuquerque Journal*).

Jessica Sanders is a remarkable Science Teacher at Berrendo Middle School in Roswell, New Mexico where she teaches 6th and 7th grade sciences. Mrs. Sanders is identified as a consistent Level III Exemplary Teacher with the district where she esteems students and the entire district staff as an imperative part of the science education structure. Mrs. Sanders has obtained her MA in Curriculum and Development from New Mexico Highlands University and plays an active role in the New Mexico Science teachers Association where she serves as President-elect. Additionally, Mrs. Sanders actively contributed to the NGSS as written with Education Secretary Hannah Skandera, and most recently at the October 16th hearing.

Mrs. Sanders not only exhibits academic excellence, she is also a compassionate leader. She demonstrates the natural ability to establish great rapport with both students and colleagues while delegating responsibility as needed. She is

determined by the knowledge of right and wrong and has an outstanding sense of good judgment. Mrs. Sanders displays the aptitude to stay optimistic and has the determination to follow through with her endeavors with integrity.

Jessica Sanders leadership in education has been inspiring; providing innovative models of education for all children, to include students with a wide range of learning, emotional, physical, neurological, and developmental disabilities. In addition she regards the gifted and talented learner with exceptional understanding. Mrs. Sanders has been pivotal in bringing her middle school and school district forward in STEM Education and she looks forward to being an educational leader with the implementation of NGSS. Mrs. Sanders is noted for providing numerous STEM opportunities to not only her student population, but furthermore to her local Girl and Boy Scouts councils. Mrs. Sanders continues to advocate for rigor in scientific content for the future of Science Education in New Mexico.

Mrs. Sanders authored and won the Devon Science Grants grant, The Prices Dairy Grant, and Girls Moving Forward in Sports Grant. She is also currently a top 16 finalist for the Golden Apple Award to be announced at the end of November 2017.

Mrs. Sanders has a passion for focusing on individual attributes while thoughtfully recognizing individual needs for support in the school community as a whole. She has a keen eye for detail and her extraordinary knowledge of education laws- alongside the various challenges that administrators, teachers, support staff, parents, and students face drives her direction.

New Mexico Academy of Science Research Symposium

ABOUT THE RESEARCH SYMPOSIUM

The 2017 New Mexico Academy of Science Research Symposium was held in Albuquerque on 04 November 2017. The Symposium was sponsored by the New Mexico Academy of Science (NMAS), the New Mexico Experimental Program to Stimulate Competitive Research (NM EPSCoR), the University of New Mexico Center for Water and the Environment, and the New Mexico Alliance for Minority Participation (NM AMP). The Symposium schedule included 32 oral presentations and 52 poster offerings from the students and faculty of New Mexico's universities and colleges. Dr. David Gutzler of the University of New Mexico provided the luncheon keynote address. Abstracts of these presentations are included in this annual volume of the NMAS *New Mexico Journal of Science*. The Symposium closed with the presentation of awards for what were judged to be the best undergraduate posters, and with the New Mexico Academy of Science's annual award for Outstanding Science Teaching.

KEYNOTE SPEAKER: DAVID GUTZLER, PHD

David S. Gutzler is Professor of Meteorology and Climatology at the University of New Mexico. His research at UNM is based on analysis of observations and climate models, with the goals of understanding the causes of climate variability and change, and improving the skill and application of climate and hydrologic forecasts on seasonal and longer time scales. He earned degrees from the University of California at Berkeley (B.S., Engineering Physics) and MIT (PhD, Meteorology). He has served as Editor of the American Meteorological Society's *Journal of Climate*. Prof. Gutzler received the Outstanding Teaching Award from the UNM College of Arts & Sciences in 2008, and a Career Achievement Award from the NM Bureau of Geology in 2014. He was a Lead Author for the chapter on detection and attribution of observed climate change for the Fifth Assessment Report (AR5), Working Group I, of the U.N. Intergovernmental Panel on Climate Change, published in 2013.

SYMPOSIUM WELCOME FROM 2017 NMAS PRESIDENT

On behalf of the New Mexico Academy of Science, I would like to welcome each of you to the 2017 Research Symposium! NMAS is pleased to partner with New Mexico EPSCoR, the UNM Center for Water and the Environment, and New Mexico AMP to sponsor this annual conference to promote science and science education in our community. Our keynote speaker, Dr. David Gutzler is a professor of Meteorology and Climatology at the University of New Mexico. He will be speaking about the changing climate and what both scientists and citizens can do about it. Join us for his lunchtime presentation as well as the award for Outstanding Teacher in our state, plus a day of interesting and engaging presentations by students and professors, as well as the student poster awards in the afternoon.

David Peters
NMAS President

ABOUT THE SYMPOSIUM SPONSORS



NEW MEXICO ACADEMY OF SCIENCE

Founded in 1902, the New Mexico Academy of Science has been in continuous existence since 1915. The Academy is a member of the National Association of Academies of Science (NAAS) and an affiliate of the American Association for the Advancement of Science (AAAS). The New Mexico Academy of Science works with teachers, state agencies, and the legislature to establish appropriate standards for the teaching of the sciences. The Academy can also act as a resource center, providing scientific advice and expertise to these groups and others. The Academy goals are to foster scientific research and scientific cooperation, increase public awareness of the role of science in human progress and human welfare, and promote science education in New Mexico. Visit www.nmas.org to learn more.

NEW MEXICO EPSCOR

The New Mexico Established Program to Stimulate Competitive Research (NM EPSCoR) is funded by the National Science Foundation (NSF) to build the state's capacity to conduct scientific research. The infrastructure and activities of Energize New Mexico are designed to support shared-use equipment, engage new research and community college faculty, and support the STEM pipeline by training teachers, undergraduate and graduate students, and post-doctoral fellows. Research findings are communicated broadly through partnerships with New Mexico's museum network, a citizen-centric web portal, and vibrant, experiential programs targeting K-12 students. Visit www.nmepscor.org to learn more about NM EPSCoR, and visit www.nsf.gov/epscor to learn more about the NSF EPSCoR initiative and other jurisdictions.

UNM CENTER FOR WATER & THE ENVIRONMENT

The mission of the Center for Water and the Environment at the University of New Mexico (UNM) is to increase the participation of underrepresented minorities (URM) in science, technology, engineering and math (STEM) professions while conducting cutting-edge research into technological and engineering-based solutions to problems with water and the environment, in a framework that considers the social, economic, policy, regulatory, and legal implications. Practical solutions to problems related to water availability in arid environments and in times of drought, and problems associated with energy generation and consumption are particularly relevant, in light of the criticality of these issues to the state of New Mexico, the southwestern United States, and their global importance. Learn more at cwe.unm.edu.

NEW MEXICO ALLIANCE FOR MINORITY PARTICIPATION

Established in 1993 with major funding from the NSF, the New Mexico AMP program is a partnership of the state's two- and four-year colleges and universities, with a primary goal of increasing the number of B.S. degrees awarded to under-represented students in New Mexico. NM AMP supports students with scholarships; research assistantships; professional development; and enhanced teaching, learning, and mentoring experiences. Program activities are designed to attend to individual student retention, development, and progression; support student progression to the STEM workforce and graduate school; and promote the replication of best practices, both within New Mexico and nationally. Since program inception, New Mexico has seen increases in the number of science degrees earned by under-represented students at the state's public 4-year universities, thereby increasing diversity in STEM. To learn more, visit www.nmsu.edu/~nmamp/.

CONCURRENT SESSION PRESENTATION ABSTRACTS

SESSION A: CHEMISTRY I

Molecular Rectification Behavior of the Pyranopterin Ligand of Molybdoenzymes

LAURA INGERSOL, UNIVERSITY OF NEW MEXICO

Molybdenum plays an indispensable role in human metabolism, global nitrogen and sulfur cycles, greenhouse gas formation, bacterial detoxification pathways, and anaerobic respiration. These processes are critical for maintaining human health and ecological balance. To become catalytically active, the Mo ion must be incorporated into a molecular scaffold by complexation with a singular ligand known as the pyranopterin, an arrangement commonly referred to as Moco, the nearly ubiquitous molybdenum cofactor found in molybdoenzymes. Molybdoenzymes typically catalyze the two-electron oxidation or reduction of a substrate coupled to formal oxygen atom transfer. The pyranopterin dithiolene (PDT) can adopt several distinct geometries that may correspond to different oxidation and tautomeric states, which we hypothesize will contribute to its suspected role as an electron transfer conduit during the redox reactions catalyzed by molybdoenzymes. Interestingly, the fully reduced tetrahydro PDT exemplifies the Van Dyke/Ratner design rules for synthetic molecular rectifiers, indicating that nature may utilize molecular rectification in catalytic processes involving vectorial electron transfer. The rectification ratio (RR) is the ratio of the amount of current that can flow at forward and reverse biases. This RR is an indicator of the efficiency of vectorial electron transfer. The RR can be modulated when the amine terminus of the tetrahydro PDT, which serves as an anchoring group to a gold electrode in the electron transport calculations, is replaced by a thiol or a nitrile group. We rationalize these findings by analyzing the nature of the current carrying molecular orbitals that derive from our computational results. This provides a basis for understanding how electron transfer processes occur in molybdoenzymes as well as informing further design criteria for novel biologically inspired synthetic molecular rectifiers.

Keywords: molybdoenzymes, electron transfer, pyranopterin, rectifier

Modeling Mo/W formate dehydrogenase catalytic intermediates

KHADANAND KC, UNIVERSITY OF NEW MEXICO

The utilization of fossil fuel increases the global demand for CO₂ sequestration due to the potential impacts of this greenhouse gas toward global climate change and ocean water acidification. Molybdenum and tungsten formate dehydrogenase (Fdh) enzymes catalyze the reversible conversion of formate to carbon dioxide ($\text{HCOO}^- \rightarrow \text{CO}_2 + 2\text{e}^- + \text{H}^+$). Understanding the mechanism of Mo- and W-Fdh enzymes is expected to contribute to a better understanding how to design new chemical catalysts. An additional impetus for these studies focuses on the use of formate as a storable form of energy in chemical bonds. We now know that these enzymes possess an ancillary ligand selenocysteine ligand (Secys) that contributes to lowering the activation energy of the reactions these enzymes catalyze. However, it is unknown how this ancillary ligand contributes to catalysis. Thus, it is critical to understand the basic electronic and geometric structure features of Fdh enzymes if we are to fully understand their catalytic mechanism. Presence of Fe-S clusters makes more difficult to get detailed electronic structures. Although a combination of EXAFS and EPR data have been collected for these enzymes, our understanding electronic structure contributions to reactivity have been hampered by the inability to optical spectroscopies to probe these active sites. This arises from the presence of other strongly absorbing chromophores that mask the electronic transitions associated with the catalytic Mo and W centers in the enzymes. To address this issue, we have synthesized the first des-oxo synthetic analogs of Fdh enzyme active sites and have studied these models using a combination of EPR, electronic absorption, and XAS spectroscopies. Here, we will present our most recent results on the synthesis, spectroscopy, and electronic structure of novel 6-coordinate EPR active analogs for Fdh enzymes that indicate a potential role for the Secys ligand in catalysis.

Keywords: catalysts, CO₂ sequestration, formate

New Multispin Phosphorescent Chromophores

JU CHEN, UNIVERSITY OF NEW MEXICO

Square-planar (bpy)Pt(bdt) (bdt = benzene-1,2-dithiol; bpy = 4-4' bipyridine) Donor-Acceptor (DA) complexes are of interest due to the remarkable nature of their lowest energy bdt \rightarrow bpy ligand-to-ligand charge transfer (LLCT) excited states. The nature of this LLCT transition results in the formation of a charge separated open shell singlet biradical excited state. These complexes readily intersystem cross (ISC) to the open shell triplet configuration with long-lived excited state lifetimes and observed photoluminescence. We have been interested in the effects of radical elaboration on the ISC rates and excited state lifetimes of LLCT complexes. As such, we have synthesized a new verdazyl (Vdz) radical elaborated (bpy)Pt(bdt-Vdz) complex and performed spectroscopic and computational studies on this interesting system. Phosphorescent emission has been observed on this complex indicating the existence of a long-lived excited state with a different spin multiplicity ($S = 3/2$) than that of the electronic ground state ($S = 1/2$). The results are discussed in terms of the excited state electronic structure, nature of the excited state magnetic exchange interactions, and the potential for generating spin polarized excited states that will contribute to dynamic spin polarization effects in the ground state.

Keywords: platinum donor-acceptor complexes, verdazyl radical, exchange interactions

Effects of Donor Substitution on Vibronic Instability in Oxomolybdenum Dichalcogenolenes

JING YANG, UNIVERSITY OF NEW MEXICO

Dithiolene distortions have long been suggested to play a critical role in electronically buffering the Mo active site of pyranopterin molybdenum enzymes against the large changes in charge that accompany Mo(IV)/Mo(V) and Mo(V)/Mo(VI) redox processes. In this work, we quantify the nature of dithiolene/diselenolene fold angle conformers via a combination of spectroscopy, bonding calculations, and the application of a vibronic coupling model. The structure of $\text{Tp}^*\text{MoO}(\text{bds})$ (**1**) (bds = benzene-1,2-diselenolate, Tp^* = hydrotris(3,5-dimethyl-1-pyrazolyl) borate) is very similar to its dithiolene analogue $\text{Tp}^*\text{MoO}(\text{bdt})$ (**2**) (bdt = benzene-1,2-dithiolate), but possesses longer Mo-E ($E = \text{Se}, \text{S}$) bonds (Mo-Se: 2.61 Å; Mo-S: 2.13 Å) and a greater metalligand envelope fold angle (**1**: 26.2°; **2**: 21.3°). Importantly, multifrequency EPR spectroscopy has revealed, for the first time, the presence of fold-angle conformers for the diselenolene ligand in **1**. The “fold up” and “fold down” conformers are populated in an approximate 80:20 ratio at room temperature. Resonance Raman spectroscopy and electronic structure calculations also provide strong evidence for the presence of these conformers in solution. We have employed a simple two-state vibronic coupling model to understand the electronic origin of the extremely soft ground state double potential well. These new results will be discussed in terms of the potential for fold angle conformers to modulate electron and atom transfer reactivity in pyranopterin molybdenum enzymes.

Keywords: molybdenum, magnetic circular dichroism, diselenolene, electronic structure

SESSION B: SPECTROSCOPY & CHEMISTRY

Spectroscopic Study on Novel Photoactive Antibacterial Agent: 2, 3 – Distyrylindole

RUWINI RAJAPAKSHA, NEW MEXICO TECH

Optical properties of novel, photoactive, indole based antibacterial chromophore system of 2, 3 – distyrylindole (23DSI) molecule studied using various spectroscopic techniques as well as density functional theory (DFT) calculations. The spectroscopic techniques involved with UV-Vis spectroscopy, Fluorescence spectroscopy, Time-resolved fluorescence upconversion spectroscopy (TRFLS), and Time correlated single photon counting spectroscopy (TCSPC) were utilized. The studies show that the molecule 23DSI has multiphoton absorption showing two photon and three photon absorptions in both solid and solution phases. The multiphoton absorption characteristics of this

molecule can be used in various applications such as fluorescence microscopy, 3-D optical storage, optical power limiting, photodynamic therapy (PDT), and photodynamic inactivation (PDI). The TRFLS studies on 23DSI molecule shows fast, single exponential decay with average time constant of 34 ps with average lifetime of 1ns. The NIR emission studies did not show any sign of singlet oxygen production of this molecule. The DFT calculations show that the 23DSI molecule has conjugated electron densities, which is responsible for multiphoton absorption. Both optical spectrum and emission wavelength using DFT calculations show excellent agreement with experimentally measured UV-Vis spectrum and emission wavelength. Combined experimental and theoretical studies suggest that relaxation of excited state electron to the singlet state (S1) by internal conversion (IC) first and latterly relax back to their ground state (S0) by emitting fluorescence. Due to the fast depopulation of S1 to S0 via fluorescence emission, there is no effective energy transferring occurs to the triplet state (T1) of molecule and hence no successful singlet oxygen production.

Keywords: multiphoton absorption, photodynamic inactivation, fluorescence decay kinetics

Semiconductor Photocatalysis of Bicarbonate to Solar Fuels: Formate Production from Copper (I) Oxide

HANQING PAN, NEW MEXICO TECH

Copper oxide-based photocatalysts, micron- and nano-sized, and silver nanoparticle-copper oxide nanocomposites (Ag/Cu₂O) were synthesized, characterized, and evaluated for the first time in the application of bicarbonate conversion to formate. The Ag/Cu₂O nanocomposite yielded considerable production improvement over pure copper oxides due to the role of silver as a plasmonic sensitizer. We attribute these marked production improvements to direct electron transfer (DET) from metal to semiconductor, and plasmon-induced resonant energy transfer (PIRET). These photocatalysts were studied in two different hole scavenger solvents (2-propanol and glycerol) using a solar simulator with air mass coefficient 1.5 and 0 (AM 1.5, AM 0) filters. Formate production increased significantly with AM 0 solar irradiation due to inclusion of the ultraviolet portion of the solar spectrum, and nano-particulate Cu₂O showed improved photocatalysis relative to micron Cu₂O. Green chemistry solvent, glycerol, proved to be a far superior hole scavenger in comparison to 2-propanol.

Keywords: copper oxide, photocatalysis, bicarbonate, formate

Electric-field Induced Dynamic Electronic Junctions in Hybrid Organic-Inorganic Perovskites for Optoelectronic Applications

HAIZHEN WANG, NEW MEXICO STATE UNIVERSITY

Organic-inorganic metal halide perovskites have attracted great attention as optoelectronic materials due to their low-cost, relatively insensitive to defects and solution-processible properties. However, some of their properties, such as thermal instability, toxicity and current-voltage hysteresis still remain elusive. Ion-migration, which has been proved to be a thermal-activated process, is regarded as one of the major origins of the hysteresis and thus detrimental to the longterm stability of the optoelectronic devices. Nevertheless, by using the external electric field to pole the perovskite, ion-migration would be possible to be utilized to create dynamic electronic junctions. In this paper, electric-field induced dynamic electronic junctions have been manipulated for photodetection and energy harvesting through the ion-migration under external electric field. Ion-migration induced p-n or n-p junction has been created successfully via tuning the polarity of the external applied voltage, which is used for photodetection with a relative fast response. By frozen out of the non-uniformly distributed ions after migration at low temperature, we demonstrate that the ion-migration induced dynamic junctions can function as an energy harvesting device with an external quantum efficiency of 20 %.

Keywords: electric field, dynamic electronic junction, photodetection, energy harvesting

Novel Hypersaline Strains of Microalgae Growing in Saline Produced Water Comparing Geothermal and Non-Geothermal Waters

JONATHAN SCHWILLING, SANTA FE COMMUNITY COLLEGE

In this study two hypersaline strains of algae, a highly enriched polyculture from produced water (PW) (“Blue-Cyano”) (BC) because of its blue color) and another, *Dunaliella tertiolecta*, obtained from UTEX Culture Collection were cultivated in dual open raceway pond (ORP) systems using PW diluted to salinities of 30‰ and 70‰. BC did not initially demonstrate high growth, but dense algae cultures were eventually established in both ORP’s. *Dunaliella tertiolecta* was out-competed by pennate diatoms, amoeba, and rotifers. 23S rRNA genes from the polyculture were sequenced using Illumina MiSeq. The results suggest the culture consisted of *Cyanobacterium aponinum* (62.4%), Uncultured organism related to *Phycisphaera mikurensis* (25.8%), *Parachlorella kessleri* (9.0%) and *Scenedesmus* sp. (1.0%). ICP-OES analysis of the PW samples after cultivation of BC showed that group II cation concentrations were reduced in the reactors. Future work will be to determine if the BC culture can remediate PW so that it can be reused by the oil and gas industry.

Keywords: geothermal waters, microalage, produced water, polycultures

Cellulolytic enzyme activity in *Galdieria sulphuraria* cultures

UJALA SEHAR, NEW MEXICO STATE UNIVERSITY

Plants convert sunlight to biomass, this biomass is primarily composed of lignocellulose which is the most abundant natural biopolymer and a potential feedstock for fuel and chemical production. The stringency and complexity of the cellulosic structures have resulted in the evolution of a wide array of cellulose degrading enzymes. Microorganisms with the potential of degrading cellulose produce enzymes with cellulolytic and non-cellulolytic domains that work harmoniously on the substrate to break it down and thus known as cellulases. The Cyanidiophyceae class members are known to be extremophiles in nature and are believed to be the most acidophilic photosynthetic organisms known so far. *Galdieria sulphuraria* is a unicellular, red alga that belongs to this class Cyanidiophyceae. *G. sulphuraria* is an extremophile with the capacity of growing both photosynthetically and heterotrophically over fifty different carbon sources due to its diverse metabolic potential. In the current study, an important paradigm of adaptation is being presented, highlighting its ability to produce cellulolytic enzymes in the presence of different carbon sources at extreme conditions. When grown under mixotrophic conditions, secretion of beta galactosidases by the cells cause digestion of carbohydrate polymers. Moreover, the activity has been observed by disintegrated cells when treated with model substrates, which leads us to believe that cellulolytic enzymes might be present on cell wall and membranes. Thus *G. sulphuraria* may serve as a biocatalyst for cellulosic sugar production.

Keywords: cellulolytic enzymes, mixotrophic, cellulose, extremophiles

Analyzing Microbial Community for Enhanced Nutrient Removal and Biomass Productivity on a Pilot-Scale Algal Turf Scrubber™ in Dairy Wastewater

JUCHAO YAN, EASTERN NEW MEXICO UNIVERSITY

Built on our ongoing research of using algae to recover nutrients in dairy wastewater on an outdoor pilot-scale Algal Turf Scrubber™ (ATS), we have used metagenomics to analyze the microbial communities for the samples collected at different locales down the floway. This is toward engineering the algal/bacterial assemblage, which is conducive to the most efficient nutrient removal and highest biomass productivity. Interestingly, our preliminary findings show that ATS is a highly dynamic system, whereby sulfur-based metabolism appears to dominate the initial floway then converts to a nitrogen-based metabolism at the terminal end.

Keywords: algae, biomass productivity, Algal Turf Scrubber

Expression Studies of DGAT Isoforms in Nannochloropsis Salina Grown Under Cold and Nitrogen Deprived Conditions

SABA GILL, NEW MEXICO STATE UNIVERSITY

Marine microalga *Nannochloropsis salina* is famous for its high oil yield, mainly triacylglycerides (TAGs) production as neutral storage lipids in response to nitrogen deprivation and environmental stresses. One most important response is accumulation of polyunsaturated fatty acid inside the cells to prevent cellular collapse and degradation of cell membranes. Genes encoding for these lipid biosynthesis enzymes can be found in various microalgae using advanced molecular techniques. We found out that *Nannochloropsis salina* can potentially accumulate more polyunsaturated fatty acids (PUFAs) under low temperatures and nitrogen deprivation as compared to optimal conditions. We recorded growth measurements along with photosynthetic measurements. We also studied the expression of genes involved in the Kennedy pathway for lipid synthesis using RT-PCR. We found out that there are four isoforms of the DGAT enzyme, which is involved in TAG formation. For current experimental setup, only one of them showed higher expression as compared to others. To compliment our gene expression studies with lipidomics, we performed FAME analysis and FT-ICR mass spectrometry to analyze lipids produced under stress conditions.

Keywords: lipidomics, RT-PCR, PUFAs, gene expression, Kennedy pathway, DGAT isoforms

SESSION D: GEOLOGY & GEOCHEMISTRY

Reactivity of Co-occurring Nano-particulate U(IV) and U(VI) phases in Abandoned Mine Wastes Under Oxidizing Conditions

CHRIS TORRES, UNIVERSITY OF NEW MEXICO

We investigated the reactivity of co-occurring nanoparticulate U(IV) and U(VI) phases in abandoned mine wastes collected from the Jackpile mine, Laguna Pueblo, NM, under oxidizing conditions by integrating laboratory experiments with various spectroscopy, microscopy and diffraction techniques. X-ray fluorescence analysis revealed U concentrations as high as 7000 mg/kg in the mine waste. X-ray photoelectron spectroscopy (XPS) of these mine waste samples suggested the co-occurrence of both U(IV) and U(VI). The co-occurring U-minerals were encapsulated by carbon based electron microprobe mapping data. Data from electron microprobe and X-ray diffraction also suggest the presence of coffinite (U(IV)SiO₄) and U-phosphates (U(VI)-P-K), similar to observations made in XPS. Furthermore, the scanning transmission electron microscopy (STEM) analysis on these nano-particulate U minerals suggested that the U-P-K phase was crystalline and the predominant U phase in the mine waste. Batch experiments were carried out in oxidizing conditions to assess the reactivity of these co-occurring U-bearing mineral phases using 18 MΩ water (DI), sodium bicarbonate (NaHCO₃), and sodium hypochlorite (NaOCl, bleach) over 2 weeks. DI exposure invoked U concentrations of ~ 300 µg/L, an order of magnitude greater than the U MCL (30 µg/L). Reagents consisting of sodium hypochlorite and sodium bicarbonate yielded U concentrations peaking at ~8000 µg/L, and 10 mM bicarbonate yielded the highest U concentrations of 24000 µg/L. These results suggest that the bulk of U release is attributed to desorption of U as a result of complexation with carbonate (CO₃²⁻) to form uranyl-carbonates (U exposure to CO₃²⁻ ions) and dissolution.

Keywords: uranium, nanoparticulates, spectroscopy, coffinites, U-phosphates

Geothermal springs in southwestern Colorado: Understanding mantle-surface connections and structural control

BENJAMIN HOLT, UNIVERSITY OF NEW MEXICO

This project investigates the role of faults as geothermal fluid conduits for rapid mantle-to-surface volatile transport. Variations in fault orientation, intersections, and reactivation by young magmatism may account for high mantle signature of geothermal fluids. The western San Juan Mountains of Colorado provide a field laboratory where the

structural setting and hydrochemistry of carbonic springs can be studied. Rico Hot Springs has a helium isotope ratio of 5.88 Rc/Ra (73% mantle helium component), a dry gas CO₂ content of 99.7%, and is located above a low-velocity upper-mantle domain. This and nearby springs are associated with basement-penetrating faults of the Rico dome, and are near young igneous rocks such as the Calico Peak (4.7 Ma) and Priest Gulch (4.0 Ma) stocks. The near-MORB mantle helium value and high CO₂ content in several springs indicate that mantle volatiles are rapidly transmitted into the groundwater system. Three types of analyses were done. 1) New water and gas chemistry analyses indicate that each Rico area spring has unique major and trace element chemistry (Piper diagram) suggesting different mixing of geothermal with meteoric water. 2) Structural compilation of faults suggests E-W trending young normal faults. 3) CO₂ flux measurements were made using an EGM-5 flux meter; these data identify cryptic fault conduits and quantify CO₂ flux across structural features. Overall, results so far show strong localized controls on water geochemistry and the importance of faults (some cryptic) for transmitting mantle volatiles via geothermal fluids from depth.

Keywords: geothermal springs, mantle-to-surface transport, CO₂

Tomographic and morphometric analysis of shallow sediments: Pamplona Zone, Gulf of Alaska

ROWAN CAHILL, THEODORE GOUJON, LISEL FAUST, AND RAMONA PARK, SANTA FE HIGH SCHOOL

Convergence and shallow subduction of the Yakutat microplate beneath North America has shaped the Pamplona zone fold and thrust belt in the northeastern Alaska subduction zone. Here, convergent tectonics and glaciomarine sedimentary processes have created patterns of deformation and deposition recorded by a shallow sedimentary sequence with varying fluid pressure, compaction, and fault activity. If the record of ice sheet advance is preserved on the seafloor and in the underlying sediments then bathymetric evidence of glaciomarine processes should overlap with evidence of overpressure, such as low velocity zones in the shallow sediments. In this study, we present a velocity model through the Bering trough as well as regional drainage shape characteristics. We use streamer tomography on a seismic survey from the St. Elias Erosion and Tectonics Project (STEEP) to determine a velocity model. We further inform our interpretation using physical properties relationships developed with data from core samples (IODP Expedition 341) taken near the seismic line. To document drainage morphology, we use smooth sheet bathymetry to identify a drainage network and query profile shapes at well distributed locations; where profile shape is determined by fit with a power function. Initial results suggest overlap between u-shaped drainage profiles towards the SE end of the Bering trough and low-velocity shallow sediments NE of the shelf break. In part, because this overlap occurs within the mapped extent of the last glacial maximum, we find our tomography results consistent with buildup of overpressure due to glacially driven loading of highly saturated sediments.

Keywords: pollution, reduction, smog, titanium oxide, urban

A Cost-Effective Approach to Geothermal Resource Discovery: Principal Component Analysis and Clustering

JEFF PEPIN, NEW MEXICO TECH

Geothermal resource exploration is expensive and highly uncertain. Improving success rates and lowering exploration costs are high priorities for energy scientists worldwide. Our work is aimed at better understanding the hydrologic, geologic, geochemical, and geophysical factors that control the presence/absence of geothermal resources within New Mexico to guide exploration efforts. We use advanced statistical learning tools, trained with information from known geothermal resources, to identify regions of high geothermal potential. The main two statistical methods used in this study are principle component analysis and Euclidean clustering. We considered eight predictors, which are readily available for most of the State: heat flow, elevation, crustal thickness, silica geothermometer temperature, dike density, volcanic vent density, seismicity, and fault density. We found a clear separation between geothermal

systems located in volcanic, active, and stable tectonic regimes, which allows us to predict where these types of geothermal systems are likely to occur. As part of this work, we performed a detailed variable selection analysis to determine which measurable parameters make the best predictors for geothermal activity. The results suggest that high heat-flow, low elevation, and low crustal thickness are key controls on the location of classic forced-convection geothermal systems within the State. Finally, the method can be used to locate unexplored portions of New Mexico that have similarities to known geothermal resources, effectively outlining areas of greater resource potential. Future work will focus on using these statistical methods to determine data-driven weights to more accurately construct statewide geothermal prospectivity maps.

Keywords: geothermal exploration, statistical learning, principal component analysis, cluster

Characteristics and Crystal chemistry of U-V bearing minerals in abandoned mine wastes

SUMANT AVASARALA, UNIVERSITY OF NEW MEXICO

We used spectroscopy, electron microscopy and diffraction techniques to determine the characteristic and crystal chemistry of a U-V bearing minerals occurring at an abandoned mine waste site in Northeastern, AZ. The diffraction lines in the X-ray diffractogram of these U-V bearing minerals showed up to 80% agreement with that of the synthetic carnotite from literature. The carbon (C) in the U-V bearing mineral phase was found to co-occur as an organic carbon inclusion based on results from the bright field transmission electron microscopy (BFTEM) imaging; energy filter transmission electron microscopy (EFTEM); and electron energy loss spectroscopy (EELS). Therefore, after excluding C from the quantitative electron microprobe analysis the elemental composition of U-V bearing minerals was 4.45% K₂O, 0.53% CaO, 62.72% UO₂, 0.04% Na₂O, 20.65% V₂O₅, 0.56 Fe₂O₃, 0.09% TiO₂ and 1.70 H₂O at a K:U:V ratio of 1:2:2.1 with an empirical formula of (K_{0.87}, Na_{0.012}, Ca_{0.088})(Ti_{0.005}, U_{0.99})O₂)₂((Fe_{0.033}, V_{1.05})O₄)₂·2H₂O. Although the simplified empirical formula (K(UO₂)₂(VO₄)₂·2H₂O) of U-V bearing minerals shows reduced potassium concentrations, its d-spacing is similar to that of anhydrous carnotite reported in literature with minor discrepancies due to degree of hydration. Furthermore, this hydrated carnotite (U-V bearing mineral) rapidly amorphized on short term exposure to the electron beam (<60s). Results from this investigation provide an improved understanding on the characteristics and crystal chemistry of naturally occurring U-V bearing minerals in abandoned mine wastes. Identification of these uranyl vanadates can be crucial to better understand and predict the long term transport of U in abandoned mine waste sites.

Keywords: abandoned mine waste, Uranium, U-V phase

SESSION E: ENVIRONMENTAL SCIENCE

Is the American Bullfrog (*Lithobates Catesbeianus*) a Successful Invader as It Seems, or Does It Receive Help from Other Invasives?

STEVEN SALINAS, NEW MEXICO HIGHLANDS UNIVERSITY

Invasive species can negatively affect the diversity of native species by disturbing native trophic interactions. Often times invaders work in synergy with other invaders so the role of each invasive difficult to tease apart. In this study we explore the importance of top-down control on crayfish population by bullfrogs, and predatory introduced trout Rainbow Trout (*Oncorhynchus mykiss*). One purpose of our study is to study the diet the invasive bullfrog throughout Northeastern New Mexico. The removed bullfrogs are then 1) dissected to examine stomach contents and 2) diet is compared by male and female food preference. The second purpose is to understand the impact of invasive Crayfish in North Eastern New Mexico rivers. The third and final purpose is to determine a connection between the two invasive species as well as a possible third invasive. Analyzing the diet of a population of American Bullfrogs we found a large proportion (over 80%) of Northern Crayfish (*Orconectes virilis*), another invasive. Our data strongly

suggest that these two predators exert important top down control on crayfish. Management programs to control these species must include a comprehensive control of all species involved to avoid the mesopredators to irrupt. This information can help maintain the invasive front of both Northern Crayfish and bullfrogs alike as they spread throughout New Mexico and other areas of the Southwest.

Keywords: invasive species, American bullfrog, crayfish

Genetic and population-level influences on Boreal toad susceptibility to the fungal pathogen, *Batrachochytrium dendrobatidis*

SARAH COREY-RIVAS, NEW MEXICO HIGHLANDS UNIVERSITY

The emerging fungal pathogen, *Batrachochytrium dendrobatidis* (*Bd*), is a major threat to the survival of many amphibians. Studies of host susceptibility to *Bd* infection demonstrate a remarkable range of responses across different species. The boreal toad, *Anaxyrus boreas*, is susceptible to *Bd* infection and many populations have declined after the arrival of *Bd* in the Southern Rocky Mountains. Boreal toads have been extirpated from New Mexico, yet other *Bd*-positive boreal toad populations persist. In this study, I raised boreal toads from sibling egg clutches to adults from a purportedly *Bd*-tolerant Utah population and a *Bd*-susceptible Colorado population. I experimentally infected lab-reared toads with a global panzootic *Bd* isolate from Colorado boreal toads. Day 7 mean *Bd* infection load was significantly greater in Colorado toads, but mean infection load was not significantly different among treatments for the rest of the 34-day *Bd* challenge. At late infection, Colorado toad body condition declined significantly compared to the control ($P = 0.012$), while Utah toad body condition was unchanged. Clinically, all Colorado toads at late infection presented advanced signs of chytridiomycosis whereas Utah toads presented mild or no signs of disease. The negative impacts of *Bd* infection observed in Colorado boreal toads were not observed in Utah toads in this common garden experiment, supporting the hypothesis that boreal toad population-level genetic differences contribute to *Bd* tolerance. Strategies to increase immunogenetic diversity among populations in the Southern Rocky Mountains are needed to conserve this species of greatest conservation concern.

Keywords: Boreal toad, fungus, pathogens

The Effects of Disturbance and Catastrophic Forest Fire on Submerged Aquatic Macrophytes in a Headwater Stream

VIRGINIA THOMPSON, UNIVERSITY OF NEW MEXICO

Submerged aquatic macrophytes (SAMs) can significantly modify conditions in their environment and can, like other inhabitants of stream ecosystems in the watershed, suffer major impacts from forest fires. Our study aimed to quantify and describe the effects that a catastrophic forest fire can have on four species of SAMs we identified in the East Fork Jemez River, a system highly impacted by the Las Conchas Fire in 2011. For these four species, life history observations were taken, instream biomass was quantified, and macrophyte effects on water quality and response to disturbances were measured. Total mean biomass from 2011-2013 peaked at over 1000 g DW/m². Disturbance events with associated high turbidity (>1000 NTU) and increased stream flow (0.8 m/s) in July/August 2011 caused a notable reduction in biomass, while a flood event in 2013 with lower turbidity (~150-400 NTU) but 4.5x higher flow (~3.6 m/s) caused a lesser drop in standing biomass. SAM biomass recovered and peaked in October 2011. Biomass measures were sensitive to disturbance events during the study period, and continuous measurements of dissolved oxygen (DO) at the site showed that instream DO levels were driven by SAMs. We illustrate the effects on the stream ecosystem by SAMs in a high elevation, low gradient headwater system as well as the delayed but sizable impacts that forest fires can have on SAM communities within affected catchments.

Keywords: submerged aquatic macrophytes; disturbance; dissolved oxygen; high elevation

Tracking an Emergent Pathogen in Boreal Toads across a Southern Rocky Mountain Watershed

ERIC BROWN, NEW MEXICO HIGHLANDS UNIVERSITY

Bd chytrid fungus (*Batrachochytrium dendrobatidis*) is an emergent pathogen with cosmopolitan prevalence. Its arrival in novel regions has led to the extirpation and extinction of various amphibian species worldwide and threatens many others. In this study, we follow *Bd* as it spreads through habitat of the Boreal toad (*Anaxyrus boreas boreas*) in the Southern Rocky Mountains from 2014 to present. Contact with *Bd* has already extirpated the Boreal toad from New Mexico and is driving population declines in Colorado, both states in which it has a state endangered species status. To quantify the spread of *Bd* across wild toad populations, we collected skin swabs from wild toads in a watershed of the Collegiate Peaks region of Colorado. During breeding seasons of 2014-2016, *Bd* prevalence the first year of detection ranged from 64-90% and average *Bd* zoospore load on individual toads was 1,073 to 25,064 ITS1 copies. In the breeding season following first detection of *Bd*, we observed dramatic declines in adults at historic breeding sites. We also tested for presence of a related pathogen, *B. salamandrivorans*, and report that it was absent on Boreal toads in this watershed in 2016. In the interest of predicting future *Bd* movement, we also evaluated landscape features associated with known *Bd* spread since 2014. Understanding how this pathogen moves through the landscape will aid in management decisions to prevent its spread and support affected populations.

Keywords: *Batrachochytrium dendrobatidis*, *Boreal toad*, *endangered species*, *amphibian pathogen*, *landcover*

Invasive American Bullfrog (*Rana catesbeiana*): Friend or foe?

JESUS RIVAS, NEW MEXICO HIGHLANDS UNIVERSITY

Disturbance on an ecosystem may bring it to a different state than before the disturbance. Recovering from this disturbance could be a simple matter of time or may involve more complex situations. Some ecosystems develop stable alternate states from which they cannot easily be restored. American Bullfrog has been introduced in a many habitats affecting variety of organisms by preying on them and by outcompeting others. However the impact that they do in the ecosystem has seldom being quantified experimentally. In this contribution we eradicated Bullfrogs from a section of the Mora River and left another one unchanged and monitored the abundance of other aquatic organism in both sites to assess the impact of Bullfrogs. Bullfrogs exert top down control on many aquatic organisms. They negatively affect the abundance of Northern Crayfish (*Orconectes virilis*), another invasive, as well as fishes and keep fish parasites to a lower level. Elimination of Bullfrogs seems to be associated with an irruption of Northern Crayfish. While the data are preliminary and we expect the response to the eradication to take several years, at this point we are asking the question of whether eliminating Bullfrogs helped or hurt the ecosystem. Northern Crayfish are an aggressive invader that can make tremendous impact on the ecosystem. Monitoring this population in the long term will allow us to know if the Crayfish crashes after the initial irruption, or if it finds an alternate state where it is more harmful to the ecosystem than when the Bullfrogs were present.

Keywords: *American bullfrog*, *Northern crayfish*, *ecosystems*

SESSION F: SOCIAL & NATURAL SCIENCE NEXUS

Importance of Food-Energy-Water-Health Nexus for New Mexico

VIMAL CHAITANYA, NEW MEXICO STATE UNIVERSITY

With continuing trends in population growth and sprawl of metropolitan areas, provision of the basic human needs of food, energy, and water to the inhabitants is seen as a major challenge. For New Mexico, this challenge takes on another dimension as the population is sparsely distributed making it difficult to provide basic needs affordably without stressing renewable and financial resources. Being net consumers of food, energy, and water, infrastructure that continues to rely on old technologies to provide these basic needs is not sustainable. Development of infrastructure

that can recover and recycle energy and materials within the food-energy-water (FEW) sectors is being recognized as one of the best options to improve the sustainability of agricultural systems. The Energy Research Lab (ERL) at New Mexico State University (NMSU) is engaged in finding solutions pertaining to the nexus issues, primarily using Algal Biosystems. In this paper, we will summarize contributions to finding sustainable solutions to the nexus issues and focus on algal based, photosynthetically driven waste-to-energy recovery system for recovering energy, water, and nutrients from wastewaters (WW). The recovered water and nutrients can be utilized for the food production. The system is capable of WW treatment, net energy production, and recovery of irrigation-quality water and high-purity crop fertilizers. The mixotrophic algal system is capable of incorporating all the C, N, and P in UWW into biomass without any energy input, without any loss of C as CO₂ in the atmosphere and with solubilized N and P in concentrated form as byproducts for recovery and use as fertilizers.

Keywords: food-energy-water-health nexus, population growth, fertilizer

Policy Effectiveness, Spatial Dependencies and Energy Market: Evidence from the Renewable Portfolio Standard

JANAK JOSHI, UNIVERSITY OF NEW MEXICO

This research estimates the effects of the Renewable Portfolio Standard (RPS) on renewable energy capacity development in the United States. The RPS is a renewable electricity policy, which mandates the electric utilities to supply a certain percentage of renewable electricity over the specified time frame. This study uses the most recent data, from 1990-2014, in 47 states. The empirical estimation uses the panel fixed effect and spatial econometric methods. The results indicate the RPS increases the overall renewable capacity by 194 MW, where the impacts are heterogeneous for each renewable capacity. The RPS contributes positively to solar and wind capacity, while the evidence remains insignificant for biomass and geothermal. The technology specific results imply the potential amplification of RPS contributions if the policy specifies the mandates for each renewable technology separately. Finally, the spatial correlation of the RPS shows that the spatial rearrangement of the RPS across the states can change the renewable capacity.

Keywords: energy policy, renewable portfolio standard, renewable resources, spatial structure

A System Dynamics Analysis of Water Demand in the Lower Rio Grande

SAEED LANGARUDI, NEW MEXICO WATER RESOURCES RESEARCH INSTITUTE

Water demand models usually lack feedback mechanisms that are inherent in socioeconomic systems. For example, they consider population trends only as exogenous scenarios that will not be affected by the internal dynamics of the system and thus leading to unreliable prediction of key system behaviors. In this study, we develop a system dynamics model that takes into account key feedback loops that impact long-term trends of water use in the Lower Rio Grande Water Planning Region. The model acts as an overlay to the NM Water Resources Research Institute's Dynamic Statewide Water Budget (DSWB) model to predict the future of water use under different scenarios. While a separate model, it uses the DSWB data outputs to define and calibrate the system relationships and behavior. The model consists of 6 modules: economy, agriculture, power use, non-ag use, urban use, and water. Stocks of surface water and groundwater interact with each other and with the rest of the model in order to simulate dynamic behavior of the hydrologic system. The model achieves minimal reliance on exogenous drivers, with only two variables (surface water inflow and precipitation) existing exogenously, making it a novel tool for policy and scenario analysis. For the next step, we will use the model to assess the implications of alternative scenarios of land management policies and strategies. The model will also help us to find leverage points of the system that may lead to sustainable use of water without sacrificing social welfare of communities.

Keywords: system dynamics, water demand, Lower Rio Grande, feedback

Differences of Opinion: How Preferences for the Environment Differ Across Observable Factors

KARA WALTER, UNIVERSITY OF NEW MEXICO

Given the diverse energy resources in the state and preferences for environmentalism, we expect improved information concerning the state's citizens will be beneficial in future energy policy design. Using survey data from a statewide survey on preferences for energy in New Mexico, we employ a number of logic models to examine which observable variables influence the heterogeneity of preferences and opinions about the environment. Dependent variables include respondent's view on carbon dioxide regulation, public land use for energy production, local hydraulic fracturing issues, and environmental preferences from the New Ecological Paradigm scale. Based on previous analysis of data and extant literature, we know that preferences for the environment are correlated with many factors. Preliminary analysis of our survey data shows that preferences are correlated not only to socioeconomic characteristics and political leaning but also to respondent's geographic location, opinion about the economy and climate change. These results suggest that differences in NM are not simply a function of political preferences or working in the energy sector. By exploring which observable factors are correlated with environmental preference, we expect that policymakers will be able to understand better and target differences in opinions about policy changes.

Keywords: logic models, opinion surveys, environment, energy preferences

Accuracy in Malaria Diagnosis: Comparing Microscopy and PCR-Based Methods

J. AMPADU ADJEI, EASTERN NEW MEXICO UNIVERSITY

Accuracy in *Plasmodium falciparum* malaria diagnosis is an important issue in preventing and eradicating the disease in sub-Saharan Africa. Accurate diagnostic techniques are needed to avoid false negatives which lead to greater disease burden, as well as cases of false positives where unnecessary treatment can result in needless expense and the development of drug resistance. There are multiple considerations that arise when selecting a particular diagnostic method. These include cost, expertise required, time to diagnosis and, most importantly, sensitivity and specificity. Two diagnostic methods (thick smear Giemsa stain and nested PCR for the *Pfcr* gene) were compared in terms of diagnosis obtained. In addition, the chloroquine sensitivity or resistance of the samples showing positive by PCR was determined using XapI restriction digestion. Out of the 89 samples collected at the Clinical Analysis Laboratory in the Dept. of Biochemistry, KNUST, microscopy identified 42 as positive while 39 were identified positive by PCR. Of the positives identified by PCR, 19 were negative by microscopy while 20 were also positive by thick smear. There were, however, 22 samples that showed positive by microscopy, but were identified as negative in the PCR. Thus, 20 samples were positive by both methods and 28 samples were negative by both methods. The higher sensitivity of PCR makes it more reliable than microscopy, which is highly operator and protocol dependent. Overall, taking nested PCR as the gold standard, diagnostic accuracy by thick smear at the lab was 54%, which is in line with numerous results reported in the literature. Of the parasites detected in the patient samples, 97% were chloroquine resistant. Thus, sensitivity to the drug does not appear to be returning in Kumasi, as has been observed elsewhere on the continent. Overall resistance may even be increasing, as this value is higher than the ~87% reported in Kumasi by Abruquah et al. (Ghana Med J. 2010 June; 44(2): 52–58).

Keywords: malaria, PCR, microscopy, Africa

SESSION F: SOCIAL & NATURAL SCIENCE NEXUS

Electronic Structure Contributions to Molecular Rectification

RANJANA DANGI, UNIVERSITY OF NEW MEXICO

Fundamental advances in our ability to design and construct electronic components at the nanoscale will require new design paradigms. One of the proposed electronic components is the molecular rectifier. The original concept of a molecular rectifier was proposed by Aviram and Ratner in 1974 by using a donor-insulator-acceptor (D- σ -A) type molecular construct. Molecular and molecule-based electronic components are advantageous to the ease of synthetic

manipulation coupled with the fact that the size dimensions of molecules are inherently at the nanoscale (0.5–3nm). Here, we study donor-bridge-acceptor biradicals as first generation models for understanding electronic structure contributions to molecular rectification. Constitutional isomers of the donor-bridge-acceptor biradical (NN-Th-Py-SQ) (S=1/2 ortho-semiquinonate, SQ; A: S=1/2 nitronlynitroxide, NN; Th = thiophene; Py = pyridine) complexes serve as constant bias analogs for molecular current rectifying devices. The efficiency of rectification is given by the rectification ratio (RR = $g_{\text{forward}}/g_{\text{reverse}}$; where g = conductance). The experimental RR that we derive from measured magnetic exchange couplings (JSQ-NN) is calculated to be RR = 1.58. The experimental RR shows good agreement with the computed RR of 1.24 at +/-2.56V. Spectroscopic studies and bonding calculations provide insight into the electronic origin of the RR, the effects of bond torsions on the RR, and the nature of the current carrying molecular orbitals. We will discuss our results in terms of newly developed molecular design rules for rectification and the roles of the bridge HOMO and LUMO in magnetic coupling and bias dependent rectification.
Keywords: molecular rectification, donor-bridge-acceptor, biradicals

Excited State Processes in Radical Elaborated Cyclometalated Platinum Complexes

SANGITA PAUDEL, UNIVERSITY OF NEW MEXICO

Understanding of the lowest triplet excited state of organo-transition metal complexes is useful for wide range of applications such as emitting materials in Organic Light Emitting Diodes(OLEDs), Light Emitting Electrochemical Cells (LEECs), chemosensors, photosensitizers etc. However, improvement of ligand design strategies for preparing highly luminescent and color tunable organo-transition metal complexes with desired triplet excited state lifetimes is still a challenge. Here, we aim to explore the influence of radical substituents on electronic structure, luminescence quantum efficiencies, and excited state lifetimes by synthesizing new radical elaborated molecular frameworks built on known cyclometalated square planar platinum(II) complexes. We are studying their excited state processes using numerous spectroscopic methods that include EPR, MCD, photoluminescence, and transient absorption spectroscopies. These spectroscopies probe both ground and excited state electronic structure and are used to calibrate the results of both bonding and spectroscopic calculations. Our present study focuses on investigating the effects of localized pendent radicals on the photophysical properties of the chromophore, specifically with respect to how the spin-doublet radical substituent may facilitate radical enhanced intersystem crossing (radical enhanced ISC) through new exchange interactions within multiple spin centers. Furthermore, this study of multi-spin excited state dynamics of radical elaborated molecular frameworks will allow direct control of dynamic electron spin polarization through exchange manipulation of the photoexcited triplet state of the chromophore.

Keywords: excited state processes, platinum complexes, organic light emitting diodes

Controlled Nanomorphology of Hybrid Organic/Inorganic Multi-Component Composites through Cooperative Non-Covalent Interactions

LINGYAO MENG, UNIVERSITY OF NEW MEXICO

Hybrid organic-inorganic materials have evolved into a remarkable class in the field of Materials Chemistry, as they combine the advantages of both the organic and inorganic worlds to be applicable for a wide range of technological applications. However, simple mixing of organic and inorganic components into one composite often results in structures that lack of long range order and precise arrangement. To solve this problem, we have developed a logical supramolecular approach to form stable and controlled hybrid nanocomposites for applications in next-generation photovoltaic (PV) technology. We demonstrate the formation of stable and controlled nanomorphology of polymer/quantum dots (QDs)/fullerene ternary blends. We show that by capping QDs with different ligands, synthesizing conjugated polymers and fullerene derivatives with different functional groups, we can specifically assemble them into a well-ordered core/shell structure through non-covalent interactions including hydrogen bonding, ionic interactions, etc. In the meantime, some added values, such as broader light absorption range when combined with PbS QDs, magnetic properties when combined with iron oxide nanoparticles, can be obtained. Our research can potentially help to gain a better control over the nanoscopic order and spatial arrangement of the inorganic building blocks relative to the organic moieties, and also contribute to a better understanding of the structure-property relationships at the microscopic and macroscopic scales.

Keywords: organic photovoltaic, conjugated polymer, quantum dot, fullerene, self-assembly

UNDERGRADUATE POSTER SESSION ABSTRACTS

Poster session participants are listed alphabetically by last name of registered presenter.

Geothermal Membrane Distillation in Industrial Greenhouse Applications

ALLIE ARNING, NEW MEXICO TECH

Masson Greenhouse is a large-scale indoor greenhouse that employs geothermal brackish water for space heating. Coupling heat exchangers with membrane distillation (MD) would allow Masson to simultaneously extract energy and purified water from the geothermal fluid. MD has the potential to replace the greenhouse's current RO system used for irrigation, and would meet their water demand at a much lower cost. Polyvinylidene fluoride (PVDF) based hollow fiber membranes (HFMs) were fabricated via the dry-jet wet-spinning process and the structure of the membranes was characterized using porometry and scanning electron microscopy. A pilot-scale MD system was set up with the PVDF HFMs to evaluate the feasibility of full scale implementation for water purification at Masson Greenhouse.

Keywords: membrane distillation, greenhouse, geothermal water

Performance improvement and sensitivity of carbon nanotube-based sensors for medical applications

SAMANTHA CEBALLES, NEW MEXICO STATE UNIVERSITY ABDESSATTAR ABDELKEFI, NEW MEXICO STATE UNIVERSITY

In recent years, the research of carbon nanotubes (CNTs) has significantly increased due to their unique material properties. These properties can include high strength and stiffness, high thermal conductivity, and high flexibility. Specifically, for their high stiffness, CNTs are considered as target candidates in medical applications, such as the detection of cancer cells. In this application, the goal is to be able to detect and identify the mass of nanoparticles in the zeptogram range deposited on a CNT based upon a frequency shift and conversion to an equivalent mass. Because experiments in this field are time consuming, difficult, and expensive, the goal is rather to develop accurate reduced-order models that capture phenomena occurring at nanoscale and eventually lead to the detection and characterization of nanoparticles. In developing these models, several different theories, their assumptions, and challenges should be considered including beam theories, shell theories, theories in nonclassical continuum mechanics, and more. In addition, different environments should be considered to most accurately reflect experimental results, i.e. CNTs in a thermal environment. In addition, the geometry of the particle should be considered for specific cases. Considering each of these factors, the limits of applicability of various theories will be discussed, along with their corresponding assumptions and formulation. In doing so, mathematical models reflecting the true behavior of CNTs as biomass sensors can be developed, along with methods for detecting the mass based upon the inherent frequency shift.

Keywords: carbon nanotubes, reduced-order models, materials science

Arsenic Comparison of Irrigated and Non-Irrigated Soils in the Middle Rio Grande Valley

DUSTIN DEALY, UNIVERSITY OF NEW MEXICO VALENCIA TRACY TERRY, UNIVERSITY OF NEW MEXICO VALENCIA
VICTOR FRENCH, UNIVERSITY OF NEW MEXICO VALENCIA

Arsenic levels in ground water of the Middle Rio Grande watershed of New Mexico (20 ppb to an excess of 600 ppb) and in the Rio Grande itself (2-16 ppb) are higher than the EPA standard for drinking water (10 ppb). Years of irrigation with these high arsenic content waters may lead to build up of arsenic in the fields and increased uptake of arsenic in crops grown in these fields for both human and livestock consumption. In order to determine the extent of arsenic build up in farmed soils due to irrigation, a map of the arsenic content of unfarmed soils is being created between the Rio Grande and the Manzano Mountains parallel to HWY 60 in northern Socorro County. Of particular interest is the depth and arsenic content of the caliche layer where salts tend to deposit after rain events. This data is being compared to the depth and arsenic content of the caliche layer of irrigated soils in northern Socorro and

southern Valencia Counties. Soil samples were taken in 6-inch increments using a soil auger until the caliche layer was visually determined in the field. Samples were dried and analyzed via X-ray fluorescence spectrometry (XRF) for arsenic content.

Keywords: arsenic, irrigation, Middle Rio Grande Valley

The Benefits and Feasibility of Converting Our Locomotive's Engines from Diesel to Natural Gas

DAVID DODD, MESALANDS COMMUNITY COLLEGE

With the global concerns of greenhouse gases, ongoing research in the conversion of locomotive engines from diesel to natural gas is extensive. Many studies show that the amount of carbon dioxide and other greenhouse gases emitted from locomotives can be lowered with the conversion of engines from diesel to natural gas. There are two different methods to convert diesel engines. One method is the use of liquefied natural gas (LNG). This method involves supercooling the natural gas to a -260 ° Fahrenheit, turning it into a liquid form. The second method is the use of compressed natural gas (CNG). This method involves compressing natural gas, consisting mostly of methane, to less than 1% of its volume at standard atmospheric pressure. Independent studies of locomotive engines converted to natural gas in use in Japan and Canada show that conversion is feasible for locomotive engines. United States governmental studies confirm the independent studies. The California Air Resource Board (CARB) found that CNG emits 20%-29% fewer greenhouse gases compared to diesel.

Keywords: natural gas, greenhouse gases

Applying GIS Tools to Verify Weather Forecasting Models over a Domain in Southern California

ULRICK FRANCISCO, NAVAJO TECHNICAL UNIVERSITY JAYVION CHEE, NAVAJO TECHNICAL UNIVERSITY
GILBERT BENALLY, JR., NAVAJO TECHNICAL UNIVERSITY

Current verification approaches have limited abilities to observe subdomain error variations and to partition them in ways that can improve atmospheric sciences. Our approach was to determine if we can employ GIS tools to assess and verify weather forecast over a terrain. We investigated the spatial analysis tools that are available within QGIS to perform forecast analysis with respect to high resolution terrain and land use variables. We demonstrated how GIS can be applied to building models through spatial analysis through remote sensing methods. Remote sensing is the study of objects from great distance, by obtaining images of the earth's surface. We classified land terrain based on its characteristics; such as vegetation, water, soils, and infrastructure. We also used GIS tools in attempts to look for trends and model errors. In an effort to correlate the mean of errors with its domain, we observed these errors with its terrain characteristics. By doing so, we assessed different aspects using remote sensing methods through GIS tools. We hope to improve errors with the use of remote sensing images of higher band resolution. Overall, we were able to use spatial data through GIS tools using remote sensing methods and bring new approaches in analyzing models from different classification perspectives.

Keywords: GIS, weather forecasting, remote sensing

Anthropogenic and Rheocrene Springs in the Cibola National Forest

BRITTANY GRIEGO, UNIVERSITY OF NEW MEXICO CORY WALK, UNIVERSITY OF NEW MEXICO
KATE MENDOZA, UNIVERSITY OF NEW MEXICO LIVIA CROWLEY, NEW MEXICO BUREAU OF GEOLOGY
TYLER PENNINGTON, UNIVERSITY OF NEW MEXICO LAURA CROSSEY, UNIVERSITY OF NEW MEXICO
REBECCA BIXBY, UNIVERSITY OF NEW MEXICO

Springs are an important water resource both for anthropogenic use and support of ecosystems in the arid Southwest. Springs are classified into several different types for purposes of better management. Five spring types are found in the Cibola National Forest in northern New Mexico: Anthropogenic, Rheocrene, Helocrene, Hypocrene, and

Limnocene. In the Cibola National Forest, anthropogenic and rheocene are dominant spring types. Some of the springs visited for this study were Cole, Big, and Upper Fourth of July (all anthropogenic) due to the human alterations to the spring itself. Torro Spring is a Rheocene type due to its flow into a stream or a river. We collected samples from the spring water itself to be analyzed in the lab, wildlife demographics, and in field water quality parameters such as flow discharge and acidity and basic levels of the water at the source. In the lab we analyzed stable isotopes, pH levels, and major solute composition. These data are also compiled into a regional database to provide important baselines for future comparison. We show here the co-parative data for all sites visited in 2017, and compare results with other regional springs.

Keywords: natural springs, geology, geothermal waters

Identification of Markers Contributing to White Mold Resistance in Peanut Using Quantitative Trait Loci Sequencing

ESTRELLA GUTIERREZ, NEW MEXICO HIGHLANDS UNIVERSITY MICHAEL GONZALES, UNIVERSITY OF GEORGIA
JOSH CLEVENGER, UNIVERSITY OF GEORGIA SCOTT JACKSON, UNIVERSITY OF GEORGIA

Peanuts are an important crop in several regions of the world for their high essential vitamin properties. Peanuts and peanut oil are used for human and animal consumption, and in a variety of consumer items including paint and furniture polish. Peanut production in the Southeast U.S. is afflicted by white mold, *Sclerotium rolfsii*, and has been for as long as peanuts have been produced in the United States. White mold is the number one cause of yield loss in a season and is particularly hard to manage with fungicides in arid climates. This study utilizes Quantitative Trait Loci sequencing (QTL-seq) to test if markers for white mold resistance can be developed faster and more efficiently. QTL-seq is an approach done by whole-genome resequencing of DNA from two populations showing a desired phenotypic trait and its opposite (i.e. resistance and susceptibility) for a rapid identification of plant QTLs. Our hypothesis is that QTL-seq methods can identify chromosomal regions and markers important to white mold resistance in peanuts. In this study, we phenotyped three years of recombinant inbred lines and ranked the top 5% mold-resistant and bottom 5% mold-susceptible phenotypes. The resistant and susceptible groups were sequenced and mapped to two reference genomes. We estimated allele frequencies at single nucleotide polymorphism sites for both groups, and we observed peaks indicating resistance on chromosomes A01 and A05. We then identified and developed markers spanning resistance hotspots on these chromosomes. These resistance markers are expected to facilitate future selection for mold resistance, which will help farmers cultivate healthier, higher yield crops and reduce the use of fungicides. With this information, the future direction would be to use QTL-seq to find resistance to other diseases, such as late leaf spot (*Mycosphaerella berkeleyi*).

Keywords: white mold, peanut, fungal resistance

Novel Inorganic-Organic Hybrid Material for Selective Uranium Adsorption from Natural Water Supplies

CHASE KICKER, NEW MEXICO TECH LILYA FROLOVA, NEW MEXICO TECH
SAMANTHA SAVILLE, NEW MEXICO TECH

Based on a novel covalent modification method of graphite surfaces we developed a new highly chemically stable adsorbent for selective uranium adsorption from natural water supplies. Commercially available graphite is chemically modified with tetracyanoethylene oxide via 1,3- dipolar cycloaddition. The modified material shows high selectivity towards uranium even in the presence of competing cations like calcium and magnesium. It further demonstrates that uranium adsorption is not hindered by the presence of many other cations or the change in the pH of the medium. The material showed high affinity and selectivity for natural samples of uranium contaminated water. We showed that overall uranium adsorption is best in basic conditions. We also demonstrated that different mineral acids have different effectiveness at stripping the column of collected uranium and the regenerating of material capacity. Finally, we studied the ability of different oxidation reagents to change the uranium adsorption properties of new material.

Keywords: materials science, Uranium adsorption, water quality

Assessing the Potential Benefits of the Fungal Endophyte to its Locoweed Host *Oxytropis sericea*

MONIQUE LOPEZ, DINE COLLEGE

REBECCA CREAMER, NEW MEXICO STATE UNIVERSITY

AZIZA NOOR, NEW MEXICO STATE UNIVERSITY

Locoweeds are *Astragalus* and *Oxytropis* sp. plants that contain the toxin swainsonine, which is produced by fungal endophytes (*Alternaria* section *Undifilum* sp.) living within the locoweed plants. When ingested by grazing animals, the alkaloid toxin causes severe neurological toxicosis. Since toxic locoweeds are found throughout the western United States, the toxicosis causes considerable losses to grazing livestock. The *Alternaria* section *Undifilum* sp. endophyte does not hurt its plant host and could help its plant host by preventing the establishment of plant pathogens. To assess the potential for *Alternaria oxytropis* endophyte to protect its locoweed host from plant pathogens, samples of *Oxytropis sericea* plants were collected from a common garden in Logan, UT, 10 with the endophyte (+) and 6 without the fungus (-). Fungi were cultured from the stems and leaves of the plants using a low stringency surface sterilization and the resulting fungi were characterized by morphology, PCR amplification of the ITS region, and sequencing of the amplified nucleic acids. Fungi were cultured from 100% of endophyte+ plants that contained the endophyte, with 90% of the leaf pieces and 45% of the stem pieces yielding fungi. Fungi were cultured from 90% of the endophyte - plants, with 26% of the leaf pieces and 17% of the stem pieces yielding fungi. The endophyte was cultured from the endophyte+ plants and only a few other fungal species were cultured. The endophyte - plants yielded a diverse set of fungi. These culture results are consistent with those for locoweeds from China.

Keywords: locoweeds, toxins, fungi

Photoexcitation in Organometallic Nickel Complexes Used to Study Ligand-to-Ligand Charge Transfer

ADRIANA LUJAN-PAEZ, WESTERN NEW MEXICO UNIVERSITY

Synthesis of metal-ligand complexes for the study of photoexcitation states involved with ligand-to-ligand (L-L) charge transfer. Target complexes focused on the use of nickel as a metal bridge, dichalcogenolene ligands as electron donors, and diimine ligands as electron acceptors. Specific bidentate compounds were chosen to bind to the nickel in a square planar geometry to optimize charge transfer between donor and acceptor ligands. These photoexcitation behaviors are often referenced when study the efficiency of photovoltaic compounds, which can be applied to solar energy materials. Various diagnostic tests can reveal more about the photoelectrical behaviors of each complex and observe efficiency based on ligands bound to the nickel. The use of nuclear magnetic resonance, mass spectroscopy, and X-ray crystallography, allow for further confirmation of each of the nickel complex structures. The use of Raman spectroscopy would allow for the observation of the donor-acceptor energy states, and compare results with existing complexes with similar characteristics. The crystal structures of a few of the complexes can be viewed and analyzed through X-ray diffraction. Synthesis of these complexes has already proven fruitful and a few of the products have visible crystalline structures. Methods used to synthesize the compounds were adapted from an existing synthesis procedure (Kamenicek, 2008). Issues with synthesizing one of the compounds were overcome by using a modified, bench-safe procedure. Further syntheses will focus on complex behaviors using different ligand structures.

Keywords: photoexcitation, charge transfer, metal-ligand complexes

Investigating the Chemical Composition of Uranium Mine Samples from New Mexico

DANIELSON MORENO, CENTRAL NEW MEXICO COMMUNITY COLLEGE

With over 28,000 unremediated abandoned mines in the US, the potential adverse health effects mine contamination has, due to run-off in the surrounding environment, is cause for study and understanding. This experiment helps understand the chemical composition of soil samples taken from the Jack Pile and Saint Anthony Mine in New Mexico. By analyzing the chemical composition, a more accurate understanding of runoff can be obtained. Since many forms of minerals and rocks that exist in mines, this study aims to explore the levels of organic carbon, uranium, and other

co-occurring metals concentrations from the solid samples. Do samples with containing uranium also contain levels of organic carbon? The techniques used include: XRD, ICP-OES, LOI and TGA. ICP-OES and XRD will indicate what types of metals and their concentrations. LOI and TGA will indicate organic carbon content. The samples studied contained elevated levels of organic carbon as well as elevated levels of uranium. Understanding the concentrations of uranium and other co-occurring metals present in organic carbon-based rocks and minerals will help us understand the overall presence of uranium and co-occurring metals at these mine sites. If the presence and concentration of these metals can be better understood, then understanding the mine and its effects on the surrounding area.

Keywords: abandoned mines, Uranium remediation, geochemistry

Climate Variability Over the Past 2,500 Years in the Southwest United States

HOLLY OLIVAREZ, UNIVERSITY OF NEW MEXICO

Scientists have documented large amounts of precipitation data in the southwest region of the United States over the last 2000 years. Precipitation patterns vary greatly, and the causes of the variations in climate are unknown. There are proven persistent climate modulators, such as ocean circulation, volcanic activity, and solar variability, which affect precipitation. The most valuable data comes from climate oscillators PDO, ENSO, and AMO, which cycle regularly in patterns that can be measured over years and decades. The Southwest's winter precipitation comes from Pacific-driven rain (PDO and ENSO), and summer precipitation comes from our monsoon season (driven by the Gulf of Mexico and Gulf of California (AMO)). The purpose of our study is to perform a time series analysis of a data set from samples obtained from stalagmites in caves in southwestern New Mexico; so that we might find correlations between the records found in stalagmite rings and precipitation pattern data already obtained. Using wavelet analysis, the data can be examined for the strength of climate variabilities in the past. Combining this analysis with another technology, called Redfit, will allow historical information (gathered from multiple sources) into one presentation; in order to determine if a cause for precipitation variability can be found.

Keywords: climate, precipitation, stalagmites

In Vivo Toxicity of Different Shaped GNPs

TRISTAN ORTEGA, NEW MEXICO HIGHLANDS UNIVERSITY JESSICA SNOW, NEW MEXICO HIGHLANDS UNIVERSITY

Due to their myriad biomedical applications, gold nanoparticles (GNPs) have recently become a focus of heavy research. However, little is known about how the shapes and sizes of GNPs correlate to toxicity, as well as how the properties confer in vivo benefits. This research focuses on what effects might arise from in vivo star and spherical shaped GNPs. Previous research indicates that when mice are administered sphere shaped GNPs, they may suffer adverse effects because of accumulation in the liver, spleen, hippocampus, stomach, and other organs. As a result, anorexia may develop from the administration of GNPs by concentrations of nanospheres inhibiting the passage of fluids. Therefore, we hypothesize that in vivo toxicity of both spherical and star-shaped GNPs will result in decreased weight gain in mice. In order to test this hypothesis, C57/bl6 mice were randomized and injected with either GNP spheres, stars, or sterile H₂O (control group). In contrast to our hypothesis, we found that mice tolerated injections of GNPs, and weight gain between groups did not differ. Future studies will address the effect of additional doses of GNPs and how they affect the major organ systems.

Keywords: gold nanoparticles, in vivo toxicity, anorexia

Use of Mayfly Habitat as Indicator of Uranium Pollution

DIONNE PAUL, DINE COLLEGE

The USEPA Region IX Cove Watershed Assessment Project (CWAP), currently conducted on the Navajo Reservation in southern Cove, AZ includes Tronox, formerly known as Kerr- McGee, a contributor to the abandon uranium mines (AUM), whom left approximately 50+ mines open and unattended. The project's focus is around the community of Cove, Apache County, Arizona. Team hike consists of several interns, scientists and project managers. The duties of lead scientists and Dine College interns is to assist in collecting samples from the streams in Cove. One section of

this study protocol, “Stream Ecosystem Monitoring (SEM)”, include Section 7.2, “collecting macroinvertebrates”. The heavy elements of concern that may be in the stream could be contaminating the Cove Watershed flood bank drains, which eventually flow to the agriculture and livestock down below into the Cove community.

Keywords: water quality, Uranium, ecosystem monitoring, mayfly habitat

Characterization of protein methyl transferases in *Caulobacter crescentus*

MARIAH PAUL, DINE COLLEGE

INOKA MENIKPURAGE, NEW MEXICO STATE UNIVERSITY

ADDI MOYA, NEW MEXICO STATE UNIVERSITY

PAOLA MERA, NEW MEXICO STATE UNIVERSITY

Methylation is the process carried out by methyltransferases to add a methyl group to proteins and then change the protein's activity. It is known that in eukaryotic cells, the methylation process regulates cytoskeletal proteins (Park et al., 2016). However, in prokaryotic it is still being studied. Our hypothesis is that a set of predicted methyltransferases have a regulatory effect on the cytoskeletal proteins in the bacterium *Caulobacter crescentus*. To test our hypothesis, we deleted 5 genes that are predicted to be the methyltransferases. I worked specifically on deleting gene CCNA_00389 from the wildtype strain. Using double recombination, I constructed the strain Δ CNA_00389, which allowed me to further investigate the gene had an effect on the entire wild type cell. I used colony PCR protocols and DNA gel electrophoresis to confirm the deletion of this gene from the chromosome. I performed growth curves of Δ CNA_00389 and of five other strains that had the other putative methyltransferases deleted. Each strain was grown in different nutrient levels: rich nutrients (PYE) and minimal nutrients (M2G) for cell growth. My results showed that the Δ CNA_00389 and Δ CNA_00389 grew faster than wildtype in PYE media. It also showed that these mutant strains grew at the same rate in M2G. I am now testing if these mutants have defects in morphology and swimming ability. The importance of my project is to gain a better understanding of methyltransferases and how they affect the cytoskeletal proteins. Having enough knowledge of a prokaryotic cell, doctors, researchers, and scientist will have better ways of killing bacterial pathogens.

Keywords: methyltransferases, bacterial pathogens, prokaryotic cells

Uranium-bearing dust dissolution in simulated lung fluid electron microscopy

SHAYLENE PAUL, DINE COLLEGE

BONNIE FREY, NEW MEXICO TECH

GAYAN RUBASINHEGE, NEW MEXICO TECH

DAN CADOL, NEW MEXICO TECH

The purpose of this research is to identify the dissolution of uranium dust bearing particles and mineral samples from two types of artificial lung fluids. The study's dissolution of the samples in the two types of lung fluid called “Artificial Lysosomal Fluid (AFL³)” and Gambles Solution. In New Mexico there are many uranium mines that are left open and unprotected from the elements of the weather. These mines are close to many communities and many of these community members worked for uranium mines. New Mexico has many dust storms that can carry dust particles for many miles. The particle size of dust is wind captured from 1.5 meters high near a uranium mine. Soil Samples are taken from a mine waste pile. The dust samples were taken from Jackpile Mine in Cibola County, NM and St. Antony mine soil sample from Laguna Reservation. The study's conclusion pointed out that the soil sample that was taken from St. Anthony mine were mineral samples of uranium and had different chemical composition than the dust particle samples. This could be described as a scenario of uranium workers working and inhaled uranium from within the mines would affect their lung tissue (AFL³). AFL³ replicates as an immune response to foreign substances that enters the lung. The dust particles from an open pit mine could blow around and affect close communities. The person could inhale uranium dust bearing particles and affect the deep lung tissues (Gambles solution). This means that the different uranium chemical composition of its changing states effects the human lung tissues differently by the dissolution dust particles and soil/mineral sample. Both can cause serious health effects and there needs to be more research done, but it gives an idea to open mines that are in the Navajo Nation. There needs to be more research due to large error bars in the data because there may have been contamination during the study. This study gives an idea to how the 1950-1967 uranium workers were affected during their time in the mines and today's long- term effects.

Keywords: microscopy, Uranium transport, lung fluid

Synthesis of First Row Transition Metal Nanoparticle for Aerosol 3D Printing

DIANA PERALES, SANDIA NATIONAL LABS

TIMOTHY BOYLE, SANDIA NATIONAL LABS

LARICO TREADWELL, SANDIA NATIONAL LABS

ADAM COOK, SANDIA NATIONAL LABS

NELSON BELL, SANDIA NATIONAL LABS

W. DERRICK REINHOLTZ, SANDIA NATIONAL LABS

DEVONTE WOODARD SANDIA NATIONAL LABS

Direct Write (DW) manufacturing methods can precisely print microcircuits, computer chips, and other electronics. Currently, DW methods have focused on silver and gold printed electronics due to their high conductivity. However, these materials are very expensive, thus, we have been investigating other metals as a more economically favorable alternative such as copper. Copper possess similar conductivity but is significantly lower in cost. In addition to copper, we have expanded our research to other first row transition metals due to their diverse properties such as magnetism, conductive abilities, and corrosion resistance. In order to print these metals effectively, nanoinks (or N-inks) need to be developed, which requires high quality nanometals. In order to generate these nanometals, a variety of tailored precursors such as metal alkoxides, amides, alkyls, as well as commercially available compounds (i.e., metal carbonyls) were explored for optimal (size and shape) nanometal synthesis. All aspects of the precursor synthesis, nanomaterials, N-ink formulation, and final properties of printed metals will be presented.

Keywords: nanometals, Direct Write methods, 3D printing

Investigating the Chemical Composition of Solid Samples from the Jackpile Sandstone Member of the Morrison Formation in New Mexico

ANTONELLA RIEGA, UNIVERSITY OF NEW MEXICO

CARMEN VELASCO, UNIVERSITY OF NEW MEXICO

ABDUL-MEHDI ALI, UNIVERSITY OF NEW MEXICO

JOSÉ CERRATO, UNIVERSITY OF NEW MEXICO

We applied spectroscopy, microscopy, and water chemistry techniques to characterize two mining sites from the Jackpile sandstone member of the Morrison formation, Saint Anthony and the Jackpile Mine; two samples from each site were studied. Specifically, Thermogravimetric Analysis (TGA), X-Ray Fluorescent (XRF), and Inductively Coupled Plasma Optical Emission Spectrometry (ICEP-OES) were used to characterize the samples from each site. Prior to performing the characterization, the material was first homogenized and sieved to a particle size of <math><63\ \mu\text{m}</math>. TGA analysis corroborates that the Loss on ignition (LOI) of the samples are on average 13.18% and 22.78% for the Jackpile Mine and Saint Anthony sites, respectively. Results from XRF for the Jack Pile Mine show that the major elements are iron (9.62%), calcium(3.70%), uranium (3.44%), potassium(1.34%) and Carbon (1.70%) while for the Saint Anthony are uranium (4.11%), iron (2.83%), carbon(2.35%), potassium(1.18%) and calcium(0.57%). The mean concentration of metal acid extractable for the Jackpile Mine are iron (6.49%), Aluminum (1.32%), uranium (0.64%), calcium(0.69%) and potassium(0.5%) while for the Saint Anthony are uranium (1.71%), Aluminum (1.36%), iron (0.38%), potassium(0.18%) and calcium(0.09%). This study identified the relevance of characterization of mines sites to better understand mobilization of different minerals and metals in the environment.

Keywords: Uranium; chemical composition; characterization; New Mexico mines

Medicinal Plant Extraction and Analysis

SHANIA SANCHEZ, UNIVERSITY OF NEW MEXICO VALENCIA

VICTOR FRENCH, UNIVERSITY OF NEW MEXICO VALENCIA

TRACY TERRY, UNIVERSITY OF NEW MEXICO VALENCIA

Traditional healers have used medicinal plants for ages while more recent efforts have yielded the isolation of plant pharmaceuticals such as aspirin, quinine, and paclitaxel. A rise in interest from across society has led to a rapid growth in the essential oils industry which is expected to double in market value between 2014 and 2020. We have begun a survey of the medicinal properties of common plants of the southwest. Steam distillation for essential oils and solvent extractions have been carried out on various locally sourced plants. These extracts have been analyzed for antibiotic properties via Kirby-Bauer assay using *E. coli* on Mueller Hinton agar. Zones of inhibition were analyzed and compared to antibiotics Ciprofloxacin, a positive control, and Penicillin, a negative control. Other assays for

biological activity will be conducted in the future. As active agents are identified, further isolation and analysis of compounds and possible synergistic effects will occur.

Keywords: traditional healing, medicinal plants, ecology

Novel Hypersaline Strains of Microalgae Growing in Saline Produced Water

JONATHAN SCHWILLING, SANTA FE COMMUNITY COLLEGE THOMAS HOPKINS, UNIVERSITY OF NEW MEXICO
SERENA INGRAM, FORDHAM UNIVERSITY ANDY SCHULER, UNIVERSITY OF NEW MEXICO
LUKE SPANGENBURG, SANTA FE COMMUNITY COLLEGE STEPHEN GÓMEZ, SANTA FE COMMUNITY COLLEGE

In this study two hypersaline strains of algae, a highly enriched polyculture from produced water (PW) (“Blue-Cyano”) (BC) because of its blue color) and another, *Dunaliella tertiolecta*, obtained from UTEX Culture Collection were cultivated in dual open raceway pond (ORP) systems using PW diluted to salinities of 30‰ and 70‰. BC did not initially demonstrate high growth, but dense algae cultures were eventually established in both ORP’s. *Dunaliella tertiolecta* was out-competed by pennate diatoms, amoeba, and rotifers. 23S rRNA genes from the polyculture were sequenced using Illumina MiSeq. The results suggest the culture consisted of *Cyanobacterium aponinum* (62.4%), Uncultured organism related to *Phycisphaera mikurensis* (25.8%), *Parachlorella kessleri* (9.0%) and *Scenedesmus* sp. (1.0%). ICP-OES analysis of the PW samples after cultivation of BC showed that group II cation concentrations were reduced in the reactors. Future work will be to determine if the BC culture can remediate PW so that it can be reused by the oil and gas industry.

Keywords: microalgae, produced water, polycultures

Osmotic Power Development: Acquiring Energy from Waste Water

SHANTAL SMART, SAN JUAN COLLEGE FRANK HUANG, NEW MEXICO TECH
LYNDA LAUMBACH, NEW MEXICO TECH RILEY REPROGLE, NEW MEXICO TECH
CAROLYN MEDIN, NEW MEXICO TECH ELIJAH NARANJO, NEW MEXICO HIGHLANDS UNIVERSITY
ALLIE ARNING, NEW MEXICO TECH

Geothermal greenhouses grow crops year-round without having to rely on natural gas for heating but still spend millions of dollars. But with the existing energy of the brackish geothermal fluid, membrane distillation can offer a great opportunity to meet the demand for irrigation with the geothermal fluid at a lower cost. Asymmetric hollow-fiber membranes were fabricated and characterized for their application to provide clean irrigation water through the use of the brackish geothermal fluid as the DCMD feed at Masson Greenhouse at Radium Springs, New Mexico. The membranes displayed a dual-layer cylindrical structure with an external sponge layer and an internal macrovoid layer. The intention is to prevent pore wetting from the hot saline fluid with the sponge layer, while using the macrovoid layer to increase the water flux and thermal efficiency of the membrane. Through the use of this irrigation system we can create clean recycled irrigable water.

Keywords: greenhouses; fiber membranes; Masson; direct contact membrane distillation (DCMD)

A Case Study of Pilot-Scale Continuous Flow Reactor for Hydrothermal Liquefaction of Algae

BRIAN TREFTZ, NEW MEXICO STATE UNIVERSITY FENG CHENG, NEW MEXICO STATE UNIVERSITY
TRAVIS LE-DOUX, NEW MEXICO STATE UNIVERSITY SCOTT WOOLF, NEW MEXICO STATE UNIVERSITY
JUANITA MILLER, NEW MEXICO STATE UNIVERSITY CATHERINE BREWER, NEW MEXICO STATE UNIVERSITY
UMAKANTA JENA, NEW MEXICO STATE UNIVERSITY

Algae-based biofuels have attracted significant research interest due to their advantages of not competing with land for food production, abilities to grow in low-quality water, higher growth rates, and strong CO₂-mitigation abilities. In recent years, research has focused on hydrothermal liquefaction (HTL) of whole, wet algae biomass. HTL uses hot, compressed water (270-350 °C and 8-18 MPa) to convert the organic constituents into an energy-dense “bio-crude

oil” that can be upgraded to liquid transportation fuels. Most HTL research studies to date have reported results from batch reactors of 100-2000 mL sizes operated at 5-20 wt.% algal solids load. In order to develop commercial scale operations, future HTL systems would need a significant technological shift from batch processes to development of continuous flow reactor (CFR) systems. CFR systems suffer from several challenges including smooth flow of biomass slurry through pumping/preheating unit/reactor units, clogging of solids, solid-liquid-gas separation/filtration, involvement of large number of unit operations and the safety and control issues. Unlike the batch systems, maintaining a high solids loads (>5%) pose a significant challenge for CFR systems. The current study presents New Mexico State University’s experience in development and modification of a pilot-scale CFR for HTL of fresh water microalgae. The goal of the reactor is to be able to perform continuous HTL on slurries with solid algae contents of 5-10 wt.%, and to produce char-free bio-oils. The presentation provides an overview of the operational issues with a continuous HTL reactor and the results of the recent runs.

Keywords: hydrothermal liquefaction, algae, water quality

GRADUATE STUDENT POSTER SESSION ABSTRACTS

Poster session participants are listed alphabetically by last name of registered presenter.

New Mexico "Continental Smokers": Geothermal Potential of Spring Vents that show Mantle Degassing and High CO₂ Content

JORDAN ANDERSON, UNIVERSITY OF NEW MEXICO

KARL KARLSTROM, UNIVERSITY OF NEW MEXICO

VALERIE BLOMGREN, UNIVERSITY OF NEW MEXICO

BENJAMIN HOLT, UNIVERSITY OF NEW MEXICO

JON GOLLA, UNIVERSITY OF NEW MEXICO

LAURA CROSSEY, UNIVERSITY OF NEW MEXICO

SHARI KELLEY, NEW MEXICO BUREAU OF GEOLOGY

CHRIS MCGIBBON, UNIVERSITY OF NEW MEXICO

CORY WALK, UNIVERSITY OF NEW MEXICO

Carbonic springs and wells in New Mexico exhibit evidence for mantle-to-groundwater connections. In addition to high CO₂ partial pressure, these vents (termed "continental smokers") have high 3He/4He ratios, major faults nearby, travertine deposits, and low mantle velocity regions below the surface. These attributes indicate crustal permeability capable of transporting fluids and heat from deep within the Earth to near-surface groundwater systems. They typically occur within tectonically extended regions of the Earth's crust with high heat flow. The term "continental smokers" arises from their similarities to oceanic smokers at mid-ocean ridges. Robust correlations exist between high 3He/4He values and regions of relatively low mantle seismic wave velocity. No strong correlation exists between helium isotope ratios and crustal thickness suggesting that regional mantle volatile sources are more essential than crustal conduit systems. Low seismic velocities in the mantle indicate partial melt, a logical source of deeply derived helium (3He) and CO₂-bearing volatiles. Springs and wells with the highest helium isotope ratios in the NM area (3He/4He in non-airlike groundwater) are located above the Valles Caldera (3.86 to 6.16 RA), Rico area of SW Colorado (4.75-5.88 RA), SE corner of AZ near the NM boarder (up to 4.23 RA), Bravo Dome (up to 3.78 RA), and Socorro magma body (NM Tech wells = 1.41 to 1.91 RA). This study also applies multiple geochemical tracer analyses to evaluate fluid mixing end members, fluid pathways, and the geothermometry of deeper fluids leading to a synthesis of geothermal resources in the New Mexico region.

Keywords: spring vents, continental smokers, geothermal

Fermentation of Wastewater-Grown Algae Through *Saccharomyces Cerevisiae* for Potential Bioethanol Production

DAVID ARELLANO, EASTERN NEW MEXICO UNIVERSITY

Utilizing a wastewater resource, cattle waste liquid, to effectively cultivate algal biomass is an extensively explored third-generation biofuel technique; the produced biomass could then be processed for fermentation to produce bioethanol. This bioremediation/cultivation pathway shows potential for a post third-generation bioethanol fuel source. Through experimentation and research this study aims to prove the viability and potential of this post third-generation bioethanol fuel source. Algal biomass is obtained from the Algal Turf Scrubber (ATS) system at Eastern New Mexico University in Portales, NM. The ATS operates with an indigenous algal community, composed of many different species and varieties including single cell and diatoms through to large filamentous species. Biomass is thoroughly lysed by using a combination of sonication and heat as proven by literature. The process sonicates the mixture, easily and quickly rupturing the cells, when followed by steam heating and pressure complete cell destruction can be attained. The resulting slurry is actively saccharified using mild acid and heat during the lysing process to hydrolyze available carbohydrates. Saccharification under these conditions renders the available complex carbohydrates into readily fermentable monosaccharides. *Saccharomyces cerevisiae* fermentation under controlled conditions has shown extensive removal of the same monosaccharides made available by lysing and then hydrolysis of algal biomass. Current inconclusive evidence suggests fermentation has occurred, however further analysis is required to determine total amount. Analysis of products of lysing and saccharification process, and of ultimate fermentation products will be done on a GC-MS.

Keywords: : Saccharomyces cerevisiae, bioethanol, algal biofuels

Hydrothermal Liquefaction of Algae Grown on Dairy Wastewaters

MESHACK AUDU, NEW MEXICO STATE UNIVERSITY

According to researchers the recent incidence of hurricane Harvey and Irma were linked to the contribution of climatic change. One of the biggest contributors to climate change is the release of greenhouse gases (especially from the combustion of fossil fuels) so the need for advance alternative energy (e.g bio fuels) cannot be over emphasized. Algae just like plants help to reduce the carbon contents in the atmosphere through photosynthesis, treat wastewater to acceptable limits and can also converted into useful energy dense biofuels. Hydrothermal liquefaction (HTL) is a thermochemical process of converting algae biomass into various bio fuels. The HTL process involves the use of sub-critical water (270-350°C and 8-18 MPa) both as a solvent and a reagent to convert the organic biomass constituents into energy-rich bio fuels. This study presents two strains of algae to analyze the influence of growth conditions on the biofuel yields. The Filamentous algae was grown in a fresh dairy water pond while the other strain we nicknamed Dr Myint's sample was grown in a brackish dairy water pond. According to the United States Geological survey (USGS) 71% of the earth is covered with water and the oceans holds about 96.5% of earths water (which is basically brine water), Since biofuels will be one of the future's alternative energy source, the need to grow algae faster and with cheaper resources to meet the market demand cannot be over emphasized.

Keywords: algae, Hydrothermal liquefaction, climate change, wastewater treatment

Post-Explosion Tracer Gas Study in Fractured Granite

SOFIA AVENDANO, NEW MEXICO TECH

CELESTE HERRERA, NEW MEXICO TECH

MELINDA HORNE, NEW MEXICO TECH

MARK PERSON, NEW MEXICO TECH

EUGENE GORMAN, NEW MEXICO TECH

ANASTASIA STROUJKOVA, NEW MEXICO TECH

JESUS D. GOMEZ-VELEZ, NEW MEXICO TECH

Radioactive noble gas detection at suspected underground nuclear test sites is the only proven way to confirm that a nuclear test has occurred. However, the migration of gas effluent through fracture networks is still poorly understood. A pilot field study of the gas migration through rock damaged by explosions was conducted in a rock quarry in New Hampshire in the summer of 2017. Tracer gas (SF₆), used as a proxy for the noble gas, was released into a cavity created by an explosion (63 kg of TNT at a depth of 13 m) during the summer of 2016. The upper 5 m of borehole were grouted with stainless steel tubing sealed in the concrete and the gas was pumped through the tubing. Before the gas release, we conducted a series of geophysical and hydrologic tests: a pump test, slug tests, a tracer test, and TEM and ERT surveys. Pressure and electrical conductivity transducers were placed in the surrounding boreholes to monitor the pressure changes and tracer arrival during the pumping. The results of the pump test show that the rock is well connected and has high permeability. We observed gas breakthrough immediately after the release. During the first minute after injection, a pressure wave was observed in two boreholes suggestive of inertial effects and hydraulic fracturing after gas release. The concentrations observed at each monitoring site are consistent with the pump testing. The results of this study will be used in our upcoming experiments and to test detailed mathematical models.

Keywords: radioactive gas, tracer gas, hydraulic fracturing

A Hydrogeochemical Analysis and Recharge Evaluation of Cienega Spring Located in the Sandia Mountains, NM

WESLEY CLARY, UNIVERSITY OF NEW MEXICO

LINDSAY WORTHINGTON, UNIVERSITY OF NEW MEXICO

LOUIS SCUDERI, UNIVERSITY OF NEW MEXICO

HUGH DAIGLE, UNIVERSITY OF NEW MEXICO

JOHN SWARTZ, UNIVERSITY OF TEXAS

Convergence and shallow subduction of the Yakutat microplate beneath North America has shaped the Pamplona zone fold and thrust belt in the northeastern Alaska subduction zone. Here, convergent tectonics and glaciomarine sedimentary processes have created patterns of deformation and deposition recorded by a shallow sedimentary sequence with varying fluid pressure, compaction, and fault activity. If the record of ice sheet advance is preserved

on the seafloor and in the underlying sediments then bathymetric evidence of glaciomarine processes should overlap with evidence of overpressure, such as low velocity zones in the shallow sediments. In this study, we present a velocity model through the Bering trough as well as regional drainage shape characteristics. We use streamer tomography on a seismic survey from the St. Elias Erosion and Tectonics Project (STEEP) to determine a velocity model. We further inform our interpretation using physical properties relationships developed with data from core samples (IODP Expedition 341) taken near the seismic line. To document drainage morphology, we use smooth sheet bathymetry to identify a drainage network and query profile shapes at well distributed locations; where profile shape is determined by fit with a power function. Initial results suggest overlap between u-shaped drainage profiles towards the SE end of the Bering trough and low-velocity shallow sediments NE of the shelf break. In part, because this overlap occurs within the mapped extent of the last glacial maximum, we find our tomography results consistent with buildup of overpressure due to glacially driven loading of highly saturated sediments.

Keywords: carotenoids, fatty acids, lipids, photooxidative stress, renewable resources, microalgae

Geochemical Characterization of Bouse Carbonates; Towards an Understanding of Bouse Diagenesis

CHRISTINA FERGUSON, UNIVERSITY OF NEW MEXICO
KARL KARLSTROM, UNIVERSITY OF NEW MEXICO

LAURA CROSSEY, UNIVERSITY OF NEW MEXICO
MICHAEL SPILDE, UNIVERSITY OF NEW MEXICO

This paper examines the Bouse Formation carbonates using stable isotope, Sr and SEM/microprobe data, and possible paleontological features to evaluate the extent to which carbonates retain their primary composition. These data could help determine marine versus non-marine depositional environment of the Bouse Formation, the record of first arrival of the Colorado River to the Gulf of California. The major goals are to decipher the diagenetic history of the Bouse and determine the nature of the tubular features found in some of the facies. Textural evidence from cut slabs and thin sections show mottled carbonate textures indicating multiple carbonate generations. Microprobe data have revealed amorphous silica intergrown with the carbonate; the silica replaces forams and other fossils and likely represents an important silica diagenetic event. Our present working hypothesis is that Bouse carbonates have undergone both silica and carbonate diagenetic events that have modified primary compositions such that interpreting and understanding the original environment relies on finding un-/ least-altered portions of the samples and then applying suitable microscale analyses. Tubular features resemble worm tubes and/or casts of vegetation; they have lengths up to several cm, sub-mm-scale inner diameters, and cm-scale outer diameter. One of the possibilities for these features is that they were formed by serpulids, a genus of tube worms. Comparison with published paleontological studies of serpulids is underway. There is one known fresh water serpulid, 5 known brackish/geothermal species, and more than 350 marine species. Thus, identification of serpulid species in the Bouse may have important depositional environment implications.

Keywords: geochemistry, Bouse Formation, carbonates

Shallow Reflectors in the Southern Albuquerque Basin from the Sevilleta Array

TORI FINLAY, UNIVERSITY OF NEW MEXICO

The Sevilleta Array was a dense seismic array deployed for 12 days in February, 2015 by collaborators from the University of New Mexico, New Mexico Tech, and Colorado State University. Approximately 800 vertical component, 10-Hz geophones were deployed across the Sevilleta National wildlife refuge in northern Socorro County, New Mexico. The array was designed to investigate the northern half of the Socorro magma body, an actively inflating mid-crustal sill. However, the data has provided an opportunity to examine shallow reflectors in the southern portion of the Albuquerque basin in addition to the magma body. Teleseismic virtual source reflection profiling (TVR) utilizes the free surface reflection of a teleseismic P-wave as a “ghost” source in dense arrays. During the deployment, the Sevilleta Array recorded 62 teleseismic events greater than M5. Applying TVR to the data collected by the Sevilleta Array, we present 2-D profiles created from the four events with the highest signal to noise ratio. Shallow reflectors

of interest dominate profiles taken from the northwestern-most quadrant of the array (near the Sierra Ladron uplift) and western edge of the Rio Grande rift. These reflectors may represent normal faulting from the region's past and present tectonic activity.

Keywords: Socorro Magma Body, seismology, Rio Grande Rift

Algal indicators of acidic inputs and intermittent flow in streams in the Valles Caldera National Preserve

APRIL FOX, UNIVERSITY OF NEW MEXICO

REBECCA BIXBY, UNIVERSITY OF NEW MEXICO

In freshwater ecosystems, there are many variables that can influence the distribution of biological communities including flow, pH, nutrients, and heavy metals. These habitats are a result of dynamic environments where physical and biological attributes vary in time and space. Diatoms and other algae often live within narrow environmental conditions, making them important ecological indicators of aquatic ecosystems. Algae respond to these environmental factors with changes in biomass and changes in species assemblages. For example, high conductivities and lower pH, caused by geothermal inputs, can dramatically influence water quality and biological communities in aquatic systems. Low pH, in combination with intermittent flow, may influence algal diversity in streams. The relationship between pH and flow in the Sulphur Creek watershed in the Valles Caldera National Preserve, New Mexico may be a contributing factor to the diversity of algal assemblages found in upstream reaches compared to communities found in geothermally influenced waters downstream. Seven sites within the Sulphur Creek watershed were sampled between May 2016-September 2016 for diatom composition, stable isotopes, major ions, and flow. Water quality and isotopologues indicate three distinct types of waters within the watershed and that geothermally influenced waters are causing episodic acidification of downstream Redondo Creek. A shift in diatom community structure is observed between upstream and downstream reaches of the watershed with acidophilic diatoms dominating waters with pH<4. Utilizing algal assemblage diversity as indicators of water quality in geothermal- influenced waters may assist in the ongoing reclassification of the Sulphur Creek watershed.

Keywords: : algae, water quality, geothermal, intermittent flow

Subsurface Characterization of Thermal Springs in Cascade Range and Olympic Mountains, Washington using Multiple Mineral Equilibria Geothermometry

JON GOLLA, UNIVERSITY OF NEW MEXICO

Alongside local (Cascades vs Olympics) lithologic (igneous rocks vs marine turbidites) and tectonic (complex fault clusters vs spaced subvertical thrusts) comparisons, estimated subsurface temperatures and mineral-fluid equilibria conditions are used to diagnose the geothermal flow paths of five Cascade Range (Carson, Bonneville, Ohanapeosh, Baker, and Carson) and two Olympic Mountains (Olympic Complex and Sol Duc) thermal spring sites. This work continues analysis of thermal spring chemistry data collected in the summer of 2016. All speciation calculations were done through SOLVEQ. Most estimated temperatures for Cascade waters (53-153 °C) are hotter than Olympic waters (53- 103 °C). These estimates generally fall within the ranges projected by some select conventional geothermometers (Cristobalite, Chalcedony, Quartz, Na/K, and Na-K-Ca). The average difference between reservoir and discharge temperatures is greater in the Cascade springs (\bar{x} difference: 53 °C vs 27 °C). Furthermore, the Cascade waters show more evidence of chemical evolution since ascent, as Carson (groundwater dilution=24%), Bonneville (CO₂ degassing=23%), and Ohanapeosh (CO₂ degassing=2%) were corrected for disequilibria. Conversely, all five Olympic springs are apparently still in equilibrium with their last reservoir. The geothermal fluids feeding the Cascade springs may be undertaking an indirect path to the surface, as reflected by a greater temperature difference between surface and reservoir and evidence of disequilibria and a structurally complex setting. On the other hand, the fully equilibrated Olympic waters appear to have been cooled to a lesser extent during upflow and cycled through thrust-imbricated turbidites, so there may be a more direct connection between the reservoir and the springs.

Keywords: thermal springs, CO2 degassing, Cascades

Invasive Bullfrogs May Not Be That Bad After All: Paine Effect and the Invasion Paradox

NICASIO GONZALEZ, NEW MEXICO HIGHLANDS UNIVERSITY JESÚS RIVAS, NEW MEXICO HIGHLANDS UNIVERSITY
CALVIN VIALPANDO, NEW MEXICO HIGHLANDS UNIVERSITY

Invasive species exert an unprecedented pressure on the trophic dynamics of an ecosystem. The American bullfrog (*Rana catesbeiana*) is well documented as an ecological threat, and is recognized as one of the most widespread and detrimental invasive species in the world. Because of their broad trophic niche they exert top-down pressure on the lower trophic levels. In northeastern New Mexico, at the Rio Mora National Wildlife Refuge, we are studying the effects that the presence of invasive bullfrogs may have on the small riparian fauna in the region. This experimental study involves the comparison a 2.4 Km stretch of river in which bullfrogs have been managed (experimental site), with a 2.4 Km stretch of river where bullfrog populations have been left intact (control site). We studied the populations of small cryptic vertebrates that use artificial cover-board objects by regularly sampling transects in each site. We compared biodiversity indices among both sites. Our preliminary data shows that diversity where bullfrogs are present is higher (Inverse Simpson=2.159, Shannon weaver =1.094, Pielou's J =.562, E-evenness = .427) than in the area without Bullfrogs (Inverse Simpson = 1.618, Shannon weaver = .827, Pielou's J = .359, E-evenness = .229). Contrary to our expectations, the presence of bullfrogs does not seem to detrimentally affect diversity. Rather, Paine effect may be contributing to the higher diversity of components of the lower trophic levels where the generalist predator is present.

Keywords: invasion ecology, Paine effect, management of invasion, Rana catesbeiana

Assessment of Episodic Hydrothermal Activity in the Rincon Geothermal System

MELINDA HORNE, NEW MEXICO TECH
JEFF PEPIN, NEW MEXICO TECH
MARK PERSON, NEW MEXICO TECH

MATT FOLSOM, NEW MEXICO TECH
JAMES WITCHER, WITCHER & ASSOCIATES
SHARI KELLEY, NEW MEXICO BUREAU OF GEOLOGY

The Rio Grande Rift is characterized by high crustal heat flow and fractured basement bedrock, giving rise to a number of low temperature (< 100 °C) geothermal systems near Las Cruces, NM. One such is the fault-controlled Rincon system north of Las Cruces. This area has shallow (~310m) temperatures up to 96 °C, and opal mineralization adjacent to the fault that dates between 2.15-1.95 Ma. The opal deposits form discrete layers deposited in Camp Rice fluvial sediment, and laterally shift to calcite away from the fault. These deposits, in combination with overturned temperature profiles from the geothermal exploration borehole SHL-1, suggest hydrothermal activity along the Rincon Fault is episodic in nature. We hypothesize that progressive opal precipitation diminishes fluid flow up the fault until a micro-seismic event reinitiates hydrothermal activity. We have developed a transient hydrothermal model of the Rincon Fault in order to conduct a sensitivity analysis that focuses on temporal variations in Rincon fault zone permeability through time. Nearby seismic events magnitude 3 or greater are being analyzed to find a source that may have caused the most recent onset of Rincon geothermal activity. Formation resistivities will be measured along the Rincon Fault using TDEM surface geophysical surveys to explore the extent of the geothermal system. Early model results indicate that the temperature overturns observed in well SHL-1 began decades ago following a century-scale period of quiescence.

Keywords: hydrothermal systems, Rio Grande Rift, opal deposits

Investigation of Patterned and Non-Patterned Poly(2,6-Dimethyl 1,4-Phenylene) Oxide Based Anion Exchange Membranes for Enhanced Desalination and Power Generation in a Microbial Desalination Cell

FRANCISCO LOPEZ-MORUNO, UNIVERSITY OF NEW MEXICO
CARLO SANTORO, UNIVERSITY OF NEW MEXICO
JOSÉ CERRATO, UNIVERSITY OF NEW MEXICO

JUAN RUBIO, UNIVERSITY OF NEW MEXICO
PLAMEN ATANASSOV, UNIVERSITY OF NEW MEXICO
CHRISTOPHER ARGES, UNIVERSITY OF NEW MEXICO

Quaternary ammonium poly(2,6-dimethyl 1,4-phenylene oxide) (QAPPO) anion exchange membranes (AEMs) with topographically patterned surfaces were assessed in a microbial desalination cell (MDC) system. The MDC

results with these QAPPO AEMs were benchmarked against a commercially available AEM. The MDC with the non-patterned QAPPO AEM (Q1) displayed the best desalination rate (a reduction of salinity by $53 \pm 2.7\%$) and power generation ($189 \pm 5 \text{ mW m}^{-2}$) when compared against the commercially available AEM and the patterned AEMs. The enhanced performance with the Q1 AEM was attributed to its higher ionic conductivity and smaller thickness leading to a reduced area specific resistance. It is important to note that Real Pacific Ocean seawater and activated sludge were used into the desalination chamber and anode chamber respectively for the MDC which mimicked realistic conditions. Although the non-patterned QAPPO AEM displayed better performance over the patterned QAPPO AEMs, it was observed that the anodic overpotential was smaller when the MDCs featured QAPPO AEMs with larger lateral feature sizes. The results from this study have important implications for the continuous improvements necessary for developing cheaper and better performing membranes in order to optimize the MDC.

Keywords: microbial desalination cell, anion exchange membranes

Modeling the Energy/Water Nexus in New Mexico

JAMAL MAMKHEZRI, UNIVERSITY OF NEW MEXICO

ELMIRA KALHOR, UNIVERSITY OF NEW MEXICO

KATIE ZEMLICK, UNIVERSITY OF NEW MEXICO

JANAK JOSHI, UNIVERSITY OF NEW MEXICO

KARA WALTER, UNIVERSITY OF NEW MEXICO

N. LU, UNIVERSITY OF NEW MEXICO

JENNIFER THACHER, UNIVERSITY OF NEW MEXICO

JANIE CHERMAK, UNIVERSITY OF NEW MEXICO

A major objective of this research is to develop a model that explores the nexus between human activity, energy, water, and the environment in New Mexico (NM). We develop a System Dynamics (SD) model that incorporates the social and natural world associated with alternative energy futures. Our goal is to compare and contrast energy futures and their tradeoffs, and to find possible policy scenarios for sustainable management of energy in NM. There are six interconnected modules designed to deliver this goal: (1) Oil and natural gas production, where drilling activity and production of oil and natural gas are modeled; (2) Hydraulic fracking and produced water disposal, in which the costs of re-using co-produced water for fracking is compared with that of fresh water resources; (3) Natural gas consumption by sector, where the demand of commercial, residential, industrial and electric sectors for natural gas are modeled; (4) Electricity generation by competing sources, where generation of electricity from fossil fuel and renewable energy sources as well as related economic implications are put in perspective, (5) Implications of energy lifecycle on health, which collects pollution outcomes of all the aforementioned modules and connects it with the number of ER visits; and (6) energy preferences survey, which captures consumers' preferences on energy sources among NM residents. Our SD model investigates all these energy-related issues at county level, between 2004 and 2054, on a monthly basis.

Keywords: energy-water nexus, system dynamics, electricity generation, energy consumption, health

Groundwater Controls on Water Chemistry in the Jemez River

CHRIS MCGIBBON, UNIVERSITY OF NEW MEXICO

LAURA CROSSEY, UNIVERSITY OF NEW MEXICO

KARL KARLSTROM, UNIVERSITY OF NEW MEXICO

TANNER GRULKE, UNIVERSITY OF NEW MEXICO

The Jemez River is a snowmelt-dominated system serving as outlet for water discharging from the Valles Caldera, with a smaller but significant contribution from springs. The groundwater inputs contain a geothermal component, which leads to degradation of water quality. This increases downstream and multiple natural tracers highlight the extent of the fluid mixing, as far as 40 miles to the south. Climate models predict less snow pack, causing a decrease in river discharge, a relative increase in spring contributions, and degradation in water quality. This degradation will affect local habitats and stake holders. Salinity/conductivity and [As] increase downstream from the headwaters in the Valles Caldera to the boarder of the study area at San Ysidro. Peak concentrations occur at Soda Dam and at San Ysidro. Major ion chemistry indicate that spring water a Soda Dam is a mixture of geothermal water from the Valles Caldera and local meteoric water. Geochemical mixing models indicate water-rock interaction with basement granites, and several tracers indicate dissolution of carbonates and evaporates in the distal regions is adding Sr with

a non-radiogenic $^{87}\text{Sr}/^{86}\text{Sr}$ value. Combining $^{87}\text{Sr}/^{86}\text{Sr}$ with conservative tracers can help to establish mixing volumes of spring and river water. These vary with river discharge: during low flow conditions, at 17 cubic feet per second (cfs), the relative component of spring contribution at Soda Dam is 5% of total river discharge. This work highlights evolution of groundwater along the flow path from the Valles Caldera to as well as potential alterations to river water chemistry/degradation.

Keywords: groundwater, geochemistry, Valles Caldera

Carotenoid And Lipid Synthesis Remodeling Events of a Chlorococcum Sp. Under Carbon Limitation

SA'RAE MONTOYA, NEW MEXICO STATE UNIVERSITY

This research is an extension of previous work that was carried out to collect data analyzing the biochemical composition, carotenoid synthesis, and lipid synthesis/remodeling events in a Chlorococcum sp. under stressed conditions. It is known that photooxidative stress causes this microalga to turn carotenogenic resulting in highly pigmented biomass. The aim of this study was to further examine the relationships that occur due to photooxidative stress. To gain a better understanding of the interactions occurring as a result of unfavorable conditions this research analyzed biomass cultivated under carbon limitation along with previously outlined conditions. These cultures were grown under constant 24-hour light, at 25°C, with no agitation under nitrogen deprived and non-deprived conditions. In addition, both culture treatments were not given additional CO₂ supplementation differing from the original treatments. Metabolite, lipid and carotenoid profile determinations were carried out and compared to the results observed by the previous study.

Keywords: carotenoid, algae, lipids

Alterations in metabolite pool and lipid content in Galdieria sulphuraria under mixotrophic growth

KHADIJEH MOZAFFARI, NEW MEXICO STATE UNIVERSITY

UJALA SEHAR, NEW MEXICO STATE UNIVERSITY

BARRY DUNGAN, NEW MEXICO STATE UNIVERSITY

F. OMAR HOLGUIN, NEW MEXICO STATE UNIVERSITY

The Galdieria sulphuraria (unicellular red microalgae) is capable of growth under extreme environments such as hot habitats with low acidity. Moreover, G. sulphuraria potentially might be used in the biofuel production, wastewater remediation and high-value products. It can grow autotrophically, mixotrophically, and heterotrophically on a variety of carbon sources. In the current research, the content and compositions of neutral and polar lipids, fatty acids and metabolites are determined under different carbohydrate supplementation. The outcome of such research is beneficial for understanding the carbon metabolism of this alga under varying carbon sources and to evaluate cellulosic hydrolysates as a source of low-cost carbon for mixotrophic cultivation.

Keywords: red alga, mixotrophy, biomass yield, metabolite pools

Integration of Product Design and Cellular Manufacturing through an Axiomatic Approach

ALEJANDRO NAJERA-ACOSTA, NEW MEXICO STATE UNIVERSITY

DELIA VALLES-ROSALES, U. AUTÓNOMA DE CIUDAD JUÁREZ

BLANCA VENEGAS-MATA, U. AUTÓNOMA DE CIUDAD JUÁREZ

In today's industrial practice there is a wide range of customer needs affecting designers in many decisions on product design to find the most suitable alternatives. The activities involved in the integral development of a product, need as a preliminary stage a clear definition of the type of product to be designed. The literature related to a rational methodology that addresses product design and manufacturing issues is limited. The design of a product determines 80% of manufacturing cost, and different ways to manufacture it can be considered. It is proposed a product design framework that integrates Axiomatic Design (AD) and Cellular Manufacturing (CM) to create associativity between the product and its manufacturing processes. In this case of study, the AD final product has two different components fabricated and transported in a manufacturing cell. The AD is based on the existence of 4 domains, which are zig-zagged for an

optimal design. It uses matrix methods to systematically analyze the transformation of customer attributes into functional requirements, design parameters, and process variables. Summarizing, the proposed framework is a logical and systematic axiomatic approach for the product design in cellular manufacturing systems, which makes it easily portable into practice, providing the guidelines for the decomposition of the design problem and independent mappings between problems and solutions. The suggested methodology provides feasible solutions that best meets the design and manufacturing objectives. It establishes scientific basis to design and to improve design activities by providing the designer with a theoretical foundation based on logical and rational thought processes and tools.

Keywords: product design, axiomatic design, cellular manufacturing, design methodology, penholder

Synthesis of Nanocrystalline Heterostructures with Dual Emission

TOM NAKOTTE, NEW MEXICO STATE UNIVERSITY

Recently, synthesis of PbSe/CdSe (core/shell) quantum dots, which display emission in both the visible and IR have been reported, opening up the system to potential applications as fluorophores for labeling and imaging. This goes along with the already realized benefits of enhanced carrier multiplication and suppressed Auger recombination, which make PbSe/CdSe quantum dots suitable for solar applications. Here, we present synthesis and characterization of PbSe/CdSe/CdS nanocrystalline heterostructures, which display enhanced IR emission as well as emission in the visible region. Visible emission is observed when the nanocrystals are excited with an infrared source, indicating that up-conversion may be occurring. Up-conversion is a process, in which a low energy photon interaction with the PbSe core causes higher-energy excitations within the CdSe/CdS shell. These excitations can then be collected in the form of photocurrent or converted into higher-energy photons for capture by a photovoltaic cell. The IR photoluminescence spectra from the PbSe cores indicate greatly increased exciton lifetimes compared to core-only and core/shell samples, which can be attributed to the reduction of the electron-hole overlap resulting from the delocalization of the electron wave functions into the outer CdS shell. The PbSe cores were synthesized using a traditional hot injection method, followed by a cation exchange from Pb to Cd to form PbSe/CdSe (core/shell) quantum dots, onto which a CdS outer-layer was grown using a modified approach of the SILAR method [4]. The nanocrystals were characterized using absorption, photoluminescence, and lifetime measurements as well as HRTEM.

Keywords: nanomaterials, quantum dots, solar cells

Custom Setup for High-Quality Organic Semiconductor Crystal Growth

*EVGENII OSKOLKOV, NEW MEXICO HIGHLANDS UNIVERSITY SERGEI RIGIN, NEW MEXICO HIGHLANDS UNIVERSITY
GEORGII BOGDANOV, NEW MEXICO HIGHLANDS UNIVERSITY GIL GALLEGOS, NEW MEXICO HIGHLANDS UNIVERSITY*

Organic electronic and optoelectronics recently are drawing significant attention due to ease of manufacturing, light weight, transparency, flexibility and other properties which is difficult to achieve using inorganic electronic materials. In recent years much attention was attracted by materials built of two and more components, for instance, donor and acceptor molecules. For such materials, strong correlation between their internal structure and properties usually exists. Main interests of our group are focused on creation of two-component organic or organic-inorganic materials with potential application as semiconductors and light emitting diodes. Variation of crystal structure of the same material (polymorphism or variation of stoichiometry) can be achieved by different crystallization conditions. At present solution crystallization is mainly used for such purpose. Gas-phase crystal growth also has been used due to its ability to produce highly pure crystalline materials from μm to cm -sized samples [1,2]. In this project, we are assembling a custom setup for gas-phase crystal growth. High-end three-zone tube furnace and precise controller will be coupled to achieve maximum quality and uniformity of organic crystals and organic thin films being synthesized, while turbomolecular pump will help to achieve high-vacuum environment to maintain high purity of produced structures. This setup would be a powerful tool in organic crystal growth, particularly for organic semiconductor crystals.

Keywords: vapor growth; organic crystal; tube furnace; organic semiconductors

Evaluation of biomass productivity and nutrient removal by *Scenedesmus Obliquus* in Municipal Wastewater for biofuel production

KAAVYA POLISETTI, NEW MEXICO STATE UNIVERSITY

The goal of this study was to determine the biomass productivity and nutrient removal by the algae *Scenedesmus Obliquus* in Municipal wastewater for biofuel production. Domestic wastewater treatment techniques that are in current use were developed decades ago for the specific purpose of meeting discharge standards to protect public health and preserving receiving water quality. Their energy needs and indirect impacts on the environment are now considered unsustainable and cost prohibitive. Microalgae can be used to reduce organic carbon and nutrient in urban wastewaters at the same time yields energy-rich biomass for biofuel production. *S.obliquus* is a freshwater microalga that is a potential candidate for biodiesel production. The microalgae *Scenedesmus Obliquus* was cultivated in different wastewater media conditions and compared to the standard BG-11 media. The biomass productivity of the algae in wastewater was higher than that of the standard media. The NH_4 and P nutrient removal rates were also observed.

Keywords: microalgae, biofuel, water quality

Elemental Composition and Reactivity of Metals in Wood Ash

ASIFUR RAHMAN, UNIVERSITY OF NEW MEXICO

JOHANNA BLAKE, UNIVERSITY OF NEW MEXICO

ABDUL-MEHDI ALI, UNIVERSITY OF NEW MEXICO

CYRENA RIDGEWAY, UNIVERSITY OF NEW MEXICO

JOSÉ CERRATO, UNIVERSITY OF NEW MEXICO

ELIANE EL HAYEK, UNIVERSITY OF NEW MEXICO

REBECCA BIXBY, UNIVERSITY OF NEW MEXICO

MICHAEL SPILDE, UNIVERSITY OF NEW MEXICO

KATERYNA ARTYUSHKOVA, UNIVERSITY OF NEW MEXICO

We investigated the elemental composition along with dissolution and adsorption of metals in wood ash under laboratory-controlled conditions using aqueous chemistry, microscopy and spectroscopy to better understand metal availability after wildfire events. Ash samples were prepared from three different tree species (Quaking Aspen, Ponderosa Pine and Blue Spruce) collected from Valles Caldera, New Mexico. Acid extractable elemental cation analysis suggested that wood ash burnt at both 3500C and 5500C have significantly higher ($p < 0.05$) metal concentrations from oven dried wood at 600C. Pine ash samples at 3500C and 5500C were associated with high concentrations of metals such as Mg, K, Ni, Cu, Si, Cr and Fe. 3500C Pine ash released the highest Dissolved Organic Carbon content (11.32+0.28 mg carbon/L) in the batch experiments. Further experiments and characterization were conducted on the Pine ash samples. We observed dissolution of Cr, Ni, Fe, Cu and Zn in solution reacting Pine ash with deionized water. In the batch adsorption experiments with Cu(II) and Cr(VI), rapid decrease in Cu(II) concentration in solution was observed, suggesting possible adsorption and/or precipitation of Cu(II) onto 3500C pine ash. Limited decrease of Cr(VI) in solution was observed suggesting repulsion of negatively charged 3500C pine ash surface and the anionic species of Cr (e.g., HCrO_4^- and CrO_4^{2-}). XPS survey scan detected presence of Cu on the reacted ash, indicating that Cu is associated with the ash “near surface” region. These results help to better understand how dissolution and adsorption processes can affect the fate of metals in water post fire.

Keywords: forest fire, wood ash, chemical composition

Assessing somatic growth of Rio Grande river cooter (*Pseudemys gorzugi*) in the Black River drainage, New Mexico

THANCHIRA SURIYAMONGKOL, EASTERN NEW MEXICO UNIVERSITY

Growth rate and body size are important life history traits that can influence reproductive success and other life history traits in turtles. Rio Grande river cooter (*Pseudemys gorzugi*) is one of the least studied North American freshwater turtle species. Currently, the species is under review by the USFWS for potential federal listing. However, the data on demographic parameters and natural history traits that would aid in the decision-making process is insufficient. The objective of this study is to estimate growth rates of *Pseudemys gorzugi* of different age classes caught within the Black River drainage from 2016 to 2017. We used carapace length of the initial captures from 2016 and recaptures

from 2017 to calculate the individual growth rates. We used ANOVA to compare the growth rates among size classes. In 2017, we recaptured 13 juveniles, 8 females, and 11 males. Straight line carapace length of initial captures ranged from 44 to 114 mm for juveniles, 124 to 172 mm for males, and 203 to 265 mm for females. Mean growth rate was 13.91 ± 6.15 mm/year for juveniles, 4.27 ± 4.56 mm/year for males, and 1.13 ± 2.30 mm/year for females. Growth rates among sexes were not significantly different ($p = 0.09$); however, growth rates among age classes showed a significant difference ($p < 0.01$). In conclusion, growth rates tend to decrease as the size of turtles increases.

Keywords: turtles, Pseudemys gorzugi, growth rates

Speciation and Reactivity of Uranium and Organic Matter in Abandoned Mine Wastes from Laguna, New Mexico

CARMEN VELASCO, UNIVERSITY OF NEW MEXICO

ABDUL-MEHDI ALI, UNIVERSITY OF NEW MEXICO

JOSÉ CERRATO, UNIVERSITY OF NEW MEXICO

SUMANT AVASARALA, UNIVERSITY OF NEW MEXICO

KATERYNA ARTYUSHKOVA, UNIVERSITY OF NEW MEXICO

CHRISTOPHER OSBURN, NORTH CAROLINA STATE UNIVERSITY

We applied spectroscopy, microscopy, and water chemistry techniques to investigate the speciation and reactivity of organic matter on uranium (U) binding from abandoned U mine waste from the Jackpile Mine in Laguna Pueblo, New Mexico. Preliminary studies using fixed angle X-ray fluorescence (XRF) analysis show 3.14% carbon (C). Results from microprobe mapping suggest that uranium particles are surrounded by carbon inclusions. We hypothesize that the presence of carbon in the mine waste influences the uranium binding and therefore its release to the environment. Loss on ignition (LOI) analysis showed that $12.98 \pm 0.25\%$ mass was lost. The change on mass after the LOI might be due to the loss of organic content of the samples. Analyses with X-ray photoelectron spectroscopy (XPS) show changes on the carbon binding after the LOI experiments and the oxidation of U (IV) to U(VI). The mean concentration of acid extractable for mine waste was $0.54 \pm 0.1\%$ U before LOI and $0.64 \pm 0.01\%$ U after LOI. Basic Extractions of the Particulate Organic Matter (BEPOM) and Excitation Emission Matrix (EMM) show the presence of humic and fulvic-like groups in the mine waste. Findings from this study are relevant to identify how the binding of U and C in mine wastes can influence U mobilization in order to inform risk assessment and reduction strategies.

Keywords: uranium, organic matter, mining legacy

Team Externship at Santa Fe Community College to Gain Experience in Algae Culture and Harvesting

HUILIN WANG, NEW MEXICO STATE UNIVERSITY

MESHACK AUDU, NEW MEXICO STATE UNIVERSITY

BRIAN TREFTZ, NEW MEXICO STATE UNIVERSITY

TIANBAI TANG, NEW MEXICO STATE UNIVERSITY

DUPLEX TCHINDA, NEW MEXICO STATE UNIVERSITY

At the end of June 2017, we travelled to Santa Fe Community College (SFCC) for two weeks NM EPSCoR externship program. The travel members include Huilin Wang, Tianbai Tang, Meshack A. Audu, who are graduate students from Department of Chemical & Materials Engineering, Duplex Tchinda, who is a graduate student from Department of Civil Engineering, and Brian Treftz, who is an undergraduate student at NMSU. During the externship at Santa Fe, we learned a lot about algae farm, cultivation, and some knowledge involved. First, we learned about aquaponics, which is a mutualism system that fish and plant benefits from the activity of each other. Next, we learned about two systems for cultivating the algae: enclosed system –photo bioreactor and open system–open raceway pond. Both systems have their merits and limitations. We also did cell counts and created a calibration curve that relates concentration versus population of the cells so that one can predict the population of cells at any given day once you know the concentration. We were also exposed to different harvesting methods that include a continuous flow centrifugation system and an ultrafiltration system; these systems also recycle the water back into the algae pond. Finally, the staffs showed us the how to make food-grade algae.

Keywords: hydrothermal liquefaction, yield, high heating value, brackish, batch reactor, algae

Biochemical characterization of *Nannochloropsis salina* under nitrogen limiting and reduced temperature conditions

STEPHANIE WILLATTE, NEW MEXICO STATE UNIVERSITY

SABA GILL, NEW MEXICO STATE UNIVERSITY

BARRY DUNGAN, NEW MEXICO STATE UNIVERSITY

OMAR HOLGUIN, NEW MEXICO STATE UNIVERSITY

The marine microalga *Nannochloropsis salina* CCMP1776 was cultivated under nitrogen limiting and reduced temperature conditions to induce alterations in the biochemical composition of fatty acids and lipid classes. Nitrogen limitation increases carbon allocation to either neutral lipid or starch granule formation in other microalgal species, while reduced temperature induces polyunsaturated fatty acid (PUFA) productivity to increase membrane fluidity. Both reduced nitrogen and temperature were used for combined treatment regimes in *N. salina* to determine how PUFAs are assembled into and remodeled between lipid classes. Intact lipids were characterized by ultra-performance liquid chromatography coupled with mass spectrometry (UPLC-MS) to identify lipid classes. Several lipid classes were detected, including two monoacylated lipid products: monoacylglycerol tri-methyl homoserine (MGTS) and monogalactosyl monoacylglycerol (MGMG). The detection of monoacylated lipid products suggests that these groups participate in lipid remodeling pathways, and the composition of lipid species within MGTS and MGMG indicates which acyl chains are preferentially retained during lipid remodeling. Similarly, polar metabolites were extracted and characterized by gas chromatography coupled with time-of-flight MS (GC-TOF-MS). Metabolic profiles were uploaded for pathway enrichment analysis in VANTED V2.6.3., and statistical differences were observed for several primary metabolites. Free amino acids, polyamine, and citrate cycle metabolite levels were altered under nitrogen limitation and reduced temperature compared to nitrogen limitation alone, which indicates that metabolic distinction occurs between treatment conditions. This suggests differential regulation of secondary metabolism under nitrogen limitation and reduced temperature vs. nitrogen limitation alone.

Keywords: algae biomass, photobioreactors, polycultures

About the New Mexico Academy of Science

The New Mexico Academy of Science was founded in 1902 to foster scientific research and scientific cooperation, to increase public awareness of the role of science in human progress and welfare, and to promote science education in New Mexico.

Membership in the Academy is open to anyone interested in science, science education, or the other goals and programs of the Academy. Individuals engaged in scientific research or teaching at all levels are particularly encouraged to become members. Applications for membership as well as more information about the Academy and its programs can be found at <http://www.nmas.org>.

CONTACT INFORMATION

The New Mexico Academy of Science
c/o The New Mexico Museum of Natural History and Science
1801 Mountain Road NW
Albuquerque, New Mexico 87104
nmas@nmas.org
<http://www.nmas.org>

OFFICERS AND EXECUTIVE BOARD 2017

OFFICERS

President: Dr. David Peters
President-Elect: Dr. John Emerson
Vice-President: Dr. Stephen Jett
Treasurer: Michael Gonzales
Secretary: Malva Knoll
Past President: Dr. Shanalyn Kemme
Director at Large: Gretchen Gurtler

DIRECTORS

Jayne C. Aubele, Museum Liason & NMAS Lecture Series
Lynn Brandvold, New Mexico Junior Academy of Science & AAAS Delegate
Deb Novak, NMAS Teacher Awards Program
Dr. Richard Nygren, National Youth Science Camp
Natalie Rogers, *Journal of Science*
Dr. Hartono Sumali, Community Relations

DIRECTORS EMERITUS

David Duggan
Dr. David Hsi
Harry Pomeroy (NMAS Fellow)
Mona Pomeroy
Dr. Maureen Romine



© NMAS 2017. All rights reserved

This is a publication by the New Mexico Academy of Science. NMAS does not discriminate on the basis of race, creed, color, national or ethnic origin, sex, physical disability, or sexual orientation.